Subsurface Flow Modelling At The Hillslope Scale: Numerical And Physical Analysis

Oscar Cainelli

UNIVERSITÀ DEGLI STUDI DI TRENTO
Dipartimento di Ingegneria Civile e Ambientale

2007

Based on the doctoral thesis in Environmental Engineering (XIX cycle)
defended in February 2007 at the Faculty of Engineering, University of Trento
Supervisors: Prof. Alberto Bellin and prof. Mario Putti

Università degli Studi di Trento
Trento, Italy
February 2007

To Elisa

Contents

Introduction **1**

1 Porous Media Flow Modeling: Theoretical Overview **7**
1.1 Introduction . . . 7
1.2 Saturated Flow Modeling . . . 7
1.2.1 The Law of Darcy . . . 7
1.2.2 The Flux Equation . . . 9
1.2.3 Momentum Balance Equation for Saturated Flow . . . 10
1.3 Unsaturated Flow Modeling . . . 12
1.3.1 The Law of Darcy-Buckingham and the Unsaturated Conductivity Function . . . 12
1.3.2 The Water Retention Curve . . . 13
1.3.3 The Richards Equation . . . 16
1.3.4 Momentum Balance Equation for Unsaturated Flow . . . 17

2 Modeling Saturated Flow and Transport in Heterogeneous Media **19**
2.1 Introduction . . . 19
2.2 Overview of The Analyzed Numerical Schemes . . . 21
2.2.1 The Galerkin Method . . . 21
The Yeh Method . . . 22
The Zhou Method . . . 22
2.2.2 The Mixed Hybrid Method . . . 23
2.3 Convergence Properties Analysis . . . 24
2.3.1 Some Theoretical Considerations . . . 24
2.3.2 Convergence Rate of The Schemes for Some Test Cases . . . 26
Convergence Application Tests . . . 28
2.4 Stochastic Analysis of The Numerical Solutions . . . 34
2.4.1 Synthetic Experiments Setup . . . 34
2.4.2 Analysis of the Covariance Functions of the Velocity Fields . . . 36
2.4.3 Numerical Schemes Structure and The Conductivity Field . . . 42
2.5 Transport Simulation by Means of The Particle Tracking Algorithm . . . 48

2.6 Summary . . . 56

3 Inertial Effects in Saturated Flow **59**
3.1 Introduction . . . 59
3.2 Dimensional Analysis of The Governing Equations . . . 61
3.2.1 Scaling Variables . . . 61
The Reference Time . . . 61
The Reference Length . . . 61
The Reference Piezometric Head . . . 62
The Reference Velocity . . . 62
3.2.2 Non-Dimensional Form of The Equations . . . 63
3.2.3 Analysis of The Non-Dimensional Coefficients . . . 64
Definition of Order of Magnitude . . . 64
Considerations on The Coefficients Structure . . . 64
The Temporal Inertial Term Analysis . . . 65
The Advection Term Analysis . . . 67
The Complete Momentum Equation . . . 69
3.3 Numerical Solution of The Momentum Equation . . . 70
3.3.1 The Numerical Scheme . . . 70
Overview . . . 70
The Staggered Grid Approach . . . 71
The Boundary Conditions . . . 71
3.3.2 Convergence Analysis . . . 73
3.3.3 Applications . . . 75
Test Case 1 . . . 75
Test Case 2 . . . 79
3.4 Summary . . . 81

4 Unsaturated Flow Modeling **83**
4.1 Introduction . . . 83
4.2 Problem Statement . . . 84
4.3 Dimensional Analysis of The Governing Equations . . . 88
4.3.1 The Scaling Variables For The Unsaturated Flow Case . . . 88
The Reference Suction . . . 88
The Variably Saturated Reference Time . . . 88
The Reference Unsaturated Velocity . . . 89
4.3.2 Non-Dimensional Form of The Variably Saturated Equations . . . 90
4.3.3 Analysis of The Non-Dimensional Coefficients . . . 90
General Considerations . . . 90
Dimensional Comparison of The Coefficients . . . 91

4.4 Numerical Solution . . . 93
4.4.1 Overview . . . 93
4.4.2 Simulations Setup . . . 94
4.4.3 Results and Discussion . . . 96
4.4.4 Numerical Application of The Capillary Barrier Concept . . . 101
4.5 Laboratory Experiment Design and Setup . . . 105
4.5.1 Column Design . . . 106
4.5.2 Instrumentation Overview . . . 109
4.5.3 Ongoing Work . . . 110
4.6 Summary . . . 111

5 Conclusions **113**

List of Figures **117**

List of Tables **120**

References **121**

Introduction

Despite a great effort has been spent in the last decades in order to better explain the mechanisms underlying runoff production and solute transport at the catchment scale, several issues are still unsolved. In this context, the processes leading to runoff generation at the hillslope scale are receiving much attention both from experimentalists and modelers because of their importance in shaping and timing streamflow and the geochemical signal. However, our modeling capability is hampered by difficulties in reproducing the relevant processes at the proper scale (there is a fundamental difficulty in upscaling processes from point to hillslope and catchment scales) and characterize spatial variability of the parameters. The complexity of processes controlling runoff production has been traditionally addressed by using sophisticated distributed modeling approaches with a large number of parameters, some of them spatially variable (i.e., the saturated hydraulic conductivity and the parameters of the suction curve). Consequently, distributed modeling is plagued by overparametrization while lack of measurements of state variables (in most cases only streamflow measurements are available) warrants only very simple models with no more than a few parameters (Jakeman and Hornberger, 1993). This dichotomy between complexity of the models and available data is one of the major and unsolved problems that hydrologists are facing. Besides that, there are also evidences that the parametrization typically utilized to model runoff generation at the hillslope scale may fail to capture the relevant processes during intense storms, in particular in coarse grained soils of forested catchments in humid regions. For instance, McGlynn (McGlynn and McDonnell (2003)) showed that the common assumption of separating hillslope runoff in two components: a fast component typically associated to surface runoff, and a slow component associated to subsurface flow, is not supported by field data they collected in the MaiMai catchment in New Zealand.

What they showed clearly is the predominance contribution to streamflow of water previously stored within the catchment (pre-event or old water), leading to the conclusion that the most part of total runoff is governed by subsurface flow and that actually fast and slow components of runoff production may be associated to the response of the saturated riparian zone and the unsaturated hillslope zone, respectively. Since the pioneering work of McDonnell (1990) a large body of evidence has been collected that surface flow is small to negligible in forested catchment in humid areas (see e.g. Neal and Rosier

(1990), Sklash (1990), McDonnell (2003), Wenniger et al. (2004) and Kirchner (2003)). From these evidences one can conclude that subsurface flow plays a key role in hillslope hydrology shedding new light into our limited understanding of the processes controlling runoff generation. Several studies observed that there is a gap between data and simulations based on physically founded fully distributed modeling approaches (see e.g. Kumar (2004), Montanari and Uhlenbrook (2004), Rigon et al. (2006) and Romanelli et al. (2006)).

Modeling accurately water movement in the near subsurface is a challenging endeavour fraught of difficulties and pitfalls. The equation describing saturated and unsaturated flow in porous media, which has been verified to apply locally to predict infiltration, has been applied to model infiltration and redistribution at the catchment scale by using virtually the same parametrization. However, several difficulties arise moving from point to hillslope scale. A first problem arises in the characterization of spatial variability of hydraulic parameters, which is typically not taken into account in distributed modeling, and related to this aspect is the relevance of preferential flowpaths. In principle spatial variability of hydraulic parameters can be introduced into most existing distributed modeling, but the fundamental issue of how to characterize this variability still remains as one of the most difficult and largely unsolved problem. The tremendous spatial variability of the hydraulic properties at the hillslope scale has been evidenced in several detailed field experiments (see e.g. Montgomery et al. (2002), Russo et al. (1997) and Zehe and Bloeshl (2004)).

Including spatial variability into distributed models calls for simulations requiring the numerical solution of the governing equations. Several numerical schemes are today available for this purpose such as finite elements *(FE)*, finite difference *(FD)* and finite volume *(FV)* schemes. There is a vast literature on the convergence properties of these methods as well as on postprocessing procedures aimed at improving the local physical representativeness of these standard solutions. However no exhaustive analyses on the accuracy and efficiency of such methods in heterogeneous formations have been performed so far. This aspect is particularly important in highly heterogeneous formations, such as those encountered when considering flow along hillslopes. Chapter 2 presents an accurate analysis of the errors arising when these numerical schemes are applied to heterogeneous formations and highlights the drawbacks of each method.

A further characteristic related to the equations governing flow in saturated and most importantly in unsaturated porous formations is their dependence on constitutive laws. A first one is the law that describes how flow is related to pressure gradients. This law is employed in both saturated and unsaturated formulations of mass conservation (see e.g. Brutsaert (2005)). In the year 1856 an engineer called Henry Darcy (1856) performed a laboratory experiment from which he deducted that flow is linearly related to the applied head gradient. Therefore, as often happen in science, this law has been in first instance obtained empirically. Further laboratory experiments showed deviations from this law when Reynolds number is large enough to make flow turbulent. The modified law that

describes this effect is called *Forchheimer's equation* (see e.g. Forchheimer (1901a), Forchheimer (1901b) and Firdaouss et al. (1997)). Nevertheless, deviation from Darcy's law has been observed at low Reynolds numbers that may be modeled with a cubic like variation of Darcy's law as it has been proposed by Fourar et al. (2004). These deviations from the Darcy's law have been obtained under the common assumption of stationary flow assuming that they can be extended to non-stationary conditions prevailing during storm events. One of the first contribution addressing the influence of non-stationary (inertial) effects during pumping test experiments is that of Torbjörn and Rehbinder (1993). They calculated a simplified first order analytical solution for inertial flow without including the advection term, comparison with the Darcy's law revealed some significant differences especially for step-changes in the boundary conditions. Levy et al. (1996) studied the occurrence of inertial flow for compressible fluid in porous media, they proposed a 1-D analytical model and made comparison with experimental results. Recent laboratory experiments and theoretical analysis (see e.g. Torres and Alexander (2002) and Germann and Di Pietro (1999)) suggested that inertial terms may be important and thus cannot be neglected in the momentum equation. In fact, Darcy's law is obtained from the momentum equation when inertial and viscous terms are negligible (the viscous term, leading to the Brinckman model, is relevant only within a thin layer at the interface from surface and subsurface flows). In chapter 3 a dimensional and numerical analysis of the momentum equation and of the relevance of inertial terms is reported for general situations of incompressible fluid flow, including non stationary regimes.

Under the hypothesis that Darcy's law applies, modeling unsaturated flow requires the definition of two constitutive laws: the water retention curve *(WRC)* and the unsaturated hydraulic conductivity function *(Kr)*.

The former one is a function describing the relationship between water content and local pressure head and is characterized by a hysteretic behavior due to processes acting at small scale. Here the pressure head, because the soil is not saturated, assumes negative values and is commonly called matric suction. To date no generally applicable parametrization of this behavior have been proposed mainly for difficulties associated to the characterization of hysteresis cycles.

Many expressions, obtained empirically or from highly idealized pore-scale models, are available (see e.g. Brooks and Corey (1964), Brutsaert (1966), Mualem (1976) and van Genuchten (1980)) and they have been applied quite extensively in the last few decades. Nevertheless, several experimental studies highlighted gaps in their modeling capability, and evidenced the dependency of this relation on many factors such as the multi-porosity structure that sometimes characterizes a porous media (Simunek et al. (2003)) or the dynamic character of motion (see e.g. Hassanizadeh and Gray (1993), Hassanizadeh et al. (2002) and Shultze et al. (1999)). These studies evidenced the complexity of the relationship between unsaturated flow and head gradient, somewhat limiting the applicability of

WRC empirical curves to highly idealized situations hardly respected in applications to hillslope hydrology. In fact, non-stationarity in the climatic forcing, i.e. the precipitation, may induce rapid variations in the velocity field that propagate down into the soil. In this situation WRC obtained under static conditions may be no longer valid while additional phenomena may arise that influence the relationship between hydraulic conductivity and water content.

In unsaturated conditions the hydraulic conductivity is typically expressed as the product of the saturated hydraulic conductivity Ks and the relative conductivity, Kr, which may assume values within the range [0,1] and is function of the water content. Typically a monotonic relationship between Kr and the water content is assumed, owing on the fact that under stationary conditions, hysteresis is small to negligible. Kr is zero at a water content in which capillary forces overcome gravity and hence holding the water immobile within the pores, and assumes a unitary value at saturation, where the hydraulic conductivity is maximum. Intermediate values describe the actual conductivity that corresponds to a given water content. An analytical approach for modeling such a function exists and is based on the pore size distribution function. However empirical formulas have also been proposed and have been widely employed for their simplicity with respect to the analytical approach.

All the empirical formulas employed for the description of the *WRC* and the *Kr* functions depend on a small number of parameters describing the soil structure. Among the most used parameters are pore size distribution, which affects the air entry value, and the slope of the falling part of the *WRC*. The heterogeneity of such soil parameters together with the saturated hydraulic conductivity exert a considerable role on the mechanisms that control water movement and more importantly contaminant transport in porous media (see e.g. Russo et al. (1997)).

To summarize, Richards equation, which is commonly utilized in hillslope studies, is based on a simplification of the momentum equation leading to the Darcy-Buckingham's equation, which in addition requires two constitutive equations relating the pressure head and the hydraulic conductivity to the water content. The conditions under which these relationships have been obtained and parametrized are hardly respected at the hillslope scale, in particular under non-stationary conditions. In fact, several problems arises when the Richards equation is applied for interpretation of accurate hillslope scale experiments (see e.g. Wenniger et al. (2004), McGlynn et al. (2004), Uchida et al. (2004), Torres et al. (1998) and Montgomery and Dietrich (2002)), many studies revealed an unexpected behavior of unsaturated soils subjected to infiltration. Among the several discrepancies observed between field experiments and their interpretation through the Richards equation the most challenging are the following two: the applicability of WRC at the field scale and the relevance of inertial terms in the momentum equation precluding the use of the Darcy's law and therefore of the Richards equation.

In applications it is typically assumed that the relationship between suction and water content is univocal, while there are overarching experimental evidences that this is not the case and a more complex hysteretical behavior is instead observed. Hassanizadeh (Hassanizadeh et al. (2002), Shultze (Shultze et al. (1999)) and others devised a model in which the WRC depends on the rate of change of water content.

The second incongruence had been evidenced by laboratory experiments by Germann and Di Pietro (1999) and Torres and Alexander (2002). These experiments were conducted by using an unsteady flow boundary condition mimicking rainfall induced flow during intense storms. Inertial terms in the momentum equation have been invoked by Germann and Di Pietro (1999) and Torres and Alexander (2002) in order to justify non-darcian flow phenomena observed in these experiments (see also Torres (2002)).

In particular, Torres and Alexander (2002) performed a column experiment in which a sandy soil was subjected to variable infiltration. Starting with a low rainfall rate applied on top of the column, the soil has been driven close to saturation, then a spike increase in rain intensity was applied for one hour, and then the rainfall intensity was let to return back to the pre-spike value. This experiment evidenced the emergence of non-darcian flux when the specific water discharge during the spike equated rainfall intensity, a flow behavior that cannot be predicted by using the Richards equation. More specifically, during the pre-spike period the water content in the column reached a constant value (stationary condition), that increased during the intense spike. However, differently from what was expected during the following period with constant rainfall intensity the water content decreased to values smaller than in the pre-spike period, even if the rainfall intensity was equal in both pre- and post-spike periods. They argued that this behavior may be due to inertial effects associated to the rapidly varying flow at the inflow cross section of the column. The relevance of the inertial terms in the momentum equation is analyzed in Section 4 with the help of a dimensional analysis of the momentum equation leading to the definition of the range of validity of the Darcy-Buckingham equation. The analysis evidenced that inertial terms were not relevant and that other mechanisms should be envisioned in order to explain the non-darcian behavior observed in the experiment. Detailed numerical simulations showed that during the pre-spike period the column stored more water than predicted by numerical simulations. An explanation of this apparent dichotomy is provided in Chapter 4 of this thesis.

Furthermore, Chapter 4 describes briefly the experimental setup of a new column experiment designed in order to better investigate flow under prevailing unsteady conditions induced by rapidly varying rainfalls.

1 Porous Media Flow Modeling: Theoretical Overview

1.1 Introduction

In this chapter the basic principles of porous media flow are illustrated. Porous media are very complex systems which physic involves the description of several phenomena at various scales. While single pore hydraulic is indeed simple to model, in order to describe the ensemble behavior of a portion of soil we need to upscale the small scale processes to the so called Darcy's scale. At this scale the target is to model the effects in the overall system due to the structure of the pore network. This requires the use of averaging rules that allow to find the upscaled form of the small scale governing equations, namely the Navier Stokes equations.

The drawback of using these rules is that they lead to the definition of the so called constitutive laws that are intended to be representative of the average behavior of some soil property taking into account most of the small scale effects. Nevertheless this procedure implies often a simplification of the problem resulting in the definition of a conceptual model that in some situations disagree with real soil dynamics. The constitutive laws employed for describing water movement in both saturated and unsaturated media are basically the Darcy's law and its unsaturated counterpart the Darcy-Buckingham's law, the Water Retention Curve concept *(WRC)* and the unsaturated relative conductivity function. The former two are a simplification of the more general momentum balance equations under the assumption of inertia free flow.

In the following paragraphs all the above mentioned concepts will be illustrated and briefly discussed

1.2 Saturated Flow Modeling

1.2.1 The Law of Darcy

In the year 1856 Henry Darcy published a report on seepage experiments of water through a cylinder filled with sand. The apparatus used in his experiment, commonly called *permeameter*, is shown in figure (1.1). He studied the rate of water flow Q through a porous soil induced by a difference in head between inlet and outlet and found that these two

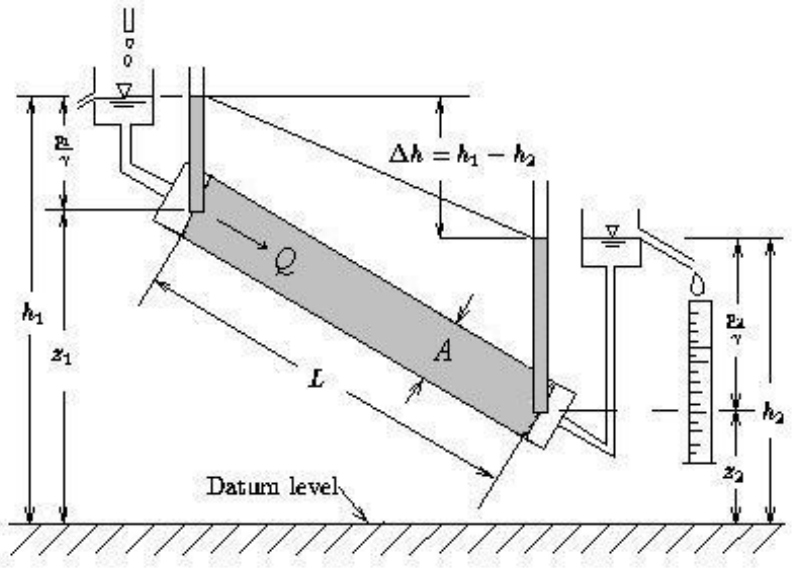

Figure 1.1: Schematization of Darcy's law experiment.

quantities were linked together by a linear relationship that depends also on the cross-sectional area of the column A and the column length ΔL and the resulted function may be formulated as follows:

$$Q = K_s A \frac{(h_1 - h_2)}{\Delta L} \tag{1.1}$$

where K_s is the coefficient of proportionality which is called *saturated hydraulic conductivity* and which has the dimensions of $[LT^{-1}]$, in table (1.1) common values for this parameter are given for a few types of soil.
The hydraulic head can be defined in the following way:

$$h = z + \frac{p_w}{\gamma_w} \tag{1.2}$$

where z is the vertical coordinate, p_w is water pressure and γ_w is the specific weight of water.

Under a continuum assumption, equation (1.1) may be reformulated in differential form for three dimensional flow in anisotropic porous media as follows:

$$\overrightarrow{q} = -\mathbf{K}\nabla h \tag{1.3}$$

where $\overrightarrow{q}$ is the flux vector and $\mathbf{K}$ is the second-order hydraulic conductivity tensor. Equation (1.3) in expanded form looks like:

Material	$K_s[ms^{-1}]$
Gravel	$10^{-2} - 10^{0}$
Clean sand	$10^{-6} - 10^{-2}$
Silty sand	$10^{-7} - 10^{-3}$
Silt	$10^{-9} - 10^{-5}$
Glacial till	$10^{-12} - 10^{-6}$
Clay	$10^{-12} - 10^{-8}$
Limestone and dolomite	$10^{-9} - 10^{-2}$
Fractured basalt	$10^{-6} - 10^{-2}$
Sandstone	$10^{-10} - 10^{-5}$
Igneous and metamorphic rock	$10^{-13} - 10^{-4}$

Table 1.1: Saturated hydraulic conductivity and capillary rise for some soil types (Freeze and Cherry, 1979).

$$\begin{aligned} q_x &= -k_{xx}\frac{\partial h}{\partial x} - k_{xy}\frac{\partial h}{\partial y} - k_{xz}\frac{\partial h}{\partial z} \\ q_y &= -k_{yx}\frac{\partial h}{\partial x} - k_{yy}\frac{\partial h}{\partial y} - k_{yz}\frac{\partial h}{\partial z} \\ q_z &= -k_{zx}\frac{\partial h}{\partial x} - k_{zy}\frac{\partial h}{\partial y} - k_{zz}\frac{\partial h}{\partial z} \end{aligned} \tag{1.4}$$

The hydraulic conductivity tensor is usually assumed to be symmetrical ($k_{ij} = k_{ji}$) and therefore may be diagonalized in order to have only three components along three principal axes. Furthermore in case of isotropic media equation (1.3) reduces to:

$$\overrightarrow{q} = -K_s \nabla h \tag{1.5}$$

where K_s is now a scalar.

1.2.2 The Flux Equation

In this section the derivation of the widely used *flux equation* is explained starting from the mass conservation equation for a consolidating porous medium which has the following form (Bear, 1972):

$$\frac{\partial \rho q_x}{\partial x} + \frac{\partial \rho q_y}{\partial y} + \frac{\partial \rho q_z}{\partial z} + n\frac{\partial \rho}{\partial t} + \rho\frac{\partial n}{\partial t} = 0 \tag{1.6}$$

where n is porosity and ρ is fluid density. The last term in equation (1.6) may be rewritten in terms of head variations as follows:

$$\rho\frac{\partial n}{\partial t} = \rho\alpha(1-n)\frac{\partial p}{\partial t} \tag{1.7}$$

where α is defined as *coefficient of soil compressibility*. Assuming that $\partial p/\partial t \cong g\rho\partial h/\partial t$ and fluid incompressibility, (1.6) becomes:

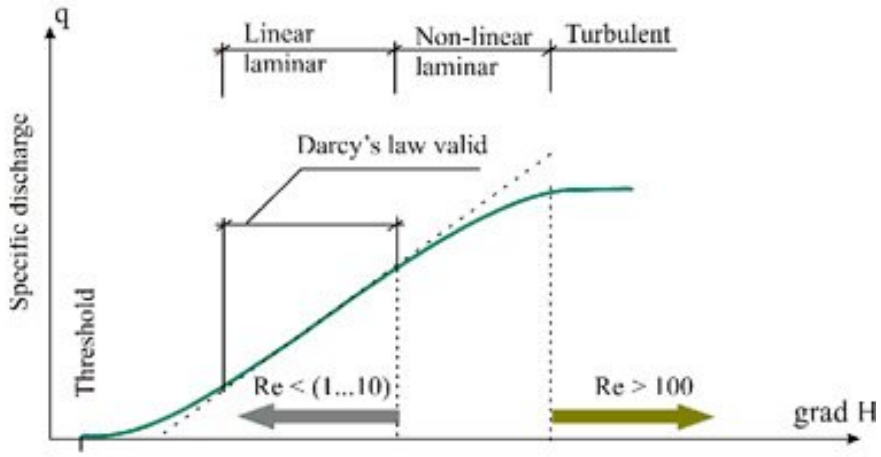

Figure 1.2: Limits of the validity of Darcy's law related to Reynolds number values.

$$\nabla \cdot \overrightarrow{q} = -\rho g \alpha [1 - n] \frac{\partial h}{\partial t} \tag{1.8}$$

we may now define a coefficient called *specific mass storativity related to potential changes* or simply *specific storage* S_s as:

$$S_s = \rho g \alpha [1 - n] \tag{1.9}$$

and rewrite (1.8) as:

$$\nabla \cdot \overrightarrow{q} = -S_s \frac{\partial h}{\partial t} \tag{1.10}$$

If we now substitute the specific discharge in (1.10) with Darcy's law as stated in (1.3), we find the form of the so called *flux equation*:

$$\nabla \cdot (\mathbf{K} \nabla h) = S_s \frac{\partial h}{\partial t} \tag{1.11}$$

Assuming the validity of the Darcy's law, the solution of the above equation describes the potential field over a saturated hydraulic conductivity domain subjected to *Dirichlet* and *Neumann* boundary conditions.

1.2.3 Momentum Balance Equation for Saturated Flow

The Darcy's law is not valid in every type of flow conditions. A first objection concerns its validity across the transition between laminar and turbulent flow. The Reynolds number is a good indicator of the type of flow regime:

$$Re = \frac{du\rho}{\nu} \tag{1.12}$$

where d is the effective pore diameter, u is the mean flow velocity, ρ_w is the liquid density and ν is viscosity. When the $Re > 100$ turbulence occur and the Darcy's law deviates from its linear behavior. However most of the natural porous media dynamics show a laminar flow character and therefore are well described with Darcy's law. Figure (1.2) shows the validity of the Darcy's law as a function of the Reynolds number and it is shown to be linear in the range $1 < Re < 10$ (According to Bear (1972)).

A second objection is that Darcy's law has been observed through the use of simple stationary experiments. The linear relationship between discharge and head gradient has been observed at equilibrium piezometric levels and assumed to be valid also for transient conditions because of the usual slow character of porous media flow.

In order to model the dependency of discharge behavior with respect to the rate of change of flow conditions, we must use the complete formulation for the momentum balance equation for fluxes. In Bear and Bachmat (1990) a full formulation for such equation is given for rigid porous media, which continuity is $\nabla \cdot \overrightarrow{q} = 0$, but under the assumption that $\nabla n = 0$ it is valid also for consolidating media. The full system of equations that governs inertial saturated flow of an incompressible fluid in deformable porous media is based on equation (1.10) and the following:

$$\frac{D\overrightarrow{v}}{Dt} = -gT\nabla h - \frac{ngT}{K_s}\overrightarrow{v} \tag{1.13}$$

where $\overrightarrow{v}$ is the velocity vector and T is the coefficient of tortuosity which can be considered as a constant scalar although in principle it is a tensor. T can be approximated in the following way (Bear, 1972):

$$T = n^{11/6} \tag{1.14}$$

Equation (1.13) is valid assuming that the velocity of soil deformation is negligible comparing to fluid velocity ($v_{s_i} << v_i$), otherwise Biot's theory or others have to be employed. In equation (1.13) a further viscosity term should appear which is though almost always negligible.

Consistency of equations (1.5) and (1.13) is easy to be verified by neglecting the rate of momentum change in (1.13) and defining fluid velocity as:

$$\overrightarrow{v} = -\frac{\mathbf{K}}{n}\nabla h \tag{1.15}$$

which means that:

$$\overrightarrow{q} = n\overrightarrow{v} \tag{1.16}$$

These simple steps allow to get back to the simple Darcy's law as stated in equation (1.5).

1.3 Unsaturated Flow Modeling

1.3.1 The Law of Darcy-Buckingham and the Unsaturated Conductivity Function

In year 1907 Buckingham postulated for the first time that Darcy's law is also valid for a partly saturated soil and that in such case the hydraulic conductivity is no more constant but depends on water content ($k = k(\theta)$). So the formulation for the newly proposed law for flow in unsaturated soils looks like:

$$\overrightarrow{q} = -\mathbf{K}(\theta)\nabla(z + \psi) \tag{1.17}$$

Equation (1.17) depends though on two state variables that are the water content θ and matric suction ψ ($\psi = -p_w/\gamma_w$) which is a negative pressure of water relative to air pressure. We will see later how these two variables are tied together and how we usually model their dependency.

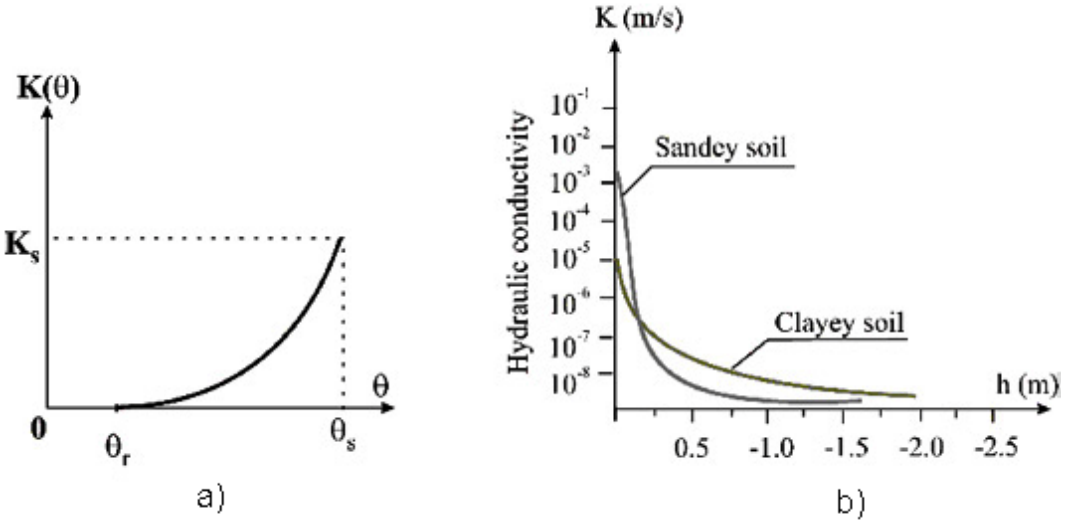

Figure 1.3: General shape of the unsaturated hydraulic conductivity: a) K(θ) ; b) K(h) ($h = z + \psi$) (Musy and Soutter, 1991).

An important concept introduced in equation (1.17) is then the unsaturated hydraulic conductivity function which typical trend is shown in figure (1.3). It states that for low

water contents the soil conductivity is low and it increases as water content increases until saturation, where the unsaturated hydraulic conductivity reaches the maximum which coincides with the saturated conductivity value.

Several empirical functions have been proposed in literature and their reliability has been tested in several laboratory works (see e.g. Brutsaert (2005) and Zaradny (1993)). Because of the interconnection between matric suction and water content, it is possible to express k as a function of either θ and ψ. One of the most diffused model has been proposed by Gardner (1958) and is based on this simple expression:

$$k(\psi) = \frac{a}{b + |\psi|^c} \tag{1.18}$$

where a, b and c are constants that satisfy $a/b = K_s$, $b = |\psi|^c$ for $k = K_s/2$ and c value ranges between about 2 for clayey soils to about 4 or more for sandy soils.

Another important model has been proposed by Brooks and Corey (1964) which is based on this simple expression:

$$k(\psi) = (\frac{\psi_{cr}}{\psi})^{2+3\lambda} \tag{1.19}$$

where ψ_{cr} [cm] is the critical pressure head (air entry pressure) and λ is a pore distribution parameter. For suction greater than the air entry value $k(\psi) = 1$. This two-part structure lead to a singular behavior of the function derivative at $\psi = \psi_{cr}$ which exerts drawbacks in numerical modeling.

In this sense van Genuchten (1980) proposed a more sophisticated expression with a smooth shape and which is one of the most used formula for unsaturated conductivity:

$$k(\psi) = K_s \frac{1 - (\alpha|\psi|)^{n-2}[1 + (\alpha|\psi|)^n]^{-m}}{[1 + (\alpha|\psi|)^n]^{2m}} \tag{1.20}$$

where α, m and n are parameters ($m = 1 - 1/n$) which typical values for different soil types are reported in table (1.2).

There are so many other models proposed in literature but the mentioned above are the most used and widely tested ones, however for a comprehensive review of them see e.g. Zaradny (1993).

1.3.2 The Water Retention Curve

As previously mentioned, the water content and the matric suction may be linked together through the use of an empirical function called *water retention curve (WRC)*, which states that for a specific moisture level there is a defined value for suction. Actually this function shows an hysteretic trend related to the state of the system, in fact it is common to observe different soil behavior in case of drainage and imbibition. For the same water content we

Soil type	θ_s	θ_r	$\alpha[m^{-1}]$	n	$\psi_{cr}[m]$	γ
Sand	0.437	0.020	14.5	2.68	0.160	0.69
Loamy sand	0.437	0.035	12.4	2.28	0.206	0.55
Sandy loam	0.453	0.041	7.5	1.89	0.302	0.38
Silt loam	0.501	0.015	2.0	1.41	0.509	0.23
Loam	0.463	0.027	3.6	1.56	0.401	0.25
Sandy clay loam	0.398	0.068	5.9	1.48	0.594	0.32
Silty clay loam	0.464	0.075	1.0	1.23	0.564	0.24
Clay loam	0.471	0.040	1.9	1.31	0.703	0.17
Sand clay	0.430	0.109	2.7	1.23	0.794	0.22
Silty clay	0.479	0.056	0.5	1.09	0.765	0.15
Clay	0.475	0.090	0.8	1.09	0.856	0.16

Table 1.2: Soil hydraulic parameters for van Genuchten and Brooks and Corey models for eleven soil classes (Shao and Irannejad, 1999).

may measure a different value for matric suction in either situations. In figure (1.4) the typical trend of the *WRC* for sandy to clayey soils is reported.

The shape of such curves show different suction ranges for different soil types, for instance sandy soils exhibit a *WRC* in the range 0 to -100 KPa ($1m = 9.81Kpa$) while clayey soils exhibit a wider range of suction variation. This aspect is strictly connected to the pore size distribution of soils (see table (1.3)) since capillary forces are greater for finer textured soils.

Several empirical formulas have been proposed in literature in order to describe soil's *WRCs*. Among them a very simple one and indeed very well known has been proposed by Brooks and Corey (1964). Defining effective saturation as:

$$S_e = \frac{\theta - \theta_r}{\theta_s - \theta_r} \tag{1.21}$$

where θ_s is water content at saturation while θ_r is residual water content, the link between suction and water content is as follows:

Soil class	*Grain size [mm]*
Gravel	> 2.0
Sand	$0.02 < d < 2.0$
coarse	$0.2 < d < 2.0$
fine	$0.02 < d < 0.2$
Silt	$0.002 < d < 0.02$
Clay	$d < 0.002$

Table 1.3: Grain size ranges for typical soil classes (Zaradny, 1993)

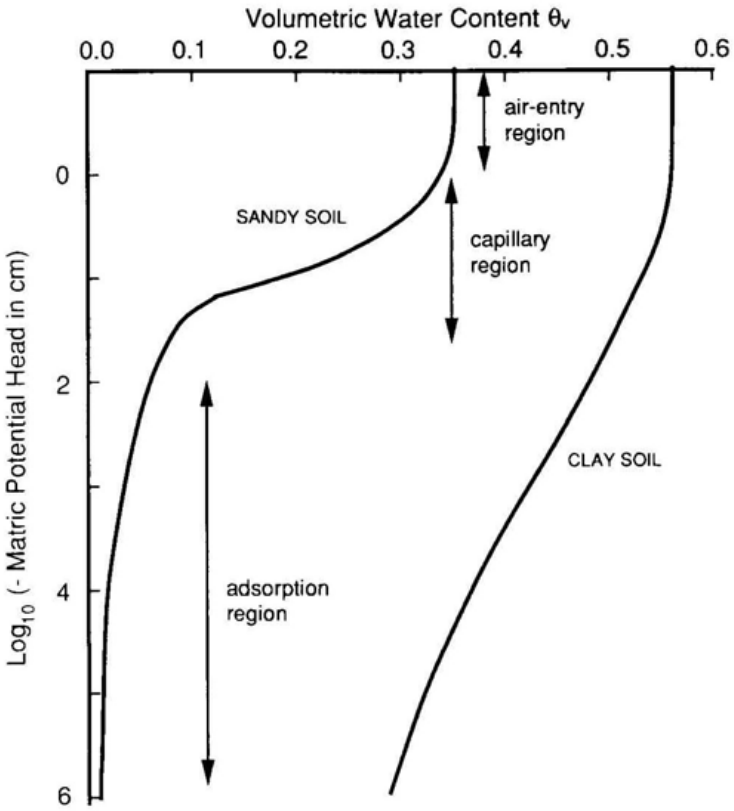

Figure 1.4: General shape of the water retention curves for some types of soil. Taken from http://research.umbc.edu/ jgwo/Courses/CompSubHydrol-I /Homework01.html.

$$\begin{aligned} S_e &= 1 \qquad\qquad for \qquad 0 < |\psi| < |\psi_{cr}| \\ S_e &= (\psi/\psi_{cr})^{-\gamma} \qquad for \qquad |\psi| \geq |\psi_{cr}| \end{aligned} \tag{1.22}$$

where ψ_{cr} and γ are constant which are characteristic for a given soil type. A major problem of model (1.22) is its derivative structure, as discussed also for the conductivity model proposed by the same authors.

In order to obtain a smooth trend through all the effective saturation range, Brutsaert (1966) proposed the following:

$$S_e = (1 + (a|\psi|)^b)^{-1} \tag{1.23}$$

where a and b are constant defined as for equation (1.18).

An extension to model (1.23) has been proposed by van Genuchten (1980) in which he introduced a further parameter in order to allow a greater function flexibility. The model is as follows:

$$S_e = (1 + (\alpha|\psi|)^n)^{-m} \tag{1.24}$$

with α, n and m the same parameters as defined for equation (1.20). The price for the more flexibility of this function seems to be related to the dependence on a third parameter (m) which though can be expressed as a function of one of the other two parameters (n).

1.3.3 The Richards Equation

The *WRC* and *k(θ)* functions together with the *Darcy-Buckingham's law* are the constitutive relations required in order to formulate an equation for flow in partly saturated porous media.

Starting from the equation of continuity in unsaturated soils:

$$\nabla \cdot \overrightarrow{q} = \frac{\partial \theta}{\partial t} \tag{1.25}$$

we may define water fluxes with equation (1.17) and substitute them into (1.25) and find:

$$\nabla \cdot (\mathbf{K}(\psi)\nabla(z + \psi)) = \frac{\partial \theta}{\partial t} \tag{1.26}$$

which depending on the two state variable (ψ and θ), might be rewritten in terms of only one of them through the use of one of the *WRC* model introduced in the previous section. Equation (1.26) is usually referred to as Richards (1931) equation. When saturation is reached, so that water content θ is equal to θ_s, we find that $k(\psi)$ is equal to k_s and hence equation (1.26) reduces to the equation of Laplace, that is $\nabla h = 0$.

In order to model both unsaturated and saturated behavior of consolidating media it is necessary to rewrite equation (1.26) in terms of suction through the use of a *WRC* model:

$$\nabla \cdot (\mathbf{K}(\psi)\nabla(z + \psi)) = C(\psi)\frac{\partial \psi}{\partial t} \tag{1.27}$$

where the term $C(\psi)$ is the derivative of the *WRC* function as $\partial\theta/\partial\psi$. Now we may introduce a further fictitious term multiplying the time derivative of suction and get an extended form for $C(\psi)$ as to take into account for soil deformability:

$$C(\psi) = \frac{\partial \theta}{\partial \psi} + S_e S_s \tag{1.28}$$

Using relation (1.28) into (1.27) allows to model the transition between the unsaturated and the saturated states of a soil accounting for soil deformability which is expressed by the specific storage term (S_s).

1.3.4 Momentum Balance Equation for Unsaturated Flow

In order to model inertial effects in unsaturated flow we may use a model proposed in Bear and Bachmat (1990), in which a formulation for multi-phase flow in porous media is given. The model states that for each phase α we may write a continuity and momentum balance equation as follow:

$$\frac{\partial \rho_\alpha \theta_\alpha}{\partial t} = -\nabla \cdot (\rho_\alpha \theta_\alpha \overrightarrow{v}_\alpha) \tag{1.29}$$

$$\rho_\alpha \theta_\alpha \frac{d\overrightarrow{v}_\alpha}{dt} = -\theta_\alpha T(\theta_\alpha) \nabla p_\alpha - \rho_\alpha \theta_\alpha g T(\theta_\alpha) \nabla z + \theta_\alpha \nabla \tau_\alpha \tag{1.30}$$

where $\nabla \tau_\alpha$ is the friction term for phase α which can be expressed as:

$$\nabla \tau_\alpha = -\frac{\rho_\alpha \theta_\alpha^2 g T(\theta_\alpha)}{k(\theta_\alpha)} \overrightarrow{v}_\alpha \tag{1.31}$$

If we now consider fluid incompressibility and model the air phase contribution with the *WRC* function, we may find a simplified formulation for the inertial unsaturated flow. The continuity equation for water is:

$$\frac{\partial \theta(\psi)}{\partial t} = -\nabla \cdot (\theta(\psi) \overrightarrow{v}) \tag{1.32}$$

The momentum balance equation for water with the aid of equation (1.31) reduces to:

$$\frac{d\overrightarrow{v}}{dt} = -gT(\theta(\psi)) \nabla \psi - gT(\theta(\psi)) \nabla z - \frac{gT(\theta(\psi))}{k(\theta(\psi))} \theta(\psi) \overrightarrow{v} \tag{1.33}$$

where subscript α has been omitted, the tortuosity factor may be evaluated with the following:

$$T(\theta) = \frac{\theta^{7/3}}{n^{1/2}} \tag{1.34}$$

where n is porosity. Equation (1.32) may be rewritten in suction terms and rearranged for the correct handling of the transition between saturated and unsaturated flow with the use of relation (1.28):

$$C(\psi) \frac{\partial \psi}{\partial t} = -\nabla \cdot (\theta(\psi) \overrightarrow{v}) \tag{1.35}$$

the model composed of equations (1.35) and (1.33) may be used as an extension to Richards equation (1.27) including unsaturated inertial flow effects.

2 Modeling Saturated Flow and Transport in Heterogeneous Media

2.1 Introduction

Mathematical modeling of flux and contaminant transport in heterogeneous porous media assumes a great relevance in several subsurface hydrological applications, with particular interests for site restoration, environmental risk assessment and for the process of runoff production. The complexity that characterizes geological formations manifest through a strong variability of the hydraulic properties, such as the permeability which shows variabilities at several different scales (Neuman and Di Federico, 2003). Starting from early '80 all the conducted studies lead to the definition of a methodology of analysis which is strongly consolidated from the conceptual point of view and through which the uncertainties related to the non perfect knowledge of the permeability field are translated in an opportune confidence interval of flow solutions. This approach then is not aimed at reducing the uncertainties connected to the poor knowledge of permeability, which would be impossible for the mole of punctual measurements needed, instead tends to quantify and minimize the confidence interval of solutions.

This approach is known as the stochastic approach, and requires the definition of a suitable geostatistical model for the variability of hydraulic properties. Analytical solution approaches are limited to weakly heterogeneous formations and for regular boundary conditions, while the applications to real cases call for the need to solve numerically the equations that describe flux and transport. The flux equation requires then to be solved over a domain where the hydraulic conductivity exhibits several scales of spatial variability, some of which are related to distances of the order of magnitude of meters in the horizontal direction and of the order of tens of centimeters in the vertical one. This requires the use of very fine grids in order to capture all these variabilities (see Bellin et al. (1992) and Chin and Wang (1992)) leading to a huge number of unknowns, and more important with conductivity value that varies from cell to cell within the domain. This latter aspect exerts a crucial role for the accuracy of the numerical solutions for the reason that the most used numerical models do not lead to solutions that satisfy the refraction laws of stream lines at the interface between adjacent cells (see e.g. Srivastava and Brusseau (1995) and Zhou et al. (2001)). These gaps exert a marginal influence if the variability is described through

a few blocks of constant permeability, which though may turn out to be appreciable when the geostatistical model assigns non negligible contrasts to the hydraulic properties of adjacent elements. It is well known that the standard finite element methods do not satisfy these laws neither in the classical Galerkin formulation (*CG*) nor in the *Yeh* formulation and nor in the classical mixed formulation. In order to remedy to this problem Srivastava and Brusseau (1995) proposed a post-processing procedure for evaluating fluid velocity that imposes the respect of such laws starting from a classical solution, and recently an analogous proposal has been presented by Zhou et al. (2001) (*ZB*). Three of these methods are based on the piezometric field evaluated through the use of the Galerkin scheme applied to the flux equation and propose various post-processing procedures to calculate the related velocity field. The alternative to such schemes is the more complex mixed finite element method (*MFE*) which solves contemporarily piezometric head and velocity field (see e.g. Meissner (1972) and Brezzi and Fortin (1991)), leading to a system of equation with a number of unknowns much greater than the other schemes. The debate on the worthiness of such method has been widely discussed, see e.g. Mosé et al. (1994) and Cordes and Kizelbach (1996) and Ackerer et al. (1996) for some contributions.

Deterministic comparisons among some of the above mentioned numerical methods applied to groundwater flow problems are reported for example in Mosé et al. (1994), Cordes and Kizelbach (1992) and Zhou et al. (2001), while one of the first stochastic comparisons of them has been proposed by Bellin (2000) for the three-dimensional case. In his analysis, Bellin did not take into account of the method of Zhou because it was not yet available, and the mixed method because in three dimensions its computational cost would be very demanding for the huge number of unknowns required. Bellin concluded that imposing with a post-processing procedure the satisfaction of the refraction laws introduces spurious effects in the flow field, which is qualitatively equivalent to a linearization of the flux equation. In this chapter the above mentioned methods applied to the stationary form of equation (1.11) in heterogeneous fields are compared in terms of the rate of convergence toward an analytical solution over simple heterogenous domains, and they are also compared from a stochastic point of view over very heterogeneous domains with the hydraulic conductivity that varies from cell to cell. An analysis on asymptotic solutions for flow and contaminant transport has been achieved in a Monte Carlo framework and the solutions of the numerical methods have been compared with first and second order analytical solutions. An important aspect arisen from the latter analysis concerns the way the conductivity fields are used within each numerical scheme leading to a modification of the field statistics with non negligible drawbacks in the flow solution. The impact of the heterogeneity level on numerical solutions is discussed together with the drawbacks on transport behavior achieved by means of the particle tracking technique.

2.2 Overview of The Analyzed Numerical Schemes

In this section a brief overview of the studied numerical schemes is given. Three of them are based on the standard Galerkin formulation for the finite element solution of the flux equation, while the fourth one is based on the mixed finite element approach, and more specifically on the mixed hybrid formulation (MH). A FORTRAN 90 code for each of them has been created and tested against theoretical behavior as will be explained later. For more exhaustive explanations about the schemes the reader should refer to the cited bibliography.

2.2.1 The Galerkin Method

The most classical numerical scheme for the solution of the flux equation in stationary conditions is the finite element method in the standard Galerkin formulation (SG), see e.g. Segerlind (1987) for the application to the groundwater problem but not only. In a saturated aquifer the flux equation in stationary form is

$$\nabla \cdot \mathbf{K} \nabla h = f \tag{2.1}$$

where f is the external forcing term which in the most common cases may be representative of either a pumping well or rainfall recharge.

Equation (2.1) is defined over a domain Ω of boundary $\partial\Omega$. Dirichlet and Neumann boundary conditions are imposed respectively over the boundary portions Γ_1 and Γ_2, under the hypothesis that $\Gamma_1 \bigcup \Gamma_2 = \partial\Omega$. The domain Ω is then divided in triangular cells (elements) for a total of n vertices and p triangles. Following the Galerkin method, equation (2.1) is first rewritten in its variational form for being solved approximating the unknown (h) as a element-wise continuous linear function (Reddy, 1993). The output of this procedure is a system of linear algebraic equations which unknowns are the piezometric head values in each node i of the grid. The system can be written as

$$\sum_{j=1}^{n} h_j \left[\sum_{e=1}^{p} \int_{T_e} \left(K_e \nabla N_i^e \cdot \nabla N_j^e \right) \, \mathrm{d}\Delta \right] - \sum_{e=1}^{p} \int_{\Gamma_2^e} q_n^e N_i^e \, \mathrm{d}\Gamma + \sum_{e=1}^{p} \int_{\Delta^e} f^e N_i^e \, \mathrm{d}\Delta = 0 \qquad i = 1, \ldots, n \tag{2.2}$$

where K_e is the hydraulic conductivity of element e and which is assumed to be constant over the entire element area T^e; N_i^e and N_j^e are the linear shape functions which value is 1 respectively in node i and node j over T^e and *zero* in the other element nodes; q_n^e is the Neumann flux defined over the element boundaries and f^e is the forcing term applied on

the element surface Δ.

The piece-wise linear interpolation used for h_j determines a univocal gradient field ∇h constant over each element, which value is determined by the slope of the plane passing by the nodal piezometric head values.

The first of the three Galerkin based methods for velocity field evaluation, namely the classical Galerkin (CG) formulation, is then straightforward, it is sufficient to substitute in equation (1.15) the element gradient as just defined.

It is possible to demonstrate that the theoretical convergence rate for such scheme is quadratic for the piezometric head and linear for velocities, under the assumption that the analytical solution is smooth enough, that the triangulation does not include degenerate angles and that all the coefficients in equation (2.2) satisfies the *Lipschitz* condition in space, which means finite first order derivative.

The velocity field obtained with CG scheme is though not always conservative, in particular this is observable in heterogeneous hydraulic conductivity fields (see e.g. Cordes and Kizelbach (1992)). In order to overcome this problem some methods try to impose further conservative conditions over the velocity field with post-processing correction procedures.

The Yeh Method

Using the variable separation principle, Yeh (1981) proposed a scheme that evaluate the velocity vector components through the variational formulation of equation (1.15). The linear interpolation of the velocity vectors determines then a linear system of algebraic equation which for each node i states an equation given by

$$\begin{aligned} \vec{v} &\approx \sum_{i=1}^{n} \vec{v^*} N_i \\ \sum_{e=1}^{p} \int_{\Omega} \vec{v^*}^e N_i^e \, \mathrm{d}\Omega &= -\sum_{e=1}^{p} \int_{\Omega} K_e \nabla h \, \mathrm{d}\Omega, \end{aligned} \tag{2.3}$$

where $\vec{v^*}$ is the nodal velocity vector components, which are the system unknowns. It is simple to see that the $\vec{v^*}$ values satisfies only the continuity condition for the normal flux component across elements boundaries but not the tangential condition (Bear, 1972). The theoretical convergence rate for the velocities evaluated with this scheme is of order 3/2, leading then to an improvement of the standard CG scheme.

The Zhou Method

Zhou et al. (2001) proposed a new post-processing approach (ZB) which extends the previous one by imposing the complete respect of the refraction laws of streamlines across

the boundaries of adjacent elements with different conductivity values (Bear, 1972). Such conditions may be written as follows:

$$\vec{v}^{+} \cdot n_e = \vec{v}^{-} \cdot n_e \qquad h^{+} = h^{-}$$

where n_e is the outward normal vector related to the interface between two elements with different hydraulic properties, while apexes $+$ and $-$ identify respectively the values of the considered quantities in the region of greater and lower hydraulic conductivity. They simply impose that the normal velocity component conserves while the tangential ones must be proportional to the hydraulic conductivity of the considered region. We then can evince that:

$$\vec{v}_n^{+} - \vec{v}_n^{-} = 0 \qquad \vec{v}_t^{+} - \frac{K^{+}}{K^{-}}\vec{v}_t^{-} = 0$$

The respect of the above mentioned laws is imposed within an iterative process which starting from the velocity field solution obtained with Yeh method leads to an improved one. Since this scheme is based on Yeh method, the convergence rate for simple cases should attest at least on order 3/2. This scheme in case of homogeneous hydraulic conductivity fields coincides exactly with the Yeh one.

2.2.2 The Mixed Hybrid Method

As an alternative to the Galerkin based methods, from the early '70 a new family of methods have been developed, the so called mixed finite elements methods. They are based on the following weak formulation (see e.g. Meissner (1972) and Brezzi and Fortin (1991)):

$$\begin{aligned} \vec{\nabla} \cdot \vec{v} &= f \\ K^{-1}\vec{v} &= -\vec{\nabla} h \end{aligned} \tag{2.4}$$

The most simple approach to solve (2.4) is based on the interpolation of h with constant basis function (ϕ_i) over each triangle, while the vector velocities $\vec{v}$ are interpolated with vectorial basis functions that are defined element-wise and linear (this approach is commonly called $RT0$ approach from Raviart and Thomas (1977)). The linear system resulting from this schematization may be better solved with a technique called hybridization, from which the name *Mixed Hybrid Finite Elements (MH)*. This approach is based on the introduction of a finite set of lagrange multipliers λ that are interpolated by means of basis functions μ_i constant along element sides and which represent the trace on the element sides midpoint of the piezometric unknown defined in the element circum-center h. Thus the problem unknowns may be summarized as follows:

$$h \approx \sum_{i=1}^{n} h_i \phi_i \qquad \vec{v} \approx \sum_{i=1}^{m} v_i \vec{w}_i \qquad \lambda \approx \sum_{i=1}^{m} \lambda_i \mu_i$$

the v_i coefficients are now the normal component of fluxes across side i. Using a weak formulation of (2.4) and introducing a further equation for imposing the continuity of normal fluxes across elements boundaries, we end up with this system of linear equations (Bergamaschi and Putti, 1999):

$$\begin{pmatrix} A & -B & C \\ B^T & 0 & 0 \\ C^T & 0 & 0 \end{pmatrix} \begin{pmatrix} \mathbf{v} \\ \mathbf{h} \\ \boldsymbol{\lambda} \end{pmatrix} = \begin{pmatrix} 0 \\ \mathbf{f} \\ \mathbf{q}_n \end{pmatrix} \tag{2.5}$$

where the elements of matrixes A, B and C are given by:

$$(a_{ik}) = \int_{T_e} K_e^{-1} \vec{w}_i^e \cdot \vec{w}_k^e \, \mathrm{d}\Delta \qquad (b_i) = \int_{T_e} \nabla \cdot \vec{w}_i^e \, \mathrm{d}\Delta$$
$$(c_{rj}) = \int_{\Gamma^e} \mu_j \vec{w}_{ie} \cdot \vec{n}_e \, \mathrm{d}\Gamma \qquad (f_i) = \int_{T_e} f^e \, \mathrm{d}\Delta$$

with in case of triangular elements $i, k = 1, 2, 3$, $j = 1, \ldots, l$, $r = 4(p-1) + i$ and $\mathbf{h} = (h_e)$, $\boldsymbol{\lambda} = (\lambda_j)$, l is the number of element sides over the entire mesh. The source term vector is defined by $\mathbf{q}_n = (q_{nj})$ where q_{nj} assumes non zero values only in correspondence to boundaries with non zero Neumann boundary conditions. The vector $\vec{n}_{ej}$ represents the outward normal vector for side j of element e. Taking advantage of the properties of matrixes A, B and C it is possible to transform the linear system (2.5) in an equivalent one which unknowns are the lagrange multipliers λ_i defined on the elements sides. The new system of equations resulting from this procedure is symmetric and positive definite, and hence is efficiently solved by means of the preconditioned conjugate gradient iterative scheme.

For a two dimensional field the number of elements sides is roughly 1.5 times the number of nodes, and this lead to a system of equations with a larger number of unknowns than for the classical Galerkin method, with obvious computational disadvantages. The theoretical convergence rate for the scheme is quadratic for all the unknowns, under the same assumptions reported for the Galerkin schemes.

2.3 Convergence Properties Analysis

2.3.1 Some Theoretical Considerations

The choice of linear shape functions to be employed in the standard Galerkin scheme guarantees the existence of a maximum principle in the numerical discretisation (see e.g. Forsyth (1991) and Putti and Cordes (1998)). It is possible to demonstrate that the

Galerkin approximation is equivalent to imposing the mass continuity over a control volume which is not coincident with the element but with the so called *Voronoi* cell, which may be found by duality from a *Delaunay* triangulation (see figure (2.1) for a schematic representation of the Voronoi cell for a mesh made of regular triangular elements). The internodal numerical fluxes may then be interpreted as first order approximations of the flux based on the arithmetic mean of the hydraulic conductivity of the two adjacent elements related to the considered internodal segment. As a consequence the local mass balance over the single element is not always satisfied since the scheme is not imposing it, instead it is satisfied over each of the Voronoi cells. This lead to the satisfaction of the tangential law of refraction of streamlines, while the normal law is not satisfied.

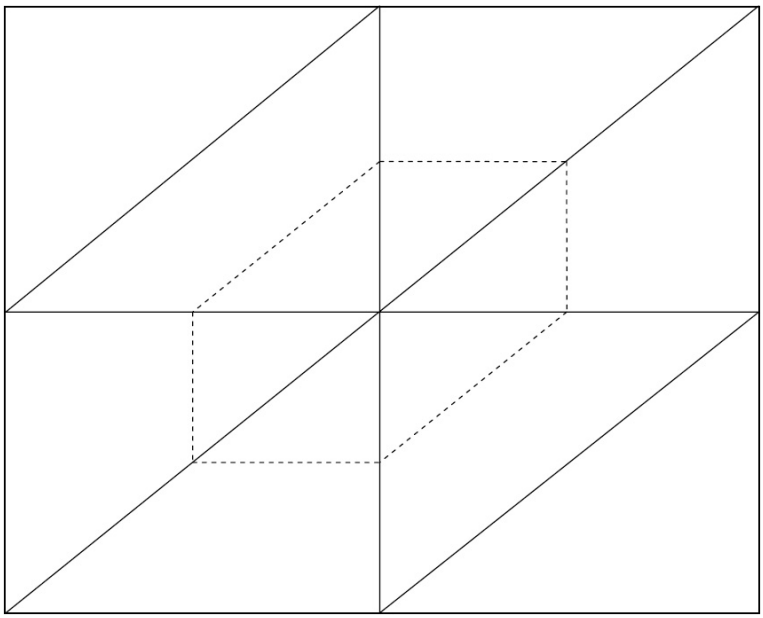

Figure 2.1: Mass balance control volume for CG scheme also referred to as Voronoi cell

In the mixed finite elements formulation the mass balance is explicitly imposed over control volumes that coincide with the elements composing the triangulation. The unknown piezometric heads are evaluated in the barycenter and in the sides midpoint of each element (Lagrange multipliers). It is possible to demonstrate that the numerical fluxes defined on each element side may be evaluated from the piezometric heads defined on the barycenter of the two adjacent elements by employing the harmonic mean of their hydraulic conductivities. The result of this is the fulfillment of the normal refraction law but not the tangential one. Furthermore, since four interconnected piezometric unknowns are defined on each element, we may find a plane passing through them all, and which slope is the approximation for ∇h over the cell, and from that we may evaluate the local velocity field, which is intrinsically conservative.

2.3.2 Convergence Rate of The Schemes for Some Test Cases

The verification of the accuracy of numerically evaluated flow fields is still an open task for research. The theoretical accuracy estimations which are based on strong assumptions such as regularity of the analytical solution and of the field coefficients (i.e. the hydraulic conductivity in our case), provide information for asymptotic conditions, that means for elements dimensions tending to zero. In real applications it is though important to achieve an extensive experimental analysis of the theoretical convergence properties for the cases where such assumptions are not valid anymore. In this section we deal with this problem by analyzing some simple analytical cases where though the hydraulic conductivity parameter shows significant variations within the considered domain.

In order to accomplish this preliminary study the method to be used is the comparison between the numerical solutions obtained with the four schemes and the analytical solution obtained with the "a-priori" technique, where the potential field is preliminarily imposed and applied to equation (2.1) from which then it is possible to infer the related external forcing field f (see for some applications Arbogast et al. (2000) and Wheeler et al. (2002)).

It is a common practice to quantify the convergence of the numerical solution towards the analytical solution by evaluating the Euclidean norm of their difference as:

$$\|e_\ell\|_2 = \sqrt{\frac{\sum_{k=1}^{N}(\delta_{k,\ell} - \delta_k)^2}{N}} \tag{2.6}$$

with $\delta = h, v$ where for instance $h_{k,\ell}$ is the numerical piezometric head value for node k and mesh refinement level ℓ, h_k is the analytical solution in the same position of node k and N is the total number of nodes in the mesh. To evaluate the convergence order p of the numerical schemes the Euclidean norm in (2.6) has been evaluated for both piezometric fields and velocity fields over structured grids in a refinement framework. For convenience at each refinement level ℓ the elements of the grid were half size the ones of the previous refinement level. In this way each refinement level comprises all the node of the previous one. The convergence order is then given by the $\log_2$ of the ratio between the two Euclidean norm of the error of two subsequent levels.

All the convergence tests analyzed in this work are based on squared domains subdivided with a structured grid obtained by first dividing the domain into squares which are further divided into triangles. Starting from a zero refinement level composed of $10 \times 10 \times 2$ triangles, at each refinement the size of the elements side is halved, then level $\ell = 1$ is composed of $20 \times 20 \times 2$ triangles and so on. Six refinement levels are studied, the last one is composed of $320 \times 320 \times 2$ elements. The number of nodes within each refinement level depends on which scheme we are treating, for instance if we are considering the Galerkin scheme applied to equation (2.1) for $\ell = 0$ we have 11×11 nodes, while for the MH scheme we have 320 nodes. Three test cases are now reported, the first one refers to a homogenous

domain, the second refers to a heterogeneous domain with smooth solution and the third refers to a heterogeneous domain with non-smooth solution.

Convergence Application Tests

Test Case 1 In this example the convergence rate analysis over a homogeneous hydraulic conductivity field is done. Only three of the four schemes are tested here since the method of Zhou is exactly equivalent to the scheme of Yeh, because of the absence of material interfaces. The objective of this test is to check the correctness of the codes by comparing the theoretical convergence rates with the numerical ones which should match. The domain is reported in figure (2.2) where the imposed analytical solution is:

$$h(x, y) = 6x^2y^2 - x^4 - y^4 \tag{2.7}$$

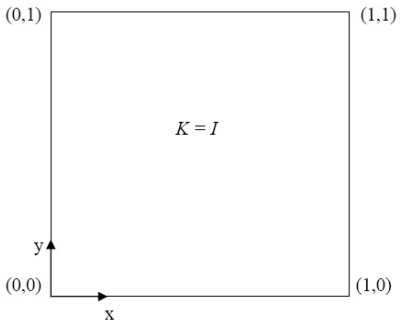

Figure 2.2: Homogeneous domain for test case 1 with unitary hydraulic conductivity.

By applying into equation (2.1) this analytical solution we can infer the related forcing field f, while the *Dirichlet* boundary conditions are evincible directly from expression (2.7) for all the domain contour by fixing opportunely x or y with their boundary values.

The hydraulic conductivity for this test case is set equal to the identity matrix ($\mathbf{I}$) which means isotropic unitary values.

The resulting convergence rates for the piezometric heads for the Galerkin based methods and the mixed hybrid one are reported in table (2.1), the statistics of the former ones are taken for the nodal piezometric heads while for the mixed case the elements barycenter piezometric unknowns are used.

As expected the rate of convergence for the piezometric head is quadratic for both methods since the solution and the parameter field are smooth and hence satisfy all the theoretical convergence rate assumptions. The same convergence rate has been observed for element sides fluxes evaluated with MH.

Furthermore in table (2.2) the convergence rate for the module of the elements barycenter velocities are reported, and the same convergence rate has been observed for single velocity components (i.e. v_x and v_y).

In this case the method of Yeh shows a better behavior by accomplishing the theoretical rate of 3/2 which has been observed also for nodal velocities. So far it seems that this

ℓ	SG	MH
0	$1.49 \cdot 10^{-03}$	$6.22 \cdot 10^{-03}$
1	$3.92 \cdot 10^{-04}$	$1.60 \cdot 10^{-03}$
2	$1.01 \cdot 10^{-04}$	$4.04 \cdot 10^{-04}$
3	$2.55 \cdot 10^{-05}$	$1.01 \cdot 10^{-04}$
4	$6.41 \cdot 10^{-06}$	$2.53 \cdot 10^{-05}$
5	$1.66 \cdot 10^{-06}$	$6.30 \cdot 10^{-06}$
p	2	2

Table 2.1: Euclidean norm for 6 refinement levels and convergence rate for piezometric heads evaluated with the standard Galerkin SG and the mixed hybrid MH schemes in test case 1.

ℓ	CG	YEH	MH
0	$2.31 \cdot 10^{-01}$	$1.11 \cdot 10^{-01}$	$2.91 \cdot 10^{-01}$
1	$1.15 \cdot 10^{-01}$	$3.72 \cdot 10^{-02}$	$1.51 \cdot 10^{-01}$
2	$5.76 \cdot 10^{-02}$	$1.25 \cdot 10^{-02}$	$7.69 \cdot 10^{-02}$
3	$2.88 \cdot 10^{-02}$	$4.31 \cdot 10^{-03}$	$3.88 \cdot 10^{-02}$
4	$1.44 \cdot 10^{-02}$	$1.49 \cdot 10^{-03}$	$1.94 \cdot 10^{-02}$
5	$7.20 \cdot 10^{-03}$	$5.25 \cdot 10^{-04}$	$9.76 \cdot 10^{-03}$
p	1	3/2	1

Table 2.2: Euclidean norm for 6 refinement levels and convergence rate for the module of velocity evaluated with the classical Galerkin CG, Yeh and the mixed hybrid MH schemes for test case 1.

method brings a great improvement to the Galerkin based family, and this is to be imputed to the fact that this scheme leads to a velocity field that is continuous everywhere as is for the analytical solution. In fact this aspect in the particular case of homogeneity implies the respect of the refraction laws of streamlines everywhere, while this is not true for the other two methods since they lead to discontinuous flow field.

Test Case 2 Here the case of a heterogeneous field with smooth analytical solution, which means that the real solution exhibits zero tangential velocity components along material interfaces, while the normal component is nonzero. Figure (2.3) shows the layout of the conductivity distribution.

The analytical solution imposed in this test is as follows:

$$h(x,y) = \frac{1}{k(x,y)} \sin(\pi(x-2)^2) \sin(\pi(y-2)^2) \tag{2.8}$$

where $k(x,y)$ assumes the scalar value of the permeability associated with the block in which the coordinates (x,y) are located.

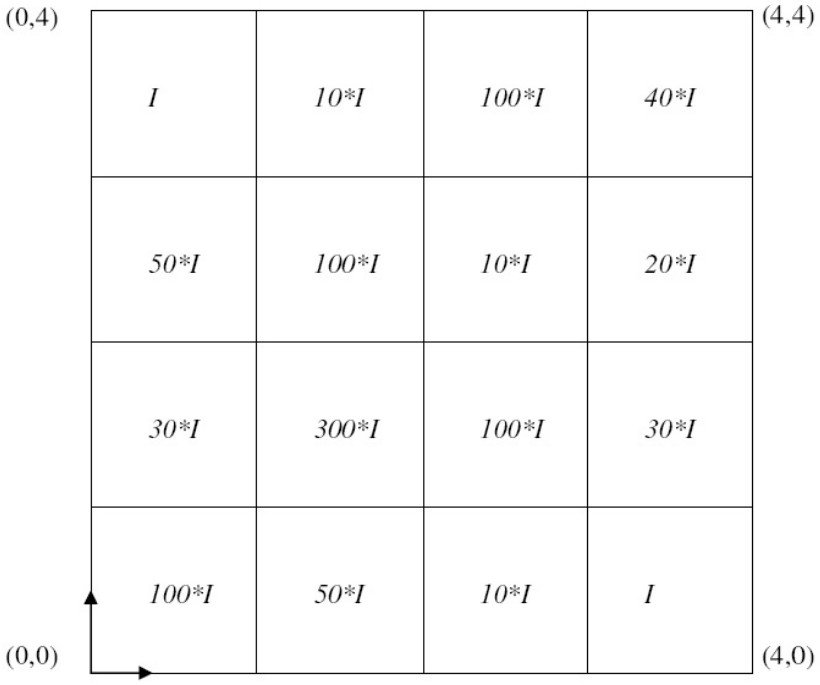

Figure 2.3: Heterogeneous domain for test case 2, all the blocks report a conductivity value which is proportional to the unitary one (**I**).

The results for the piezometric convergence rate are reported in table (2.3), because of the conductivity layout only the higher refinement levels have been evaluated and for computational reasons no further levels have been considered. This aspect may imply that we are not yet in asymptotic conditions and the convergence rate may be not yet stabilized.

For the piezometric heads the convergence is though stabilized and the quadratic rate is satisfied even if the field is heterogeneous. Things are almost the same for the convergence

ℓ	SG	MH
0	–	–
1	–	–
2	$1.53 \cdot 10^{-02}$	$6.47 \cdot 10^{-03}$
3	$3.73 \cdot 10^{-03}$	$1.55 \cdot 10^{-03}$
4	$9.31 \cdot 10^{-04}$	$3.83 \cdot 10^{-04}$
5	$2.33 \cdot 10^{-04}$	$9.54 \cdot 10^{-05}$
p	2	2

Table 2.3: Euclidean norm for the 4 higher refinement levels and convergence rate for piezometric heads evaluated with the standard Galerkin SG and the mixed hybrid MH schemes in test case 2.

ℓ	CG	YEH	ZB	MH
0	–	–	–	–
1	–	–	–	–
2	$1.17 \cdot 10^{-00}$	$5.82 \cdot 10^{-01}$	$5.65 \cdot 10^{-01}$	$5.53 \cdot 10^{-00}$
3	$5.77 \cdot 10^{-01}$	$1.57 \cdot 10^{-01}$	$1.59 \cdot 10^{-01}$	$2.13 \cdot 10^{-00}$
4	$2.91 \cdot 10^{-01}$	$4.52 \cdot 10^{-02}$	$4.69 \cdot 10^{-02}$	$8.11 \cdot 10^{-01}$
5	$1.45 \cdot 10^{-01}$	$1.38 \cdot 10^{-02}$	$1.43 \cdot 10^{-02}$	$3.19 \cdot 10^{-01}$
p	1	$> 3/2$	$> 3/2$	> 1

Table 2.4: Euclidean norm for the 4 higher refinement levels and convergence rate for the module of velocity evaluated with the classical Galerkin CG, Yeh, Zhou ZB and the mixed hybrid MH schemes for test case 2.

of the velocity fields, see table (2.4), where the convergence rates are stabilized only for CG while the other three schemes show a non stable convergence order which though tend to settle to the definite values reported in the table.

Here the solution is still smooth because no real discontinuities arise from the presence of the material interfaces, and this is reflected in the velocity convergence rates which reveal the same behavior as for the previous test case. Furthermore the application of ZB does not bring any improvement to the Yeh's solution, instead for the same mesh level this scheme shows a higher error. This aspect is probably due to the smooth character of the exact solution, and in such cases ZB introduces spurious effects in the numerical flow field where it should not.

Test Case 3 The last reported case deals with a heterogenous conductivity field with non-smooth solution, that is where the tangential velocity component along material interfaces is non-zero. A domain composed of four blocks with different hydraulic conductivity is investigated (see figure (2.4)). While in the previous heterogeneous smooth case it was relatively simple to impose an exact solution and to recover from that the forcing field, this is not so easy for this type of test cases. In order to do that we need to impose that the potential field is a continuous function which has to be not constant along material interfaces, leading to non-zero tangential velocities. In test 2 it was constant and equal to zero along such interfaces and hence with zero tangential velocities.

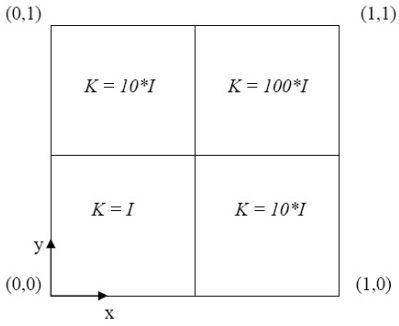

Figure 2.4: Heterogeneous domain for test case 3, all the blocks report a conductivity value which is proportional to the unitary one (**I**).

In this test the imposed solution is as follows:

$$h(x,y) = \begin{cases} sen\,(10xy) - x^3y^4 + 1 & 0 \le x,y \le 1/2, k = I \\ sen\left(10\frac{2x+9}{20}y\right) - (\frac{2x+9}{20})^3y^4 + 1 & 0 \le y \le 1/2, 1/2 \le x \le 1, k = 10I \\ sen\left(10\frac{2y+9}{20}x\right) - x^3(\frac{2y+9}{20})^4 + 1 & 0 \le x \le 1/2, 1/2 \le y \le 1, k = 10I \\ sen\left(10\frac{2x+9}{20}\frac{2y+9}{20}\right) - (\frac{2x+9}{20})^3(\frac{2y+9}{20})^4 + 1 & 1/2 \le x,y \le 1, k = 100I \end{cases}$$

The convergence results for the piezometric head are reported in table (2.5), they reveal that both numerical scheme families lose one order of convergence rate for this unknown and furthermore the MH approach seems to give better results in terms of Euclidean norm at every refinement level.

Analyzing the convergence rates for the velocity fields they highlight some interesting results (see table (2.6)). First of all the post-processing schemes which are YEH and ZB schemes lose one order of convergence rate, with ZB giving better results than the other one which means that it introduces some type of improvements to the standard YEH scheme. Second, the convergence rate for the remaining two schemes holds to the same

ℓ	SG	MH
0	$5.15 \cdot 10^{-02}$	$2.04 \cdot 10^{-02}$
1	$2.42 \cdot 10^{-02}$	$8.46 \cdot 10^{-03}$
2	$1.03 \cdot 10^{-02}$	$3.53 \cdot 10^{-03}$
3	$6.51 \cdot 10^{-03}$	$2.21 \cdot 10^{-03}$
4	$2.61 \cdot 10^{-03}$	$8.77 \cdot 10^{-04}$
5	$1.63 \cdot 10^{-03}$	$5.43 \cdot 10^{-04}$
p	1	1

Table 2.5: Euclidean norm for 6 refinement levels and convergence rate for piezometric heads evaluated with the standard Galerkin SG and the mixed hybrid MH schemes in test case 3.

values as in the previous test cases, although they are based on piezometric fields of a lower convergence rate.

ℓ	CG	YEH	ZB	MH
0	$3.84 \cdot 10^{-00}$	$3.79 \cdot 10^{-00}$	$3.26 \cdot 10^{-00}$	$4.62 \cdot 10^{-00}$
1	$1.86 \cdot 10^{-00}$	$2.77 \cdot 10^{-00}$	$1.63 \cdot 10^{-00}$	$2.45 \cdot 10^{-00}$
2	$9.27 \cdot 10^{-01}$	$1.76 \cdot 10^{-00}$	$1.02 \cdot 10^{-00}$	$1.21 \cdot 10^{-00}$
3	$4.62 \cdot 10^{-01}$	$1.20 \cdot 10^{-00}$	$5.97 \cdot 10^{-01}$	$6.05 \cdot 10^{-01}$
4	$2.32 \cdot 10^{-01}$	$8.46 \cdot 10^{-01}$	$3.37 \cdot 10^{-01}$	$3.06 \cdot 10^{-01}$
5	$1.15 \cdot 10^{-01}$	$5.95 \cdot 10^{-01}$	$2.11 \cdot 10^{-01}$	$1.51 \cdot 10^{-01}$
p	1	1/2	1/2	1

Table 2.6: Euclidean norm for 6 refinement levels and convergence rate for the module of velocity evaluated with the classical Galerkin CG, Yeh, Zhou ZB and the mixed hybrid MH schemes for test case 3.

The main result revealed by this test case concerns the robustness of the analyzed numerical schemes. It is evident that the postprocessing schemes are weaker than the other two, despite they are supposed to improve the results of the classical Galerkin scheme for the velocity field they fail to keep the theoretical convergence order. This is extremely important because it demonstrates that these postprocessing schemes are not well suited to model very heterogeneous domains, and hence real porous media flow where the hydraulic conductivity parameter is highly variable. Therefore this aspect reveals the higher strength of the classical schemes CG and MH. Although not reported a few of further heterogeneous test cases have been done and they show convergence results in line with the exposed ones, revealing the same behavior of the models.

For this reason in the stochastic analysis of the numerical schemes applied to highly heterogeneous porous media the attention will focus on these two schemes.

2.4 Stochastic Analysis of The Numerical Solutions

The convergence analysis achieved in the first part of this chapter highlighted some particular features of the analyzed numerical schemes, in particular it demonstrated how CG and MH are considerably more robust than ZB and YEH. However, the findings that the observed error convergence rates for the former two methods are the same for both and do not change as the field parameters heterogeneity increases is not sufficient to demonstrate the equivalence of their accuracy.

The two methods have indeed a very different structure, the control volume over which they impose the flux balance is not the same since CG refers to the Voronoi cell while MH refers to the element itself. This aspect is particularly relevant for the conservation of the refraction laws of streamlines between two material interfaces, in fact the CG structure leads to the conservation of the tangential refraction law while the MH structure leads to the conservation of the normal flux. This difference may have serious drawbacks when the hydraulic conductivity field is very heterogeneous, that is when the geostatistical model for such parameter assigns to each element a different conductivity value. It is then imperative to analyze deeply the influence of the models structure on their solution over very heterogeneous fields. In order to accomplish this task one possible way is to examine the stochastic characteristics of the velocity fields obtained with the two numerical schemes hoping it would be helpful for underlining their differences.

2.4.1 Synthetic Experiments Setup

According to sites data, gathered over experimental fields, the function $Y = lnT$, in which T is the hydraulic transmissivity of a porous formation, may be modeled with a spatial random function SRF normally distributed with mean $<Y>$ and variance σ_y^2 which are constant. Moreover the spatial variability of Y is describable with the following geostatistical model (Rubin, 2003, chap. 1):

$$C_Y(r) = \langle [Y(\vec{x}) - \langle Y \rangle] [Y(\vec{x} + \vec{r}) - \langle Y \rangle] \rangle = \sigma_Y^2 e^{-r/I_Y} \tag{2.9}$$

in which $\vec{x} = (x_1, x_2)$ is the position vector in the plane, $r = \sqrt{r_1^2 + r_2^2}$ is the distance between the two point respect of which the covariance value C_Y is evaluated and I_Y is the horizontal integral scale of variability.

The stochastic properties of flow fields have been evaluated within a Monte Carlo framework in which 1500 realizations of $T = e^Y$ obtained with the spatially distributed random field generator for correlated properties developed by Bellin and Rubin (1996) have been solved for flow with both CG and MH. The computational domain is a square with dimensions $40I_Y \times 40I_Y$ divided into squared cells of dimensions $0.25I_Y \times 0.25I_Y$. Each cell is then divided into two triangles. The resulting grid is of a Delaunay type and for

linear shape functions for the finite elements methods it respect the maximum principle as required in Forsyth (1991) and Putti and Cordes (1998). A value for Y, and then for T, is generated for each square cell and so assigned to both the triangular elements defined in its inside. The imposed boundary conditions are a unitary constant gradient in the longitudinal direction, that is Dirichlet boundary conditions of constant piezometric heads at lateral sides in $x_1 = 0$ and $x_1 = 40I_Y$, and Neumann boundary condition of zero flux across the remaining two sides of the domain ($x_2 = 0$ and $x_2 = 40I_Y$). Equations (2.1) and (1.15) have been solved in their non-dimensional form obtained by scaling distances respect to I_Y, piezometric head respect to JI_Y, in which J is the mean gradient imposed by the boundary conditions, and velocity respect to its mean stochastic value that is $U =< \vec{v} >= (T_G J/n)$, in which $T_G = e^{<Y>}$ is the geometric mean of the transmissivity. The stochastic analysis of the covariance functions have been done by sampling the flow velocity over a regular squared grid of cells dimensions of $0.25I_Y$ with the position of the nodes of the grid coincident with the barycenter of the upper triangular element of the computational cells.

Simulations of transport has been achieved by injecting contemporarily 160 particles aligned regularly over a vertical segment of origin $(6I_Y, 10I_Y)$ and length $10I_Y$. Their movement has been simulated by means of the particle tracking technique using the following equations:

$$X_1(t) = X_1(t - \Delta t) + v_1 \left[(X_1(t), X_2(t))\right] \Delta t \tag{2.10}$$

$$X_2(t) = X_2(t - \Delta t) + v_2 \left[(X_1(t), X_2(t))\right] \Delta t \tag{2.11}$$

in which X_i is the i^{th} component of the particle trajectory and Δt is the time step used for trajectory calculation. Δt has been chosen in a way that each particle step is shorter than the elements size of $0.25I_Y$, in particular we searched for the maximum velocity module numerically obtained over the domain and Δt has been set equal to $0.25I_Y/V_{max}$. Furthermore when the particle crosses the boundary between two adjacent elements within a time step (that is for the most of the cases), its movement has been modeled by dividing the time step into two contribution. The first one is used for the movement within the starting element and the second one for the movement within the arriving element. Obviously the velocities used for this two step movement are not the same, but refer to the element in which the particle is currently positioned.

At each time step the spatial moments of the particle plume have been calculated and compared to analytical expressions of first order accuracy in $[\sigma_Y^2]$ taken from the literature (Dagan (1989)). The stochastic analysis has been accomplished for four cases of different conductivity variance, that is for $\sigma_Y^2 = 0.2$, 1, 2 and 4.

2.4.2 Analysis of the Covariance Functions of the Velocity Fields

The structure of a flow field may be synthetically described by the longitudinal, u_{11} and transversal, u_{22} covariance functions of its velocity components. Figures (2.5a) and (2.5b) show respectively $u'_{11} = u_{11}/(U^2\sigma_Y^2)$ and $u'_{22} = u_{22}/(U^2\sigma_Y^2)$ for $\sigma_Y^2 = 0.2$. The same quantities for $\sigma_Y^2 = 1, \quad 2, \quad 4$ are reported in figures (2.6a,b), (2.7a,b) and (2.8a,b). It is important to notice that for allowing the correct comparison of the numerical solution with the covariance functions they have been reported in dimensionless form obtained by dividing them with $U^2\sigma_Y^2$, so that the first order analytical solutions proposed by Rubin (1990) are independent of σ_Y^2. In each figure it is shown the covariance functions trend with respect to two aligned point in the longitudinal ($\vec{r} = (r, 0)$) and transversal ($\vec{r} = (0, r)$) directions. In all cases the velocity field statistics have been evaluated taking into account of an internal subregion obtained by neglecting the outer part of the domain for a thickness of $5I_Y$.

From a first analysis of the results we can see in figure (2.5a) that for $r > 0$ the numerical covariance functions are in perfect accordance with the analytical solution of order $O[\sigma_Y^2]$, at least for $\sigma_Y^2 = 0.2$. However for $r = 0$ the numerical values reveal a significant difference between each other and with the analytical solution. In particular the variance of the velocity component $v_1 = u_{11}(0, 0)$ evaluated with CG is greater than the one evaluated with MH which instead seems to be in good agreement with the first order theory for which, according to Rubin (1990), $u_{11}(0, 0) = 3\sigma_Y^2/8$. We also observe that this gap increases as the conductivity field variance σ_Y^2 increases as we can see in figure (2.6a) for $\sigma_Y^2 = 1$, (2.7a) for $\sigma_Y^2 = 2$ and (2.8a) for $\sigma_Y^2 = 4$. This is obvious if we think that for $\sigma_Y^2 << 1$ the first order theory and the numerical solutions differ a very little from the exact solution, while for variances greater than 1 the solution of order $O[\sigma_Y^2]$ is not valid anymore.

Looking at the values of $v_2 = u_{11}(0, 0)$ we can notice that for weakly heterogeneous fields ($\sigma_Y^2 = 0.2$) the difference between the first order solution and both the numerical ones is almost zero (see figure (2.5b)). For higher conductivity variances we notice that both numerical schemes overestimate the first order solution and diverge from each other as shown in figure (2.6b) for $\sigma_Y^2 = 1$, 2.7b) for $\sigma_Y^2 = 2$ and 2.8b) for $\sigma_Y^2 = 4$.

Furthermore if we compare the values of the numerical velocity variances with second order solutions taken from Hsu et al. (1996) and Hsu and Neuman (1997)(see table 2.7) we see a specular behavior of the two numerical schemes. In fact, for $u'_{11}(0, 0)$ we see that the analytical solution stays between the two numerical ones, while lower differences are shown for $u'_{22}(0, 0)$ (see figure (2.5b)) where both methods underestimate the analytical value and it is evident a better performance of CG as reported also in Hsu et al. (1996). As for the first order case this behavior is emphasized with increasing conductivity variance σ_Y^2.

		σ_Y^2		
		0.2	1	2
$u'_{11}(0,0)$	GC	0.432	0.479	0.536
	MH	0.348	0.352	0.358
	$O[(\sigma_Y^2)^2]$	-	0.407	0.451
$u'_{22}(0,0)$	GC	0.123	0.160	0.204
	MH	0.119	0.136	0.152
	$O[(\sigma_Y^2)^2]$	-	0.168	0.211

Table 2.7: Non-dimensional velocity field variances for longitudinal ($u'_{11}(0,0)$) and transversal ($u'_{22}(0,0)$) components. Second-order analytical values reported in Hsu et al. (1996)

It is important to notice the opposite behavior of the two numerical schemes as field variance increases. The difference in $u'_{11}(0,0)$ tends to be more pronounced at higher σ_Y^2 where CG shows always overestimated values while MH shows underestimated values. Instead, for $u'_{22}(0,0)$ we can see that CG is in good accordance with the solution of order $O[(\sigma_Y^2)^2]$ also for high conductivity variances. Indeed the validity of first and second order solutions is limited for low values of σ_Y^2, nevertheless Englert et al. (2006) reports on this topic that velocity variance estimation is accurate up to $\sigma_Y^2 = 2$ for second order approximation (see also Salandin and Fiorotto (1998) and Hassan et al. (1998)) and up to $\sigma_Y^2 = 1$ for first order approximation.

From these results it is evident that the numerical flow fields obtained with CG show a higher heterogeneity level which are in accordance with second order solutions, while MH tends to limit the velocity fields variance. A particular aspect of MH is that the normalized variance of its longitudinal velocity component is almost constant as the conductivity field variance increases as reported in table (2.7), while this is not the case for the transverse velocity component. Furthermore this latter method exhibits velocity variances in good accordance with the first order solutions, therefore it seems that it introduces some type of linearization effect in its velocity fields. The explanation for this opposite behavior of the two numerical schemes is not trivial, some speculations on that are reported in next section.

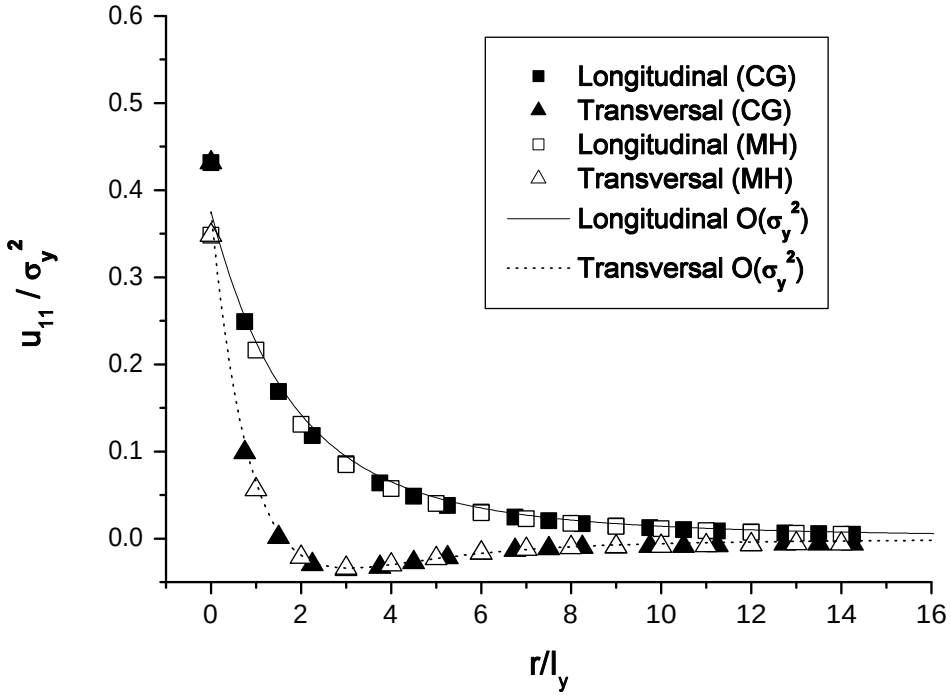

(a)

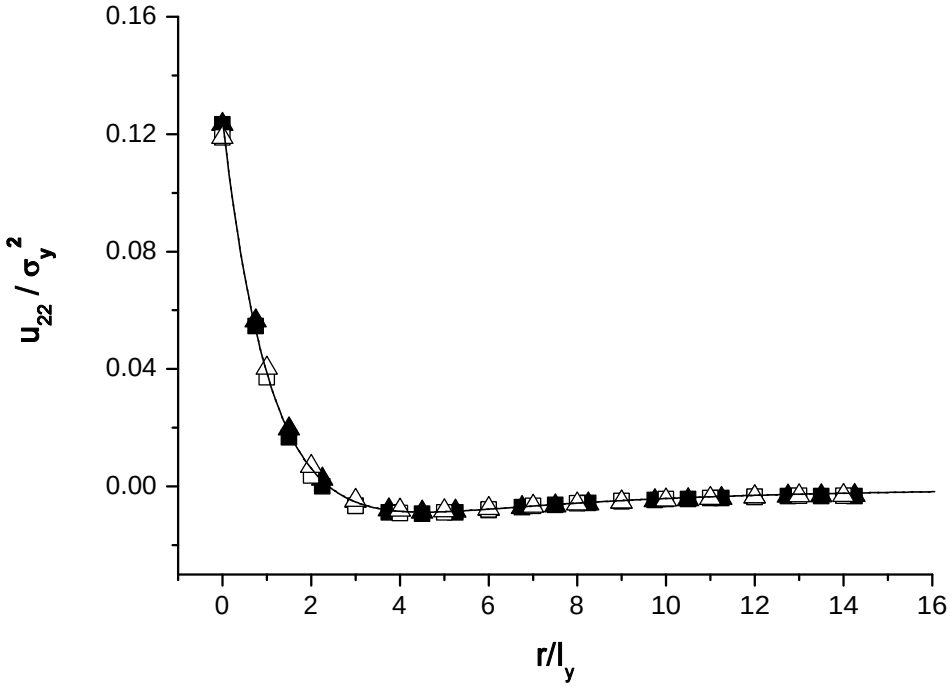

(b)

Figure 2.5: Comparison between first order analytical solution according to Rubin (1990) and numerical longitudinal (a)u_{11}) and transversal (b)u_{22}) velocity covariance functions for $\sigma_Y^2 = 0.2$.

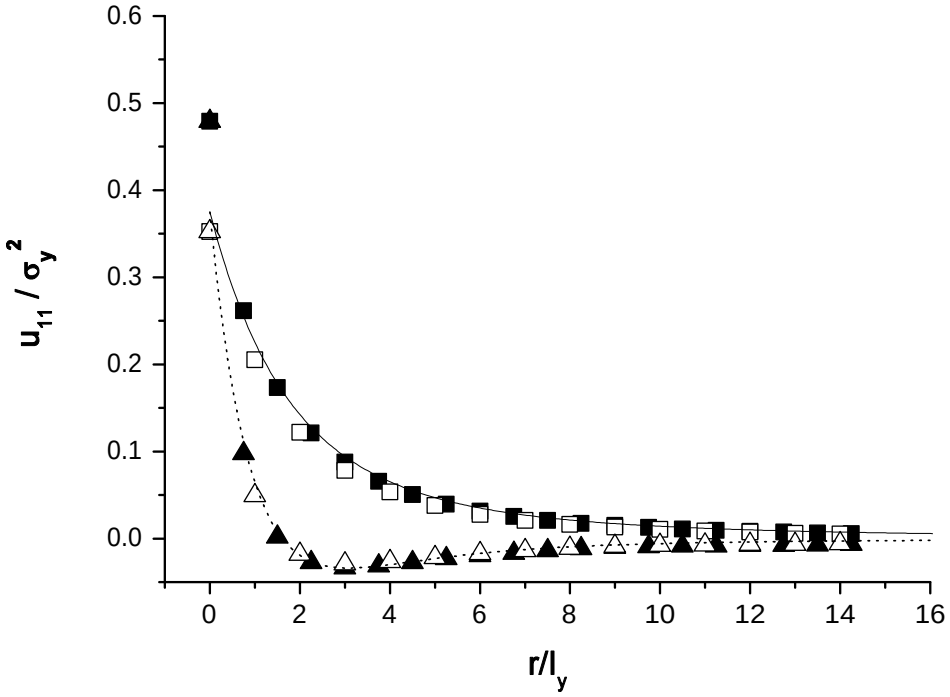

(a)

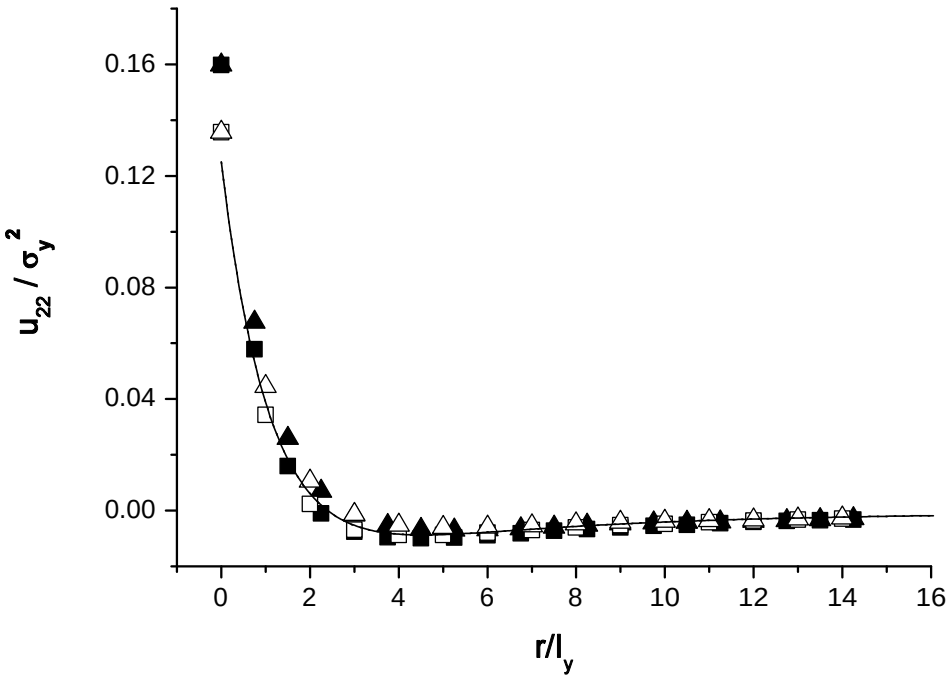

(b)

Figure 2.6: Comparison between first order analytical solution according to Rubin (1990) and numerical longitudinal (a)u_{11}) and transversal (b)u_{22}) velocity covariance functions for $\sigma_Y^2 = 1$.

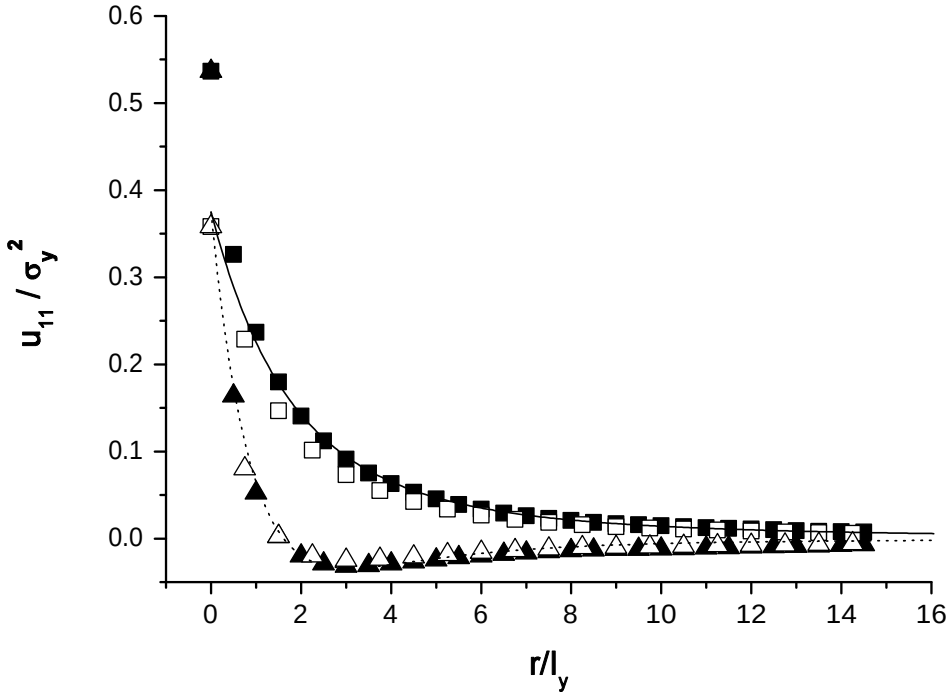

(a)

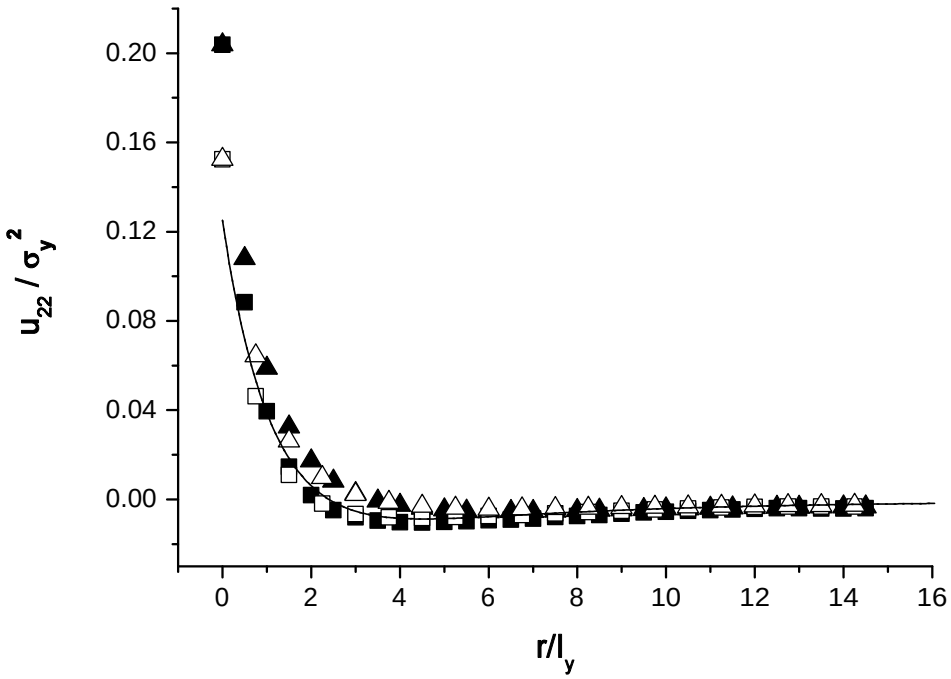

(b)

Figure 2.7: Comparison between first order analytical solution according to Rubin (1990) and numerical longitudinal (a)u_{11}) and transversal (b)u_{22}) velocity covariance functions for $\sigma_Y^2 = 2$.

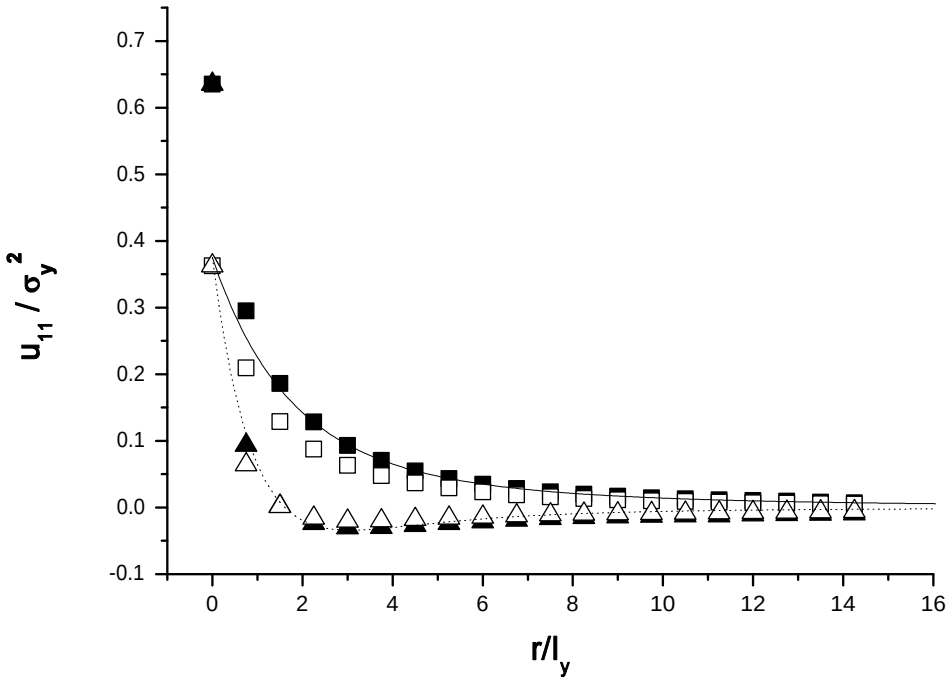

(a)

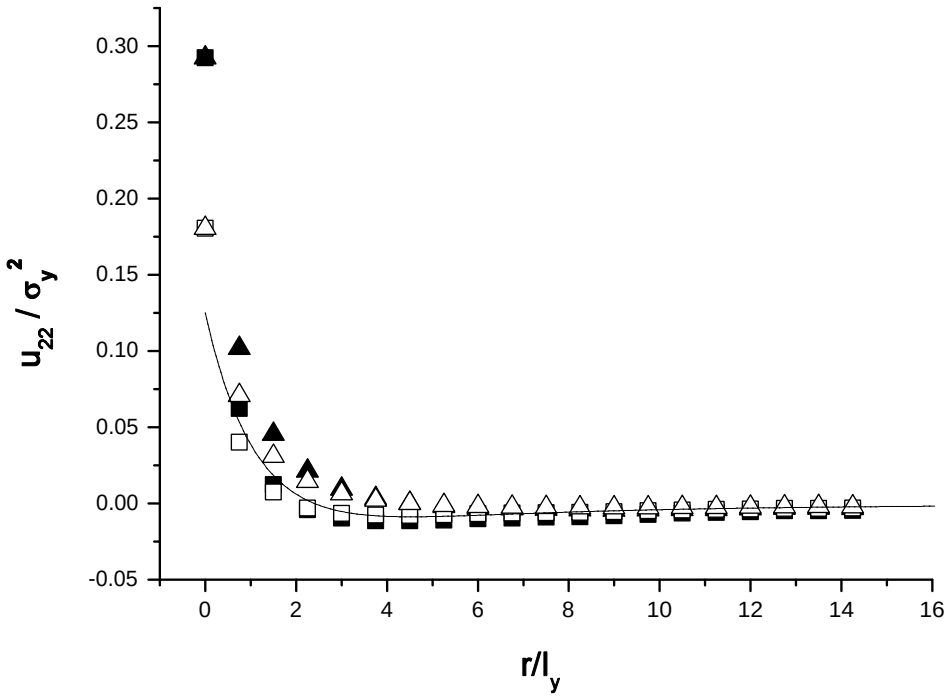

(b)

Figure 2.8: Comparison between first order analytical solution according to Rubin (1990) and numerical longitudinal (a)u_{11}) and transversal (b)u_{22}) velocity covariance functions for $\sigma_Y^2 = 4$.

2.4.3 Numerical Schemes Structure and The Conductivity Field

An important aspect arisen in the previous section is the different heterogeneous character of the flow fields evaluated with the two numerical methods, CG and MH. The synthetic experiments highlighted an important difference between these two schemes. The target now is to find an explanation for that, and possibly to highlight the innate weaknesses of the methods. Indeed this is not an easy task, also because we cannot assert which of them reflects better the analytical behavior for the limited range of validity of the first and second order solutions, on which basis we made the reported comparisons. Yet we can make our own conjectures and speculations.

We started by analyzing the structure of both schemes in order to understand what they are actually doing. According to Putti and Cordes (1996) and Cordes and Kizelbach (1996) the mixed finite element formulation is equivalent to the simple finite volume formulation under the assumption of sources/sinks absence, in which the mass balance is achieved for a control volume coincident with the element itself. In figure (2.9a) it is shown the flux balance across elements interfaces, for this particular case the piezometric unknown defined in the circum-center of the element coincides with the Lagrange multiplier positioned in the midpoint of the triangle hypotenuse ($H_0 = \lambda_0$). On the other hand the Galerkin scheme is equivalent to imposing flux balance across the so called Voronoi cell, which for a regular mesh is as reported in figure (2.1). It is simple to verify this latter conjecture by writing in expanded form the Galerkin equation for the node within the Voronoi cell to see that it is perfectly coincident with writing directly the flow balance for such control volume. Furthermore since flow balance is verified for each subarea within a single element the Voronoi control volume is extensible to the squared control volume reported in figure (2.9b), which for usefulness will be called the extended Voronoi cell.

These two are the control volume structures for the two numerical schemes. The problem is what do they imply on the accuracy of the numerical solution of the flow field over a heterogeneous conductivity domain. We speculate that the way a scheme employs the elemental conductivity values within its water balance equations defined over the control volume exerts a crucial role in affecting the variability character of the resulting flow field. In the mixed scheme, in order to impose water balance over the control volume of figure (2.9a), that is the central squared element, we need to approximate the intercell fluxes for each element side as a function of the harmonic mean of the hydraulic conductivities of the elements connected with that side. The global balance will then be the sum of the so defined fluxes. On the other hand if we do the same analysis for the Galerkin approach and write the balance fluxes on the basis of figure (2.9b), we see that in order to impose water balance on the extended Voronoi cell we need to approximate the intercell fluxes as a function of the arithmetic mean of the conductivities of the two elements crossing each of the extended Voronoi cell sides.

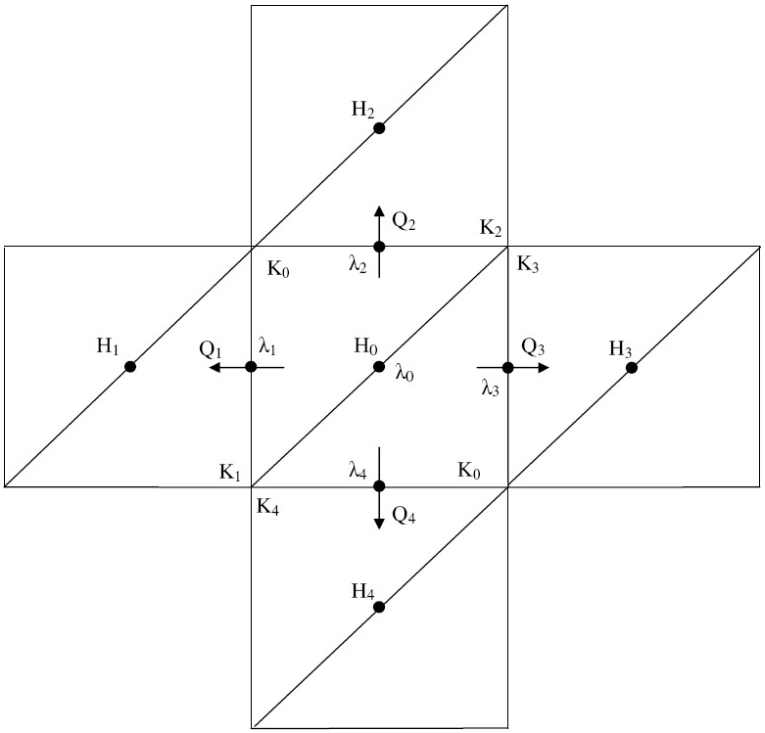

(a)

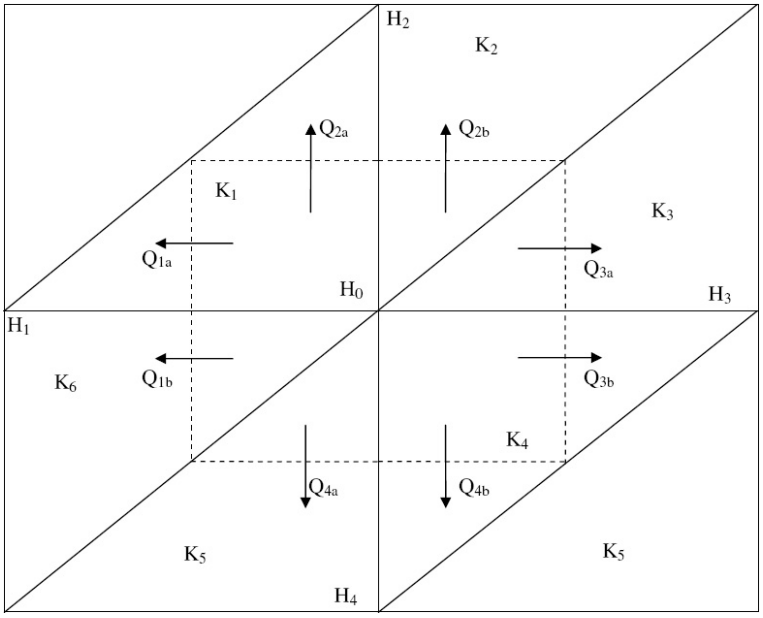

(b)

Figure 2.9: Flux balance for (a) MH over a squared control volume coincident with two triangular elements (Cordes and Kizelbach, 1996) and (b) CG over the extended Voronoi cell.

For instance Q_{1a} and Q_{1b} may be formulated as a single flux through the whole left side of the extended Voronoi cell, in which the hydraulic conductivity is the arithmetic mean of K_1 and K_6, and with a corresponding gradient equal to $H_0 - H_1$. Moreover it is easy to check that along the Voronoi cell sides the refraction laws of streamlines are totally respected, considering that they do not coincide with any material interface and that the flow field is constant within each element.

However the considerations reported so far put in evidence that both schemes do not employ the values of the real conductivity field in imposing the fluxes balance over the relative control volume. MH employs the local harmonic mean and CG employs the local arithmetic mean of the real conductivity values. Then we can say that each scheme are not solving the flow over the generated conductivity field but over a modified one. For MH the modified field is composed by the set of the harmonic mean of the conductivity values defined locally over each element side within the domain. Instead CG lead to a modified conductivity field which values are the local arithmetic mean of the conductivity values connected to each node in the domain.

Upon these objections we may now compare the modified conductivity fields statistics with those of the original field. In order to accomplish this task we generated one conductivity field for each of the considered field variances (0.2, 1, 2 and 4). The field dimensions were $100I_Y \times 100I_Y$ with grid spacing of $0.25I_Y$. For each of these fields we compared the cumulative density function (CDF) of the conductivity values with those of the modified fields. Figure (2.10) reports the comparison of the three CDFs for each of the field variances. As you can see the curves are not coincident, for instance the CDFs of MH conductivity fields are very different compared to the real ones (RE), and this is observable for any of the considered variances. Instead the CG modified field CDFs are very close to RE ones.

As expected, since the harmonic mean gives more weight to the low values and the arithmetic one does the opposite, we can observe that this peculiarity has a strong drawback on the MH field at every variance while it seems to be negligible for CG at low field variances (see figure (2.10a)) which though tend to be emphasized as the RE field variance increases. For instance, if we look at figure (2.10d) which is relative to field variance of 4, we see that the CG CDF starts to show noticeable differences to the RE one. In table (2.8) are reported the values of mean and variance of the modified conductivity fields for the four generated cases. If our speculations are correct, we can infer that when we apply a numerical scheme to solve flux over a conductivity field we are actually solving the problem with respect to a different conductivity field with different statistical properties. For instance the use of MH leads to flow solutions for conductivity fields with roughly one fourth of the mean and the variance of the real ones, while CG tends to keep more or less the same stochastic properties of the real fields.

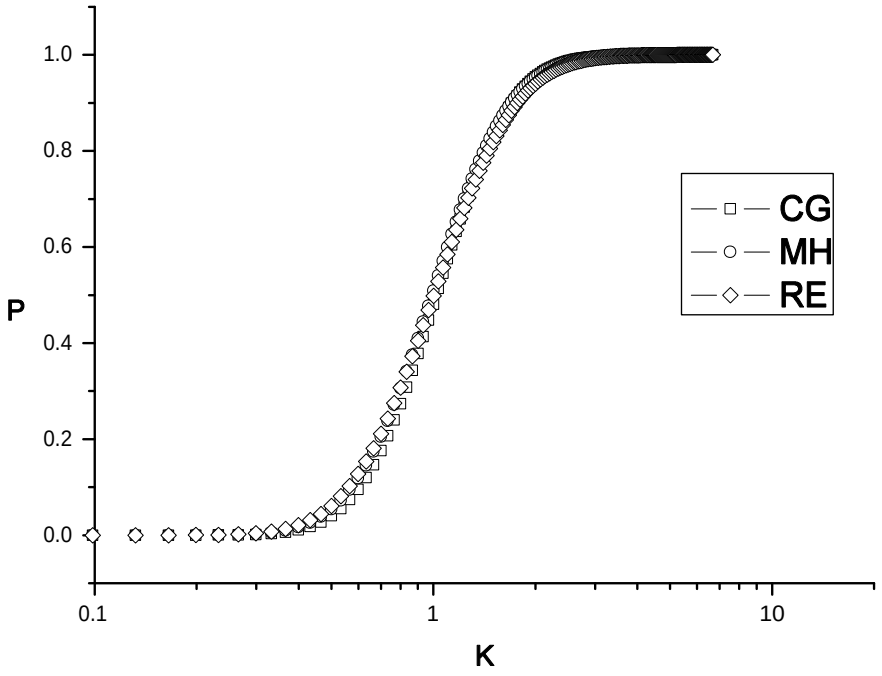

(a)

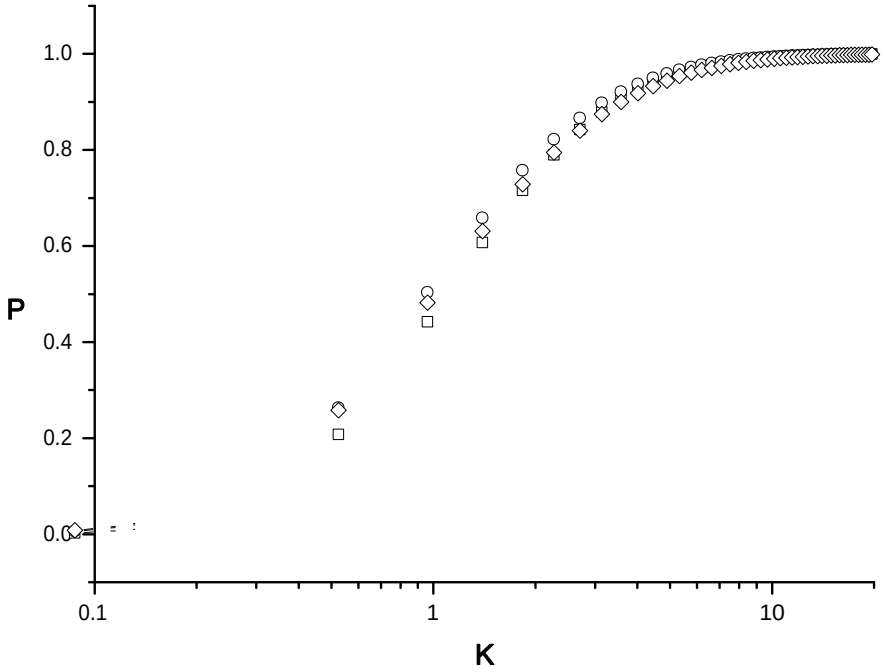

(b)

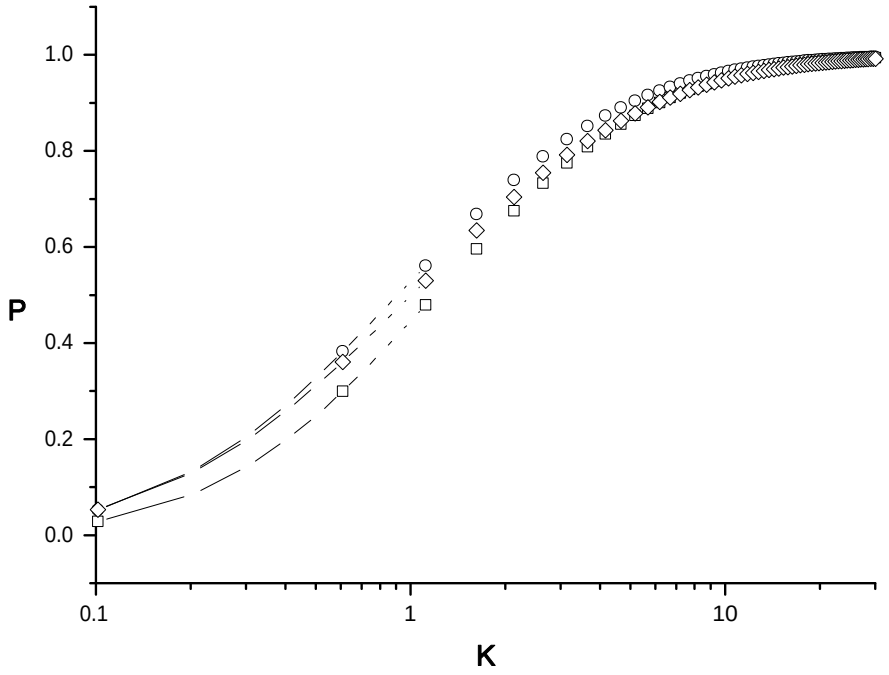

(c)

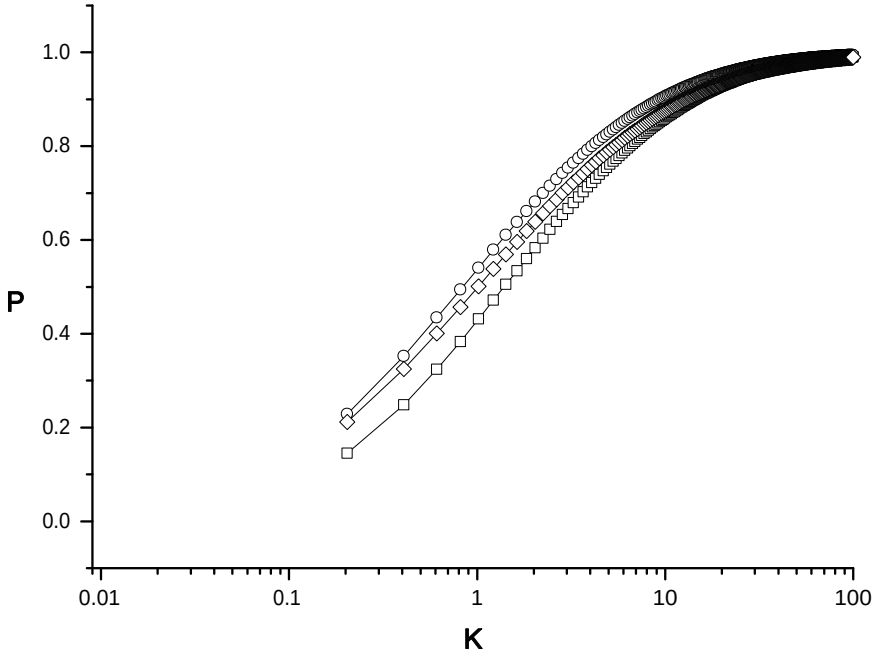

(d)

Figure 2.10: Hydraulic conductivity values CDFs of the real (RE), modified CG and MH fields for RE variances of a) 0.2, b)1, c)2 and d)4.

		σ_Y^2			
		0.2	1	2	4
$Mean$	GC	$1.10 \cdot 10^{00}$	$1.64 \cdot 10^{00}$	$2.71 \cdot 10^{00}$	$7.34 \cdot 10^{00}$
	MH	$1.08 \cdot 10^{00}$	$1.47 \cdot 10^{00}$	$2.19 \cdot 10^{00}$	$4.87 \cdot 10^{00}$
	RE	$1.10 \cdot 10^{00}$	$1.64 \cdot 10^{00}$	$2.71 \cdot 10^{00}$	$7.34 \cdot 10^{00}$
$Variance$	GC	$2.14 \cdot 10^{-01}$	$3.28 \cdot 10^{00}$	$2.65 \cdot 10^{01}$	$7.77 \cdot 10^{02}$
	MH	$2.25 \cdot 10^{-01}$	$3.03 \cdot 10^{00}$	$2.11 \cdot 10^{01}$	$4.84 \cdot 10^{02}$
	RE	$2.68 \cdot 10^{-01}$	$4.44 \cdot 10^{00}$	$3.97 \cdot 10^{01}$	$1.41 \cdot 10^{03}$

Table 2.8: Mean and variance of the real and modified conductivity fields for the four heterogeneity levels considered.

2.5 Transport Simulation by Means of The Particle Tracking Algorithm

Tracer movement within a heterogeneous flow field may be described with the first and second spatial moment of the plume evolution in time, which from a mathematical point of view for the two dimensional case are:

$$R_i(t) = \frac{1}{M}\int_\Omega x_i(t)C(\overrightarrow{x},t)d\overrightarrow{x} \qquad i = 1,2 \tag{2.12}$$

and

$$S_{ij}(t) = \frac{1}{M}\int_\Omega [x_i(t) - R_i(t)][x_j(t) - R_j(t)]C(\overrightarrow{x},t)d\overrightarrow{x} \qquad i,j = 1,2 \tag{2.13}$$

where $C(\vec{x},t)$ is the plume concentration at position $\vec{x}$ for time t, and $M = \int_\Omega C(\vec{x},t)d\vec{x}$ is the total mass of the tracer injected into the aquifer. The two first spatial moments, $R_i(t)$ for $i = 1,2$, describe the two dimensional trajectory of the plume barycenter, while the two second spatial moments, $S_{i,j}(t)$ for $i = 1,2$, provide the evolution of its momentum of inertia.

Splitting the total mass M in a number NP of particles that move independently along the trajectories evaluated with (2.10), we obtain the following approximations:

$$R_i^v(t) \simeq \frac{1}{NP}\sum_{k=1}^{NP} X_{i,k}^v(t) \qquad i = 1,2 \tag{2.14}$$

$$S_{ij}^v(t) \simeq \frac{1}{NP}\sum_{k=1}^{NP}[X_{i,k}^v - R_i^v(t)][X_{j,k}^v - R_j^v(t)] \qquad i,j = 1,2 \tag{2.15}$$

in which $X_{i,k}^v$ represents the position of particle k at time t in the v realization of the conductivity field within the MC framework. For $NP \to \infty$ it is demonstrable that (2.14) and (2.15) converge respectively to (2.12) and (2.13). It has then been fixed a proper number of particles to be used within the numerical experiments in order to achieve convergence of the statistical quantities. In other words we made the simulations with a number of particles injected within each of the 1500 independent conductivity fields of about 100, then the same has been done with 160 particles and the transport statistics were evaluated as will be explained later. From the comparison of the results we could infer that the two experiments were described with the same values of the stochastic quantities. This means that in our transport experiments the stochastic convergence was achieved.

Because of the uncertainties beneath the knowledge of the real spatial distribution of the conductivity field, the moments expressed in (2.12) and (2.13) are unknown. The stochastic approach allows to evaluate the expected values of $R_i(t)$ and $S_{i,j}(t)$, which are the best possible estimation for the real plume moments, accordingly with the knowledge

of the spatial structure of the conductivity field.

From the operative point of view one proceeds by evaluating the first and second moment approximations with equations (2.14) and (2.15) for a large number MC of realizations. The average of these sets of values are respectively the first and second effective spatial moments of the plume, which are:

$$< R_i(t) >= \frac{1}{MC} \sum_{v=1}^{MC} R_i^v(t) \qquad i = 1, 2 \tag{2.16}$$

and

$$< S_{ij}(t) >= \frac{1}{MC} \sum_{v=1}^{MC} S_{ij}^v(t) \qquad i, j = 1, 2 \tag{2.17}$$

The convergence of the moments in (2.16) and (2.17) has been obtained for a number $MC = 1500$ of independent realizations.

The numerical simulations evidenced that for low conductivity field variances (i.e. $\sigma_y^2 = 0.2$) the mean velocity of the plume, that is the average of the barycenter velocity of the plumes obtained for all the MC realizations, is constant and perfectly agrees with first order analytical solution of the mean Eulerian velocity, U, as required by the linear theory proposed by Dagan (1989) (see figure (2.11a)). However when the conductivity field variance increases we observe a reduction in the plume velocity for both numerical methods with higher emphasis for the CG one, as reported in figures (2.11b), (2.11c) and (2.11d) respectively for conductivity variances of 1, 2 and 4. The reason for this greater slowing down in the plume movement for the CG scheme is the result of its higher velocity field variance. In fact the greater variances of both longitudinal and transversal velocity components for CG solutions conduct the single particle to move along a path of higher tortuosity, often leading it to pass through low conductivity zones resulting in a slower longitudinal motion.

In figure (2.12) is reported the evolution of the velocity of the plume barycenter along the path for all the considered field variances. It is evident that the CG scheme shows a completely different behavior than MH. As soon as the particles are injected into the field, the mean of the velocities with which the particles start their motion is higher for CG, yet as the plume moves ahead this average velocity decreases significantly. On the other hand the MH method shows a fairly constant mean plume velocity along the experiments. From this aspect we evince that MH tends to channelize the particles along faster paths than CG, which on the contrary leads the particles to enter rather into slow zones than into fast ones. This may be inferred by the change of the mean barycenter velocity of the plume modeled with CG, in fact at the beginning the particles mean velocity is high and suddenly decreases as if they were conveyed from initial fast paths into slow ones.

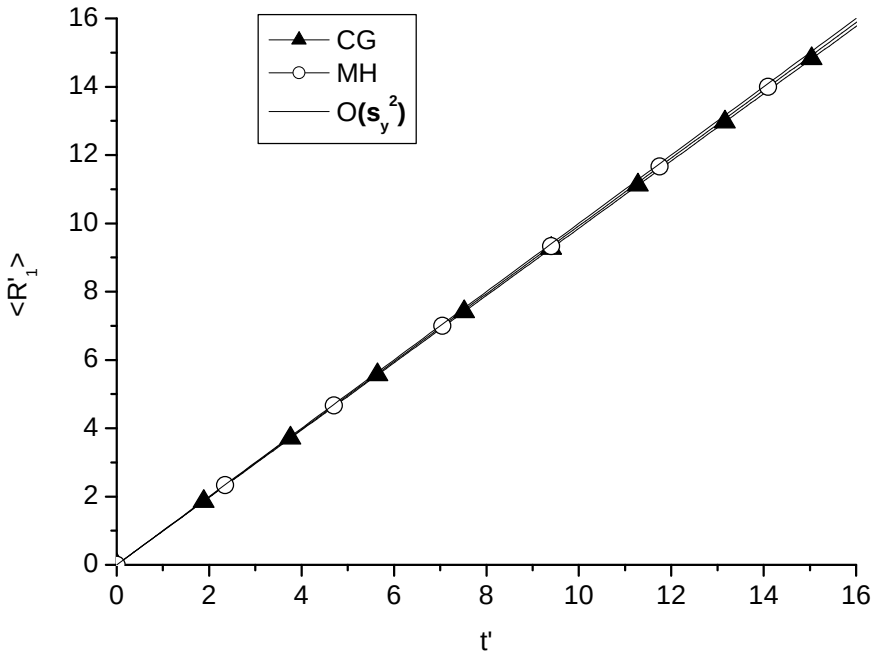

(a)

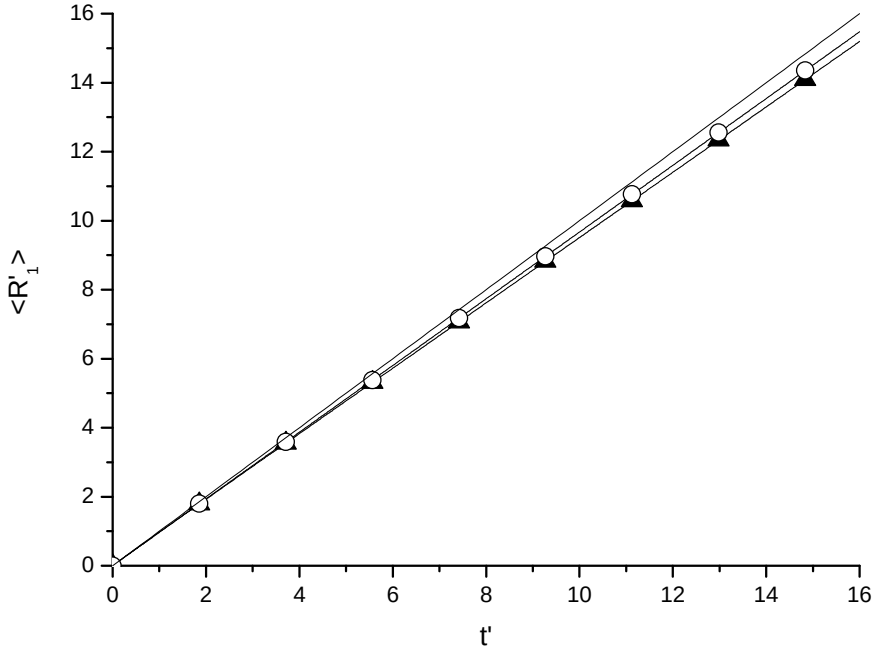

(b)

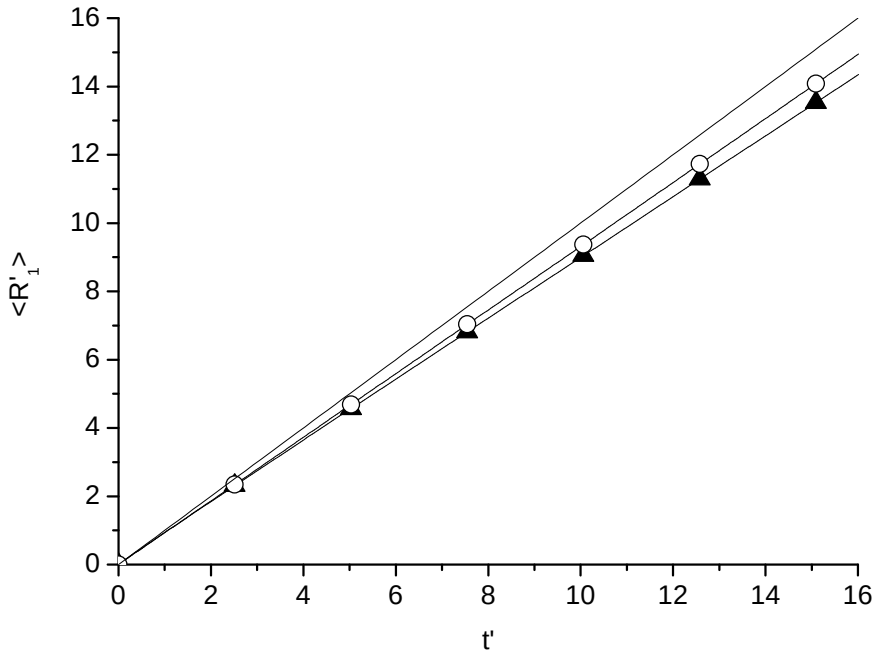

(c)

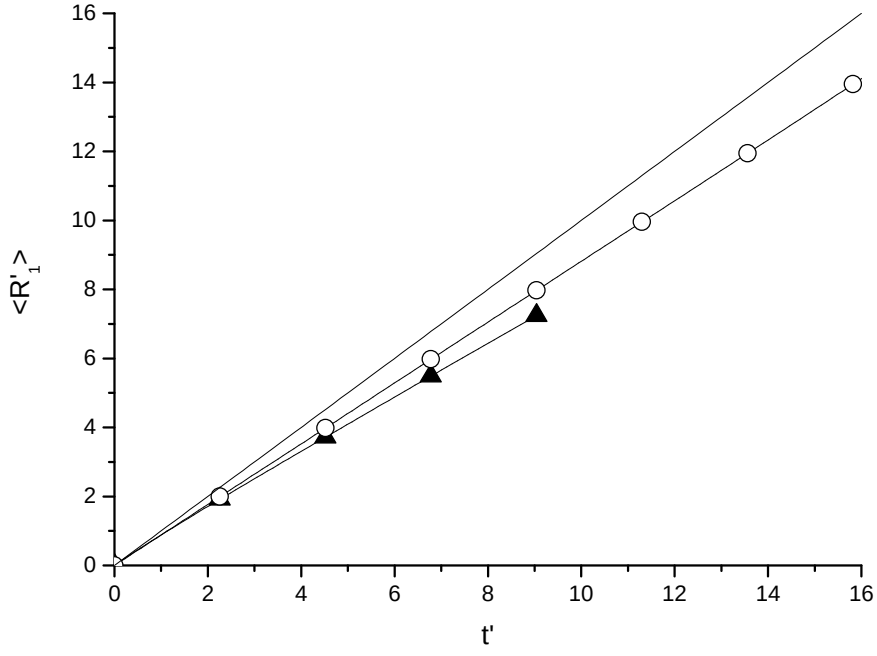

(d)

Figure 2.11: First effective moment comparison between the first order solution (σ_Y^2) and the transport solutions based on CG and MH flow fields for conductivity field variances of a) 0.2, b)1, c)2 and d)4.

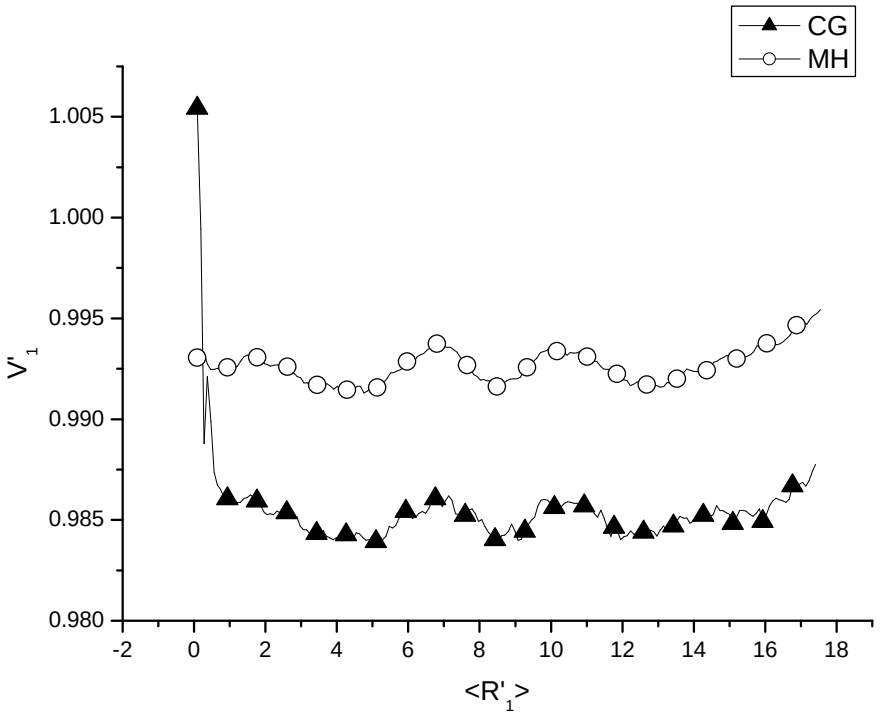
CG
MH
1.005
1.000
0.995
0.990
0.985
0.980
V'1
-2
0
2
4
6
8
10
12
14
16
18
<R'1>

(a)

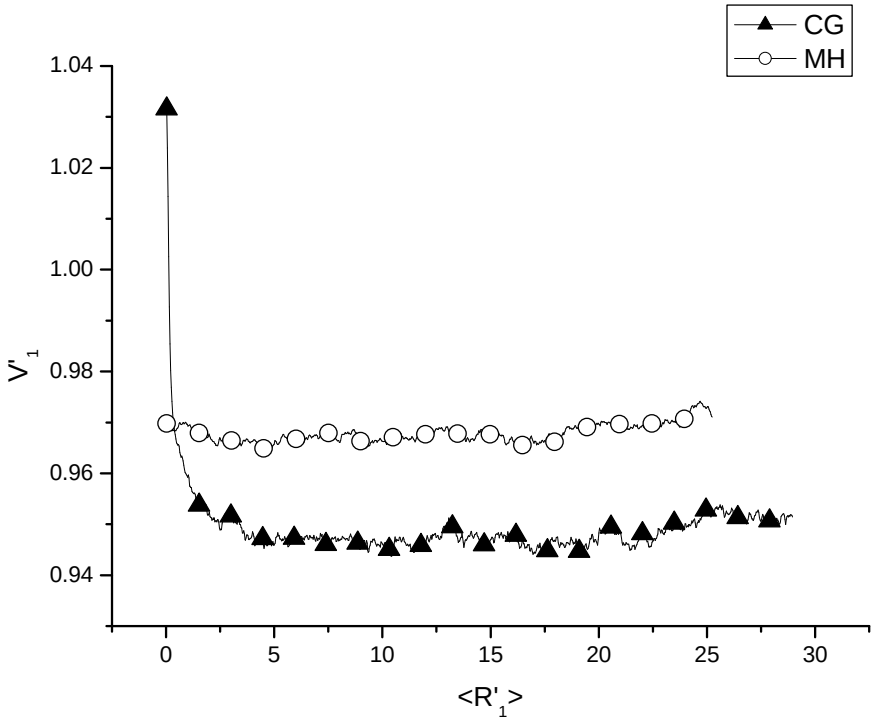
CG
MH
1.04
1.02
1.00
0.98
0.96
0.94
V'1
0
5
10
15
20
25
30
<R'1>

(b)

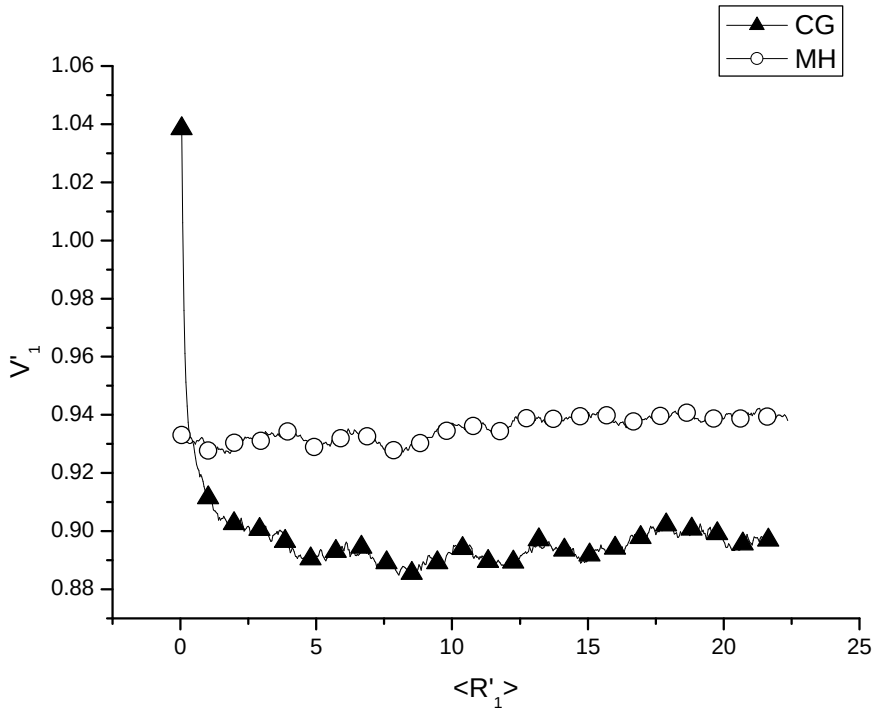

(c)

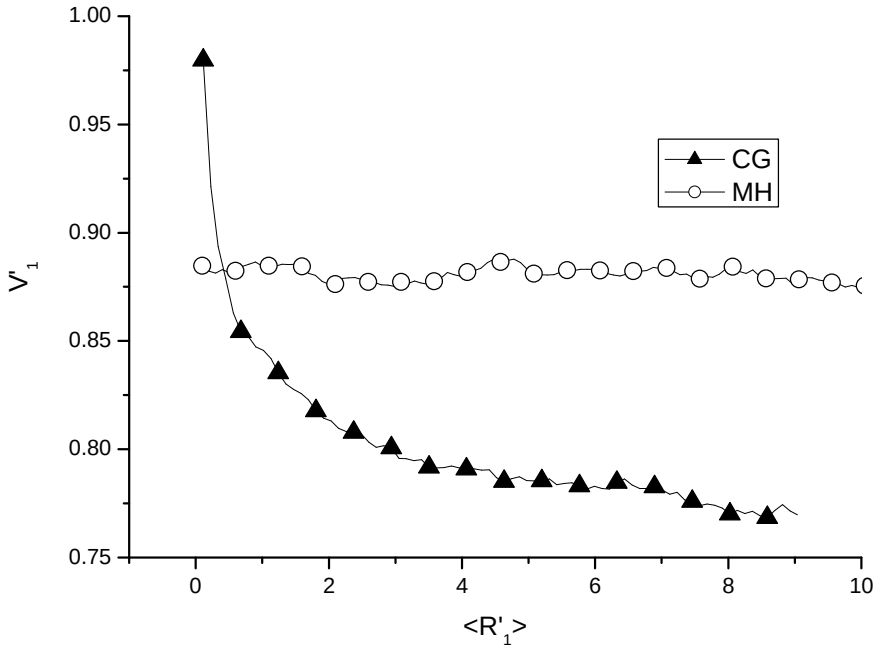

(d)

Figure 2.12: Evolution of the plume barycenter velocity for the two numerical schemes for conductivity field variances of a) 0.2, b)1, c)2 and d)4.

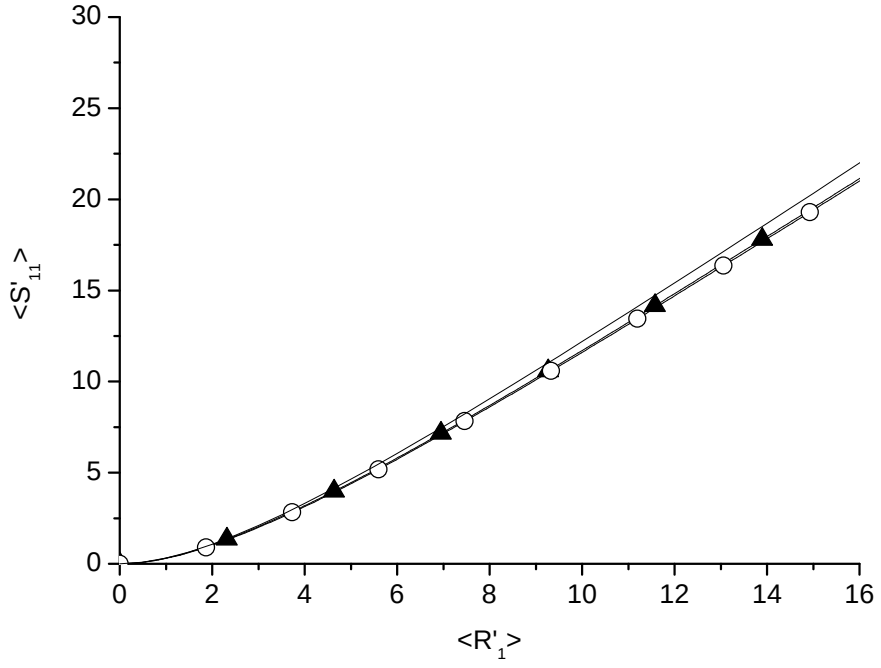
30
25
20
15
10
5
0
<S'11>
0
2
4
6
8
10
12
14
16
<R'1>

(a)

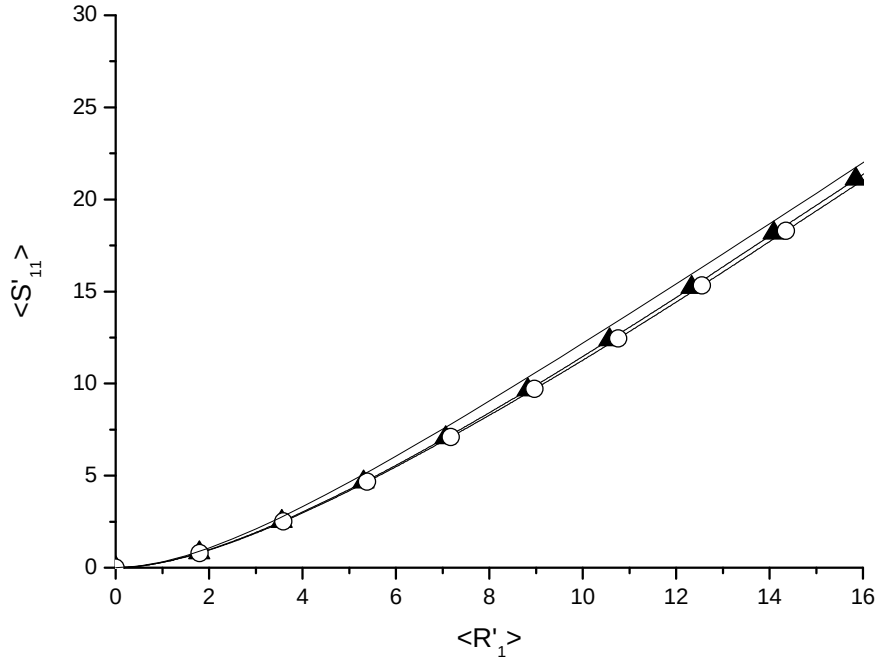
30
25
20
15
10
5
0
<S'11>
0
2
4
6
8
10
12
14
16
<R'1>

(b)

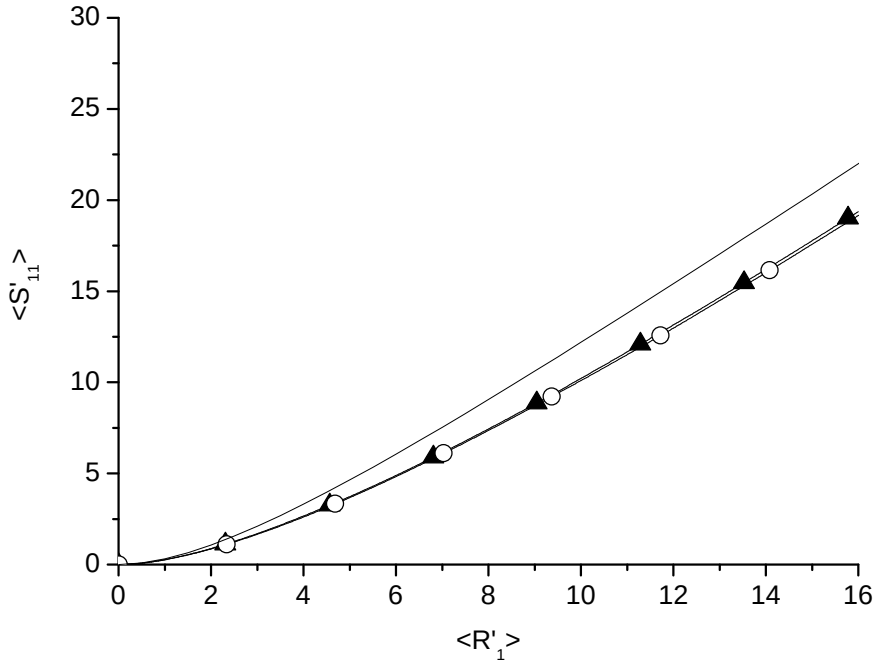

(c)

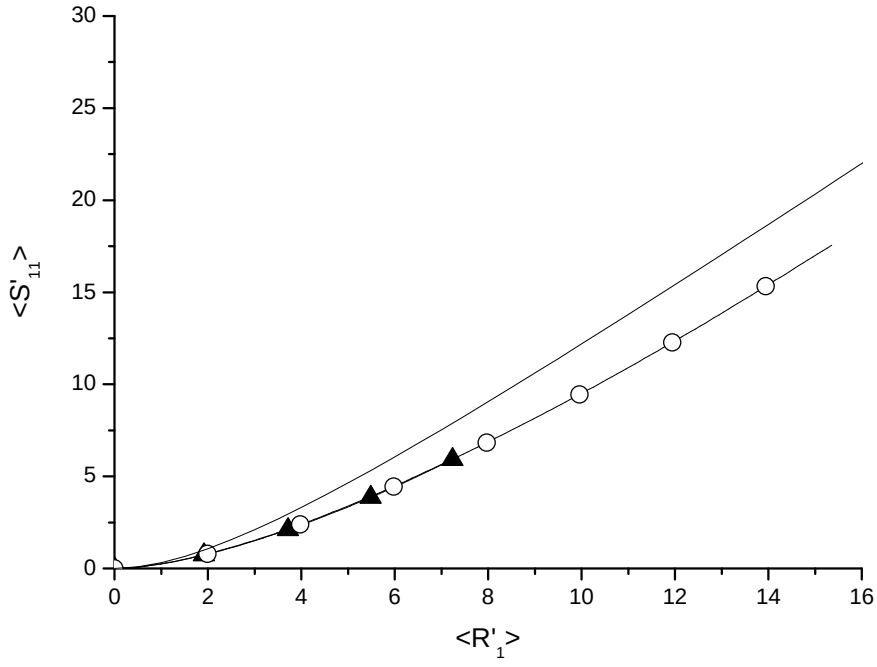

(d)

Figure 2.13: Trends of the second effective moments Vs the first effective moment for conductivity field variances of a) 0.2, b)1, c)2 and d)4.

Figure (2.13) shows $< S'_{11} >=< S_{11} > /(\sigma_Y^2 I_Y^2)$ as a function of $< R'_1 >$ respectively for field variances σ_Y^2 of a)0.2, b)1, c)2 and d)4. From the plots it is evincible that the two numerical schemes show negligible differences regarding the spreading of the plume along its path. Furthermore the difference between the numerical and the first order solutions is negligible for low conductivity variances, when the numerical mean plume velocities are very close to U. This means that for weakly heterogeneous formations (see figure (2.13a) for the case of $\sigma_Y^2 = 0.2$), both the numerical schemes used for the flux evaluation, provide solutions in good accordance with the linear theory of transport. For high conductivity variances (see figure (2.13d) for $\sigma_Y^2 = 4$) both schemes show the same longitudinal dispersion at a same distance from the injection point yet sensibly lower than the first order one.

2.6 Summary

The performed analysis highlighted several issues on finite element modeling of flow in heterogeneous porous formations. First of all it has been evidenced that the classical FEM schemes for velocity field evaluation show a more robust structure than the newly proposed ones. This has been shown by means of convergence analysis toward analytical solutions, in which the four analyzed schemes show different behaviors as the heterogeneity level of the conductivity field increases. The classical CG and MH schemes maintain the same rate of convergence as exhibited for homogeneous conductivity cases. In the other hand ZB and YEH show better performances than the former two in case of homogeneous conductivity field and in case of smooth analytical velocity field (that is a flow field in which at an interface between two different materials the tangential velocity is zero), while they lose in efficiency when non smooth analytical solutions are imposed over heterogeneous media. Hereby we decided to focus the attention on the classic schemes only, CG and MH. The stochastic analysis over very heterogeneous random fields (i.e. the log-conductivity varies cell by cell and has an exponential covariance structure with definite mean and variance) revealed some particular features of these schemes. For every level of heterogeneity analyzed the two numerical schemes lead to similar solutions except for the variances of the velocity fields. In particular the MH scheme shows velocity field variances perfectly matching those required by the first order theory, while CG leads to more heterogeneous flow fields. Furthermore the comparison with second order solutions evidenced a better performance of CG particularly for the variance of the transversal velocity component which matches perfectly with the analytical one. We speculate that the way the conductivity parameters are employed within the schemes is partly responsible for the different heterogeneity level of the numerical flow fields.

Both schemes approximate the inter-cell fluxes as a function of local averages of the real conductivity values, in particular CG employs the arithmetic mean while MH em-

ploys the harmonic mean of inter-cell conductivities, leading the schemes to actually solve conductivity fields with modified statistics than the real generated ones. Upon this conjecture the MH scheme modifies significantly the variance of the conductivity field being solved, reducing it to up 1/4 of the real value, while CG tends to minimize the discrepancy between numerical and real variance values.

Transport experiments by means of the particle tracking technique show different behavior concerning the mean velocity movement of a particle plume. In particular the CG flow fields seem to slow down the advance of a plume of particles, while MH tends to move it faster with a better matching with the first order transport theory. No differences in terms of particles dispersion are shown between the numerical solutions at the same plume barycenter position.

The greater heterogeneity level of the velocity fields evaluated with CG seems to exert a crucial role in the performance comparison between the two numerical schemes. In fact the stochastic analysis is nowadays an important tool for aquifer modeling, and in general for flow in porous formations, especially in cases of poor knowledge of the sites conductivity spatial distribution. Stochastic modeling has a very extended application to aquifer simulations but may be applied to any type of porous formations such as hillslopes and for both saturated and unsaturated conditions. For instance one of the most studied site catchments, that is the CB1 catchment in the Oregon Coast Range (Montgomery et al., 2002), shows a conductivity distribution with a strong variability, with values ranging over several orders of magnitude. In order to simulate flow in such a catchment using a distributed model the perfect knowledge of the conductivity distribution is required yet impossible. The possible choice is to employ a geostatistical model for conductivity generation and in such case we may be in a situation in which we have to solve variably saturated flow in a heterogeneous conductivity field. Within this framework, the analysis conducted in this chapter are of some help in order to warn on the reliability of the numerical model to be employed in such situation. From our models comparison we inferred that the performance of such simulation may be strongly affected by the numerical scheme adopted for flow evaluation. People needs to be aware of the intrinsic weaknesses of numerical models.

Although the analysis conducted so far are not giving definitive answers, they are of some advice to improve the understanding of numerical models reliability. The heterogeneity character of porous formations is not to be neglected by employing simplified conceptual models for the conductivity distribution, since its effect may exert a fundamental role in the dynamics of the system, either flow or transport phenomena.

3 Inertial Effects in Saturated Flow

3.1 Introduction

In this chapter the relevance of inertial terms in the momentum equation leading non-darcian effects is investigated for saturated flows. In the previous chapter we analyzed the effects of the numerical model employed on the solution of flow and transport in heterogeneous media. We found some peculiarities to be taken into account when deciding which type of numerical scheme to be used for particular situation, especially in cases of very variable hydraulic properties within the domain.

Besides the numerical argument we are also interested in analyzing the physical reliability of the equations usually employed for the description of the flow phenomena. Such equations are often based on simplifying assumptions which allow to neglect terms in the governing equations that are deemed to be small to negligible with respect to the dominating terms. For instance, the Darcy's law (1.15) which is assumed to be representative for the description of the velocity field dynamics is actually a simplification of the more general momentum balance equation (1.13) in which the inertial terms are neglected (see e.g. Bear (1972) and Bear and Bachmat (1990)). This is done under the common assumption that variations in the flow velocity are small enough to be negligible.

In this chapter we analyze the role of inertial terms in equation (1.13) in order to understand when they are negligible and when not. Former studies on that topic are based on simplified analytical solutions, for instance Torbjörn and Rehbinder (1993) analyzed the influence of inertia in case of pumping wells. Their study is based on a 1-D first order simplified analytical solution of equations (1.10) and (1.13) in which they neglect advection and impose boundary conditions in the form of heavy-side functions. They argue vaguely that there might be some influence for impulsive phenomena such as those occurring in pumping tests.

Another case, not treated here, is devoted to the occurrence of inertia in flow at high Reynolds numbers, when turbulence occurs and the friction factor for flow changes. For instance Andrade et al. (1999) studied these effects and found that the occurrence of inertia, experimentally evidenced, might be modeled also in the laminar flow regimes without including turbulence.

A large body of literature is devoted to compressible fluids and hence is not relevant to the present study. A comprehensive treatment of flow for compressible fluids can be found

in Levy et al. (1996) for single phase fluid flow, and Sorek et al. (2005) for a complete analysis of multi-phase flow for compressible fluids.

However, in the following sections we first describe a dimensional analysis of the 1-D governing equations in order to show under which theoretical conditions the inertial terms are of the same order of magnitude of the Darcy's terms. This part of the work is very illuminating from a qualitative point of view, because it can tell us on the temporal and spatial influence of such terms related to the field hydraulic properties. The links to the boundary conditions is shown to be relevant only for the advection term.

The second part is devoted to the numerical solution of equations (1.10) and (1.13). A 1-D numerical model is explained and developed. It has been tested for convergence in the case of step changes in boundary conditions. Simulations are reported for some test cases, trying to see if there is a correspondence between the dimensional analysis and the numerical solutions.

The work reported does not take into account of effects that might occur at high flow velocity, for Reynolds numbers in which the viscous drag is not proportional to the pressure drag anymore. In such cases the latter factor increases faster than the former one and additional terms have to be included in the governing equations for taking into account of the occurrence of turbulence. For instance Fourar et al. (2004) studied this phenomena numerically and concluded that the Forchheimer's equation (see e.g. Forchheimer (1901a) and Forchheimer (1901b)) is very suitable for accurately describing such effects for the 3-D cases, while this is not true for 2-D ones. See also Skjetne and Auriault (1999) for further theoretical analysis and some applications about non linear flow in porous media.

3.2 Dimensional Analysis of The Governing Equations

In order to perform a dimensional analysis of equations (1.10) and (1.13) it is necessary to rewrite them in non-dimensional form. The first step for the accomplishment of this procedure is the definition of some dimensional scaling variables, needed to re-scale all the quantities appearing into the equations (Bear and Bachmat, 1990). Once the scaling quantities are determined they are used to define the non dimensional variables to be employed within the equations. The result of this procedure is a set of non-dimensional coefficients depending on the scaling factors. The comparison of the magnitude of such coefficients gives a simple yet efficient overview of the dominant terms within the equations for specified field properties and boundary conditions.

3.2.1 Scaling Variables

The Reference Time

The most important scaling quantity is certainly the reference time, which should be comparable to the temporal window that we want to study. In our case we defined the reference time as:

$$t_r = \frac{S_s T^2 L_r^2}{K_s} \tag{3.1}$$

where S_s, T and K_s are respectively the specific storage, the tortuosity coefficient and the saturated hydraulic conductivity as defined in chapter 1. L_r is a scaling length which significance will be further discussed later on. Using the reference time defined in (3.1) we can define the non dimensional time t^* as:

$$t^* = \frac{t}{t_r} \tag{3.2}$$

The Reference Length

For scaling distances we should define a reference length as well. Every single scaling variable states a definite magnitude or, in other words, a size for the window in which the dynamics of the real variables are monitored. We will see that for convenience we may use the same length L_r introduced for the reference time. In what follows the dimension of L_r may be set to be equal to the size of the considered domain when the target is to study the influence of some particular effect at a global scale. However, as an alternative it may be left undefined ”a priori” and the non-dimensional coefficients magnitude may then be studied as a function of its value. With this procedure we are able to state the range of variability of L_r within which a chosen coefficient is of one order of magnitude or another. In other words this latter procedure will tell us the distance over which the studied effect exerts its influence in the overall physical process. In the results section a

discussion about this aspect is reported. The reference length will be used for defining the non-dimensional form of time and space differentials:

$$\partial x^* = \frac{\partial x}{L_r} \tag{3.3}$$

The Reference Piezometric Head

This reference value is not definable through the use of some domain properties as is for the reference time. It depends on the boundary conditions changes over the domain, and more specifically on the piezometric head fluctuations along the monitoring period. Naturally, the reference head should be related to the Dirichlet boundary conditions to be imposed in the practical simulation for which the dimensional analysis is to be done. For convenience we will refer this quantity (H_r) to the maximum drop in piezometric head that is supposed to occur during the simulation. The reference piezometric head will be used for the non-dimensional form of the piezometric differentials:

$$\partial h^* = \frac{\partial h}{H_r} \tag{3.4}$$

The Reference Velocity

As for the piezometric scaling variable the reference velocity should be related to the real field dynamics that are to occur along the period of time in which the system will be simulated. So far we defined a piezometric reference head, which in our case we decided to be referred to the maximum head drop occurring over the flow field, moreover we also defined how to choose a reference length, if we now employ these two quantities together with a reference value for the saturated hydraulic conductivity (which we may imagine to be constant over the domain) into the Darcy's law, we find a quantification of the reference velocity as a function of the Dirichlet boundary conditions and some of the field properties. The reference velocity so defined looks as follows:

$$V_r = -\frac{K_s}{n}\frac{H_r}{L_r} \tag{3.5}$$

where n is the porosity as defined in chapter 1. The non-dimensional velocity may then be defined as follows:

$$\partial v^* = \frac{\partial v}{V_r} \tag{3.6}$$

which may be employed for both velocity and differential velocity terms.

3.2.2 Non-Dimensional Form of The Equations

The above quantities are the scaling factors to be employed in order to rewrite the governing equations in non-dimensional form. For our test case a 1-D horizontal model has been analyzed, which for convenience is reported here:

$$\frac{\partial h}{\partial t} + \frac{n}{S_s}\frac{\partial v}{\partial x} = 0 \tag{3.7}$$

$$\frac{\partial v}{\partial t} + \frac{\partial v^2/2}{\partial x} + gT\frac{\partial h}{\partial x} = -\frac{ngT}{K_s}v \tag{3.8}$$

We may now substitute within the above equations the dimensional variables with the non dimensional coefficients multiplied by the scaling factors, i.e.:

$$\delta = \delta^* \cdot \delta^r \tag{3.9}$$

with $\delta = \partial h, v, \partial v, \partial x, \partial t$, we find after some mathematical arrangements that equation (3.7) becomes:

$$\frac{\partial h^*}{\partial t^*} + \frac{nL_rV_rT^2}{K_sH_r}\frac{\partial v^*}{\partial x^*} = 0 \tag{3.10}$$

If we now substitute V_r with the expression in (3.5) we can further simplify the above expression which then becomes:

$$\frac{\partial h^*}{\partial t^*} - T^2\frac{\partial v^*}{\partial x^*} = 0 \tag{3.11}$$

The same procedure applied to equation (3.8) leads after some arrangements to the following non-dimensional form:

$$\frac{\partial v^*}{\partial t^*} + \left(\frac{V_rS_sT^2L_r}{K_s}\right)v^*\frac{\partial v^*}{\partial x^*} + \left(\frac{gT^3L_rH_rS_s}{K_sV_r}\right)\frac{\partial h^*}{\partial x^*} = -\left(\frac{ngT^3S_sL_r^2}{K_s^2}\right)v^* \tag{3.12}$$

Substituting expression (3.5) into this equation lead to:

$$\frac{\partial v^*}{\partial t^*} - \left(\frac{S_sT^2H_r}{n}\right)v^*\frac{\partial v^*}{\partial x^*} - \left(\frac{ngT^3S_sL_r^2}{K_s^2}\right)\frac{\partial h^*}{\partial x^*} = -\left(\frac{ngT^3S_sL_r^2}{K_s^2}\right)v^* \tag{3.13}$$

Equations (3.11) and (3.13) represent the non-dimensional form of the 1-Dimensional horizontal saturated flow model.

3.2.3 Analysis of The Non-Dimensional Coefficients

Definition of Order of Magnitude

As reported in Bear and Bachmat (1990):

A number N is said to be of order of magnitude 10^n, n being an integer, if

$$n - \frac{1}{2} < log_{10}|N| < n + \frac{1}{2} \tag{3.14}$$

The order of magnitude of a function, f, defined over a certain range, means the order of magnitude of a number M, where M is the maximum (or the least upper bound), of $|f|$ over that region.

We shall employ the symbol O(N), to indicate that a function is 'of the order of magnitude of the number N'. For example,

$$O(f) = O(1) \qquad implies \qquad 10^{-\frac{1}{2}} < |f|_{max} < 10^{\frac{1}{2}} \tag{3.15}$$

In less mathematical terms, the order of magnitude of a function in some region is an estimate of the function's maximum absolute value, for independent variables in the given region.

Considerations on The Coefficients Structure

Equation (3.11) shows clearly that the only coefficient that links together its two terms is T^2 which may be considered as a constant, in fact the value of the tortuosity factor is usually defined by (1.14), however if we set it equal to 1 we are not introducing a huge error. From this consideration we evince that the non-dimensional terms in equation (3.11) are perfectly balanced for timescales of the order of the reference time, which is a function of the field properties and of the dimensions of the analyzed domain window.

Different considerations have to be done for equation (3.13). In this case the non-dimensional coefficients depend on both the domain properties, K_s, S_s and L_r, and the magnitude of the boundary conditions, that is H_r. There are a lot of ways to study the influence of these four parameters into the various coefficients. If we pay attention to the non-dimensional equation, we see that the coefficients multiplying the third and fourth terms, i.e. the Darcy's terms, are the same, and this means that they are of the same order of magnitude for any value of the domain properties yet for a timescale which depends on such properties. Our objective is to study the influence of inertial terms in porous fluid motion, so we can seek for the conditions in which the coefficients multiplying the inertial terms are of the same order of magnitude of the Darcy's ones.

The problem is that there are two inertial terms, the temporal one and the advective one. We may try to find when all the four terms in the equation are of the same magnitude or in alternative when only one of the inertial terms at a time is of the order of the Darcy's

ones. In this latter case the temporal term is the simplest to be studied since its coefficient is constant and equal to 1. The conditions of equal magnitude between this term and the Darcy's terms require that the Darcy's non-dimensional coefficients have to be of the same order of magnitude of 1, and hence order 0. These coefficients fortunately depend on three domain properties only, which are the conductivity, the specific storage and the reference length. It is therefore possible to study the order of magnitude of such coefficients as a function of two of these properties, allowing to find what is the range of variability of the third one for the satisfaction of the criteria in (3.14).

The second inertial term requires a less restrictive criteria of evaluation in terms of domain properties, yet it introduces the boundary conditions into the analysis. Its dependency to the specific storage is the same as for the Darcy's terms, and hence we may neglect this parameter in the dimensional comparison. This aspect is obvious since in stationary regime the system of equations loses its dependency to such parameter, and there is no reason that it might have effects to the advection term in non stationary situations.

Applying to a specific situation this two analysis, in order to understand when we have to use the complete momentum balance equation, is then straightforward. We have all the four parameters to account to, the field properties and the boundary condition. In order to accomplish this analysis we need to fulfill sequentially the above two steps.

The Temporal Inertial Term Analysis

The coefficient to be analyzed in this case is the one multiplying the Darcy's terms in equation (3.13), that is:

$$\frac{ngT^3 S_s L_r^2}{K_s^2} \tag{3.16}$$

In this term we have the dependency to the saturated conductivity, the specific storage and more importantly to the reference distance L_r. Our target is to find what are the combinations of these three parameters in order to have that (3.16) satisfies the criteria in (3.14). The best thing to do is to find boundary values for the parameter L_r as a function of the other two parameters. In other words we have to solve for:

$$L_1^2 = \frac{10^{1/2} K_s^2}{ngT^3 S_s} \tag{3.17}$$

and

$$L_2^2 = \frac{10^{-1/2} K_s^2}{ngT^3 S_s} \tag{3.18}$$

In figures (3.1a) and (3.1b) are reported respectively the contour lines for L_1 and L_2, for which calculation we set $n = 0.35$ and $g = 9.81$, the tortuosity has been evaluated with (1.14).

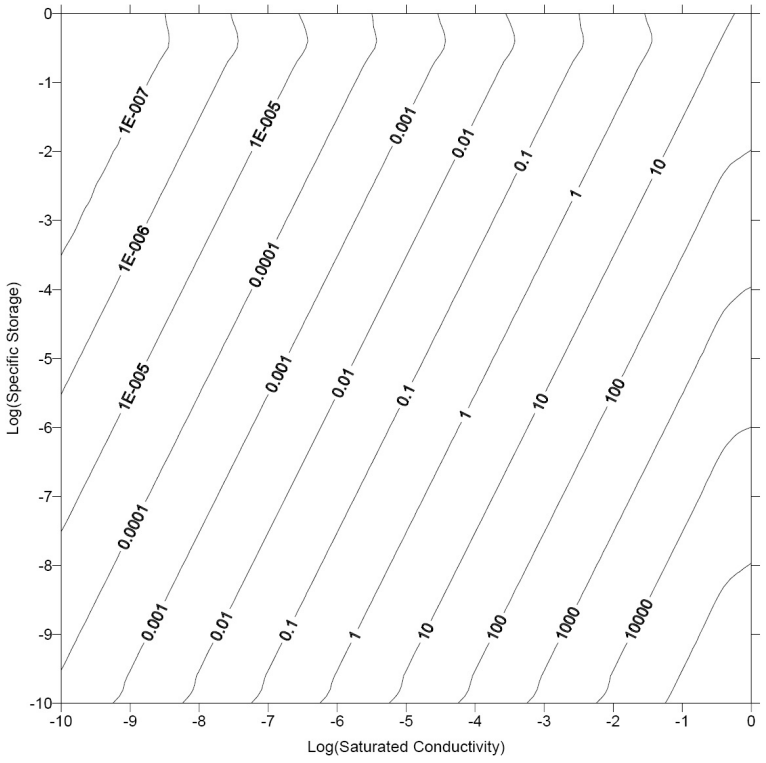

(a)

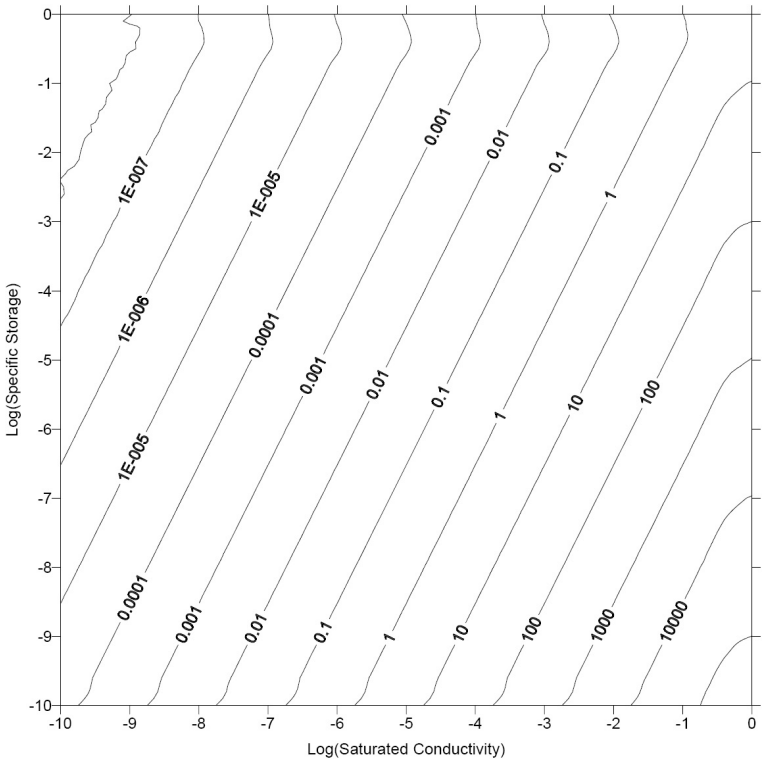

(b)

Figure 3.1: Upper (a) and lower (b) values for the reference distance L_r for which the temporal inertial term is of the same order of magnitude as the Darcy's terms.

The use of these two graphs is very simple since having a value for S_s and K_s we find a range of the magnitude of L_r which states the distances over which the temporal inertial term is not to be neglected for a temporal scale as defined in (3.1).

Figures (3.1a) and (3.1b) defines a three region problem. These are the regions that state either the dominance of one term over the other or their equivalence. For instance if $L_r < L_2$ the Darcy's terms are of one or more orders of magnitude lower than the temporal inertial term. In the other hand for $L_r > L_1$ we are in the opposite situation, that is when the Darcy's terms are dominant. Between these two boundaries we have the dimensional equivalence of them.

The Advection Term Analysis

The magnitude analysis for this term is similar to the previous one yet it is linked to the magnitude of the boundary conditions H_r instead of the specific storage coefficient. The coefficients to be compared are (3.16) and the following:

$$\frac{S_s T^2 H_r}{n} \tag{3.19}$$

Assuming that the temporal inertial term is negligible we might study the ratio between the remaining two coefficients. As said before they both depend on S_s which then might be neglected from the comparison. Their ratio is therefore:

$$\frac{n^2 g T L_r^2}{H_r K_s^2} \tag{3.20}$$

In order to have that the two coefficients are of the same magnitude, this ratio has to be of order $O(1)$, and hence:

$$10^{-\frac{1}{2}} < \frac{n^2 g T L_r^2}{H_r K_s^2} < 10^{\frac{1}{2}} \tag{3.21}$$

Also in this case we turn out with two boundaries for a region in which the criteria in (3.21) is satisfied, and which are reported in figure (3.2). All the calculations have been performed by setting $n = 0.35$ and $g = 9.81$ as for the previous case.

Having the value for K_s and for the head drop applied to the domain, the plots allow to find a range of values for L_r for which the advection term and the Darcy's terms are of the same order of magnitude. The temporal scale here has no sense, since this study is not linked with temporal variations in the system state because it is valid also at stationarity. Here the reference length refers to the distance over which the head drop occurs and hence, together with the H_r, defines what is the gradient range for which, at a specified saturated conductivity value, the advection term is not to be neglected in the study.

As for the previous case we have a three regions problem. The dominance of the advection term over the remaining ones is satisfied for values of L_r below the limit defined

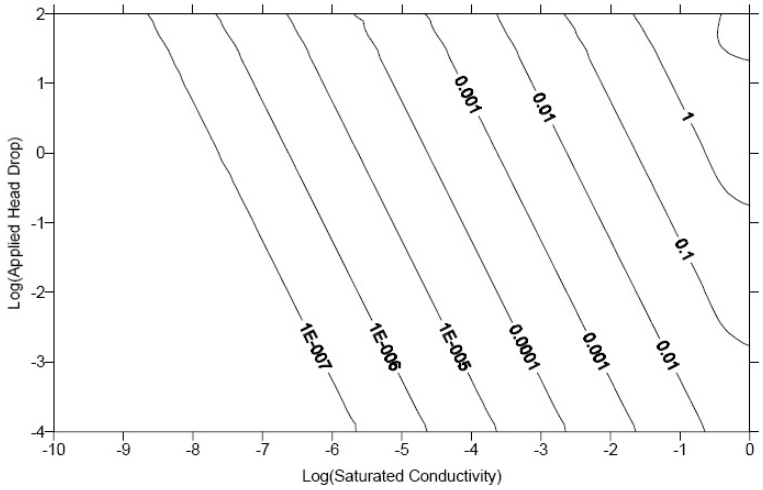

(a)

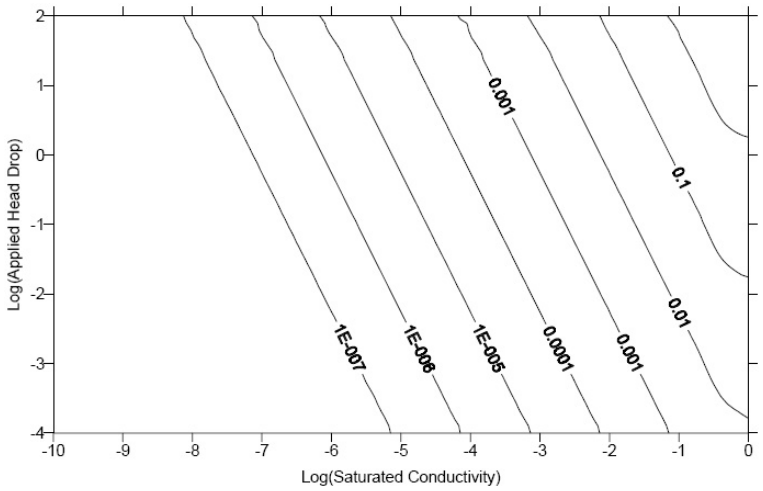

(b)

Figure 3.2: Upper (a) and lower (b) values for the reference distance L_r for which the advection inertial term is of the same order of magnitude as the Darcy's terms.

by figure (3.2b), while its negligibility is satisfied for values above those defined in figure (3.2a). The middle region states the dimensional equivalence of the terms.

In non stationary regimes, where for instance the piezometric head is initially constant and an instantaneous gradient is applied to the field boundaries, we are in a situation in which the pressure profile is evolving with time. At the beginning the head gradients might be very steep close to the boundaries and tend to smooth as time advances and the head front propagates, until a stationary profile of constant gradient is reached over the whole field. In such case we might be in the situation in which the gradient is locally high enough to require the advection term to be taken into account, while as time proceed the gradient diminishes as the front advances. However, when this type of situations occur, we might be in the case of high Reynolds number flow across the front, and further terms

need to be added to the momentum equation to take into account of turbulence effects.

The Complete Momentum Equation

The situations in which the momentum equation shall not be simplified in any of its terms occur when both the previous criteria are satisfied. From the operative point of view the usual starting point is the knowledge of the field parameters S_s and K_s. These two parameters, which are rather simple to characterize, let us to see which is the range of L_r for which the temporal term is not negligible and hence what is the timing scale for which the momentum equation is influenced by this term. Having the values of the mentioned parameters, it is now possible to enter figure (3.2) to see if for the boundary conditions which we expect to occur within the domain, the corresponding reference length matches with the reference length found in the previous step.

Obviously most of the situations will show the dominance of the Darcy's terms, yet for some specific cases such as pumping wells or applications to deep aquifers we might have to analyze deeper the problem before assuming the negligibility of the inertial terms influence on the flow dynamics.

3.3 Numerical Solution of The Momentum Equation

The numerical solution of equations (3.7) and (3.8) is explained in this section together with some applications. Connections with the study proposed within the previous section are reported in the sense that the dimensional analysis is applied and discussed to the test cases exposed in the following paragraphs. After some attempts on using standard finite difference schemes which performances did not produce good results, a staggered grid approach has been employed for the numerical solution of the governing equations. The convergence of this scheme has been accomplished with respect to a very refined grid solution and the resulting convergence rates are reported and discussed. The solution of the standard flux equation in (1.11) is then compared with that of the momentum equation.

3.3.1 The Numerical Scheme

Overview

The attempts to apply standard finite difference schemes for the solution of equations (3.7) and (3.8) lead to solutions that exhibit spurious effects. The problem arises because in these equations there are three terms of gradient form, each of which have to be modeled with either upwind, downwind or centered approximations for the derivatives. Using various combinations of these types of approximations lead always to non-physical results, disclosing sometimes oscillating trends or other type of spurious effects.

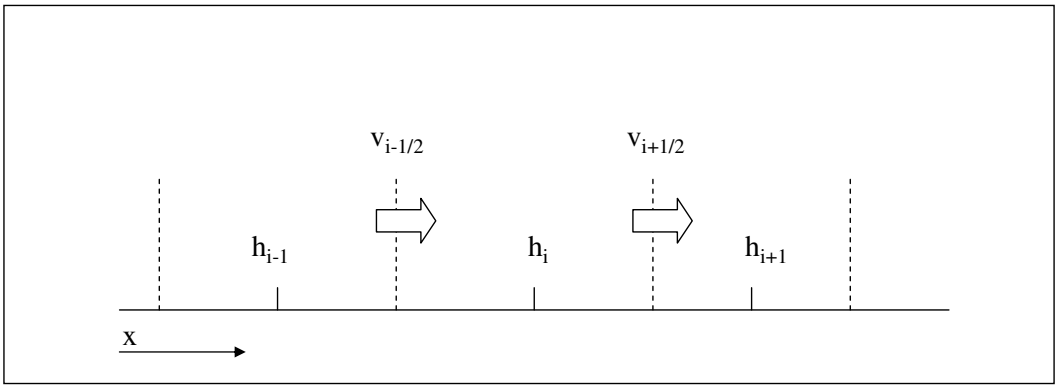

Figure 3.3: Staggered grid layout used for the solution of the inertial system of equations.

To solve this problem we employed a staggered grid approach, for which the two unknowns of the equations are defined over non matching grids as reported in figure (3.3). The reason for the better performance of such scheme is that two of the three gradients within the equations refer to the variable conserved in the other equation, and consequentially such gradients are exactly balanced across the point in which the conserved variable

is defined. For instance equation (3.7) conserves the piezometric unknown and contains the gradient for the velocity which is the variable conserved within equation (3.8). In the other side this latter equation contains a gradient for the piezometric head which refers to the former equation. The only gradient that do not satisfy this peculiarity is in the advection term in (3.8). This term may be modeled with an upwind or a centered scheme, and however as will be explained afterwards it is rather negligible for most of the situations. The system's non-linearity arisen from the advection term is treated with the Picard iterative scheme for the solution of non-linear systems.

The Staggered Grid Approach

On the basis of the staggered grid of figure (3.3) and numbering the discretized unknowns as h_i for $i = 1..m$ and $v_{i+\frac{1}{2}}$ for $i = 1..m-1$ we may write the discrete form of equations (3.7) and (3.8) as follows:

$$\frac{h_i^{n+1} - h_i^{n+1}}{\Delta t} + \frac{1}{\Delta x}\frac{n}{Ss}(v_{i+1/2}^{n+1} - v_{i-1/2}^{n+1}) = 0 \tag{3.22}$$

$$\frac{v_{i+1/2}^{n+1} - v_{i+1/2}^{n}}{\Delta t} + \frac{(v_{i+3/2}^{n+1})^2 - (v_{i-1/2}^{n+1})^2}{2\Delta x} + gT\frac{h_{i+1}^{n+1} - h_i^{n+1}}{\Delta x} = -\frac{ngT}{K_s}v_{i+1/2}^{n+1} \tag{3.23}$$

In this case the advection term in (3.23) has been developed in centered finite difference form. However we performed the experiments with all the possible discretization for such term, but we did not notice any difference in the solution. At the domain boundaries the formulation for this term and for the velocity gradient in equation (3.22) is delicate because of their dependent stencil that falls outside the domain, the solution to that problem depends on what type of boundary conditions are applied to the domain. In the next paragraph this aspect is discussed.

The Boundary Conditions

For the one dimensional problem modeled by equations (3.7) and (3.8) we need to impose one boundary condition at each end of the domain. In the applications being presented afterwards assuming to have a domain of length L, the boundary condition applied to the first end of the domain (that is in $x = 0$) is a Dirichlet type boundary condition in which we impose a variable piezometric head. At this end the only problem remaining by applying such condition is in the advection term of the momentum equation. To deal with this term we may apply the following discretization:

$$\frac{\partial v^2/2}{\partial x} \cong \frac{1}{2}\frac{(v_{3/2}^{n+1})^2 - (v_0^{n+1})^2}{3/2\Delta x} \tag{3.24}$$

Then we may assume zero velocity at $x = 0$ and the term further reduces to:

$$\frac{\partial v^2/2}{\partial x} \cong \frac{1}{2}\frac{(v_{3/2}^{n+1})^2}{3/2\Delta x} \tag{3.25}$$

At the other end of the domain we assume a reflective boundary condition of the velocity, for which across node m:

$$\left.\frac{\partial v}{\partial x}\right|_1 = 0 \tag{3.26}$$

This condition, which is still a Dirichlet boundary condition, reduces the continuity equation for node m to:

$$\frac{\partial h}{\partial t} = 0 \tag{3.27}$$

which means that at the right boundary the piezometric head remains unchanged during the simulations.

Since condition (3.26) basically states that $v_{m+1/2}^{n+1} = v_{m-1/2}^{n+1}$, the advection term in the momentum equation written for node $m-1$ may be rewritten in terms of $v_{m-1/2}^{n+1}$ and $v_{m-3/2}^{n+1}$ as:

$$\frac{1}{2}\frac{(v_{m-1/2}^{n+1})^2 - (v_{m-3/2}^{n+1})^2}{2\Delta x} \tag{3.28}$$

In some application a Neumann type boundary condition is applied to the left end of the domain, in which a variable inflow is applied to the continuity equation. In such case the continuity equation in $i = 1$ will be subjected to the Neumann flux which will cover the value for $v_{-1/2}$. In the same way the advection flux for the momentum equation in $1/2$ will depend on the Neumann flux as well.

3.3.2 Convergence Analysis

In order to verify the accuracy of the numerical scheme employed for the solution of the inertial problem we may perform a convergence analysis towards an analytical solution as the grid is refined. Unfortunately we do not have a test case for which the analytical solution is available, therefore we performed the analysis towards the solution obtained over a very fine grid.

The test case used for this analysis is based on the impulsive change of boundary conditions at the left end of the domain. The initial condition is of constant zero head over the field. The change event in the boundary condition occurs every second and is of the form of a square wave function in which the head level rises instantaneously from zero to one meter and at the next second falls again to zero and so on. The field properties are: domain length equal to $L = 5m$, specific storage $S_s = 10^{-5}\text{m}^{-1}$, porosity $n = 0.35$ and hydraulic conductivity 10^{-3}m/s. These characteristics are representative of a conductive and rigid sandy soil, for which we could see in the numerical solution the occurrence of an inertial propagating front at each boundary condition change rather than a simple diffusive head evolution.

Time (sec)	Mesh				
	99	197	393	785	1569
2	3.83484867	3.69568712	4.03488776	4.19716303	4.99868031
3	3.55898631	3.95647051	4.04105635	4.19740431	4.99867212
4	3.51245302	3.98637484	4.04197337	4.19743126	4.99866566
5	3.67929898	3.9932907	4.04225822	4.19743495	4.9986621
6	3.8079489	3.99527702	4.04237623	4.19743516	4.9986575
7	3.81954025	3.74074569	4.04605427	4.22947057	4.94930227
8	3.66111606	3.97247464	4.05648866	4.2510806	4.91674199
9	3.52690116	3.99908044	4.05515562	4.24292649	4.92877958
10	3.6383954	4.00527028	4.05352962	4.23597706	4.93899668
11	3.76531442	4.00726998	4.05217904	4.23071711	4.94672956
12	3.8512823	4.00792171	4.05108638	4.22664957	4.95268968

Table 3.1: Resulting rates for the convergence test of the inertial system. The convergence rates attest around order 2.

The convergence errors have been evaluated at each second, right after the pressure spike occurrence, therefore when the inertial front is visible. The refined grids ranged form 50 nodes to 99, 197, 393, 785 and 1569, while the most refined grid of 3137 nodes has been considered as the analytical solution. At each refinement level the grid contains all the grid-nodes belonging to the previous level, so the Eulerian norm in (2.6) could be evaluated for the same points. Figure (3.4) shows the trend of the norm at seconds 2 to 12 of the simulation results. Furthermore table (3.1) reports the evolution of the convergence rate along the mesh refinement at every second. As reported form the table

the convergence order attests at around order 2.

The adopted staggered grid scheme is very similar to the mixed finite element approach, for which the theoretical convergence rate of the piezometric head for homogeneous conductivity fields should be of order 2, as is for the present case.

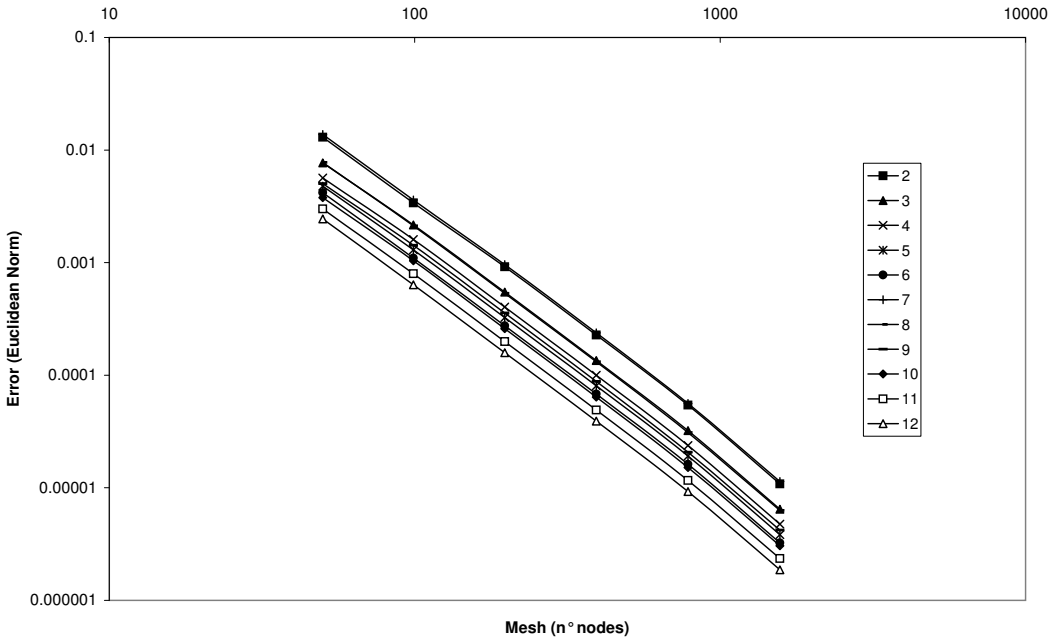

Figure 3.4: Convergence trend at each second of the solution of the saturated inertial system obtained for the test case in which the upstream boundary condition is a square wave.

3.3.3 Applications

Two numerical applications are reported in the following paragraphs, yet they are useful for showing inertia occurrence in saturated flow. The first one concerns an experiment similar to the one used for the convergence test. For this application the propagating fronts relative to the rising and falling of the piezometric boundary condition are compared with the solution obtained from the classic flux equation. Connections with the dimensional analysis of the equation terms are briefly discussed. The second application regards the imposing of a high frequency square wave upstream boundary condition. This latter test case is reported and discussed because it shows clearer the inertial terms influence in space, therefore it permits an easier and more reliable comparison with the dimensional analysis. The practical application of this experiment within the hydrological processes framework is rather useless, but for our objectives it has the great merit of acknowledging the dimensional analysis reported in the previous section.

Test Case 1

This test case is similar to that used for the convergence analysis of the numerical scheme employed for the solution of equations (3.7) and (3.8). The aim of this further analysis is to show the differences between the propagating front evaluated considering the inertial terms in equation (3.8) and the front obtained by neglecting such terms. For this test case the same field properties as for the convergence test case are used, the only difference is in the domain length which is set to 10 m.

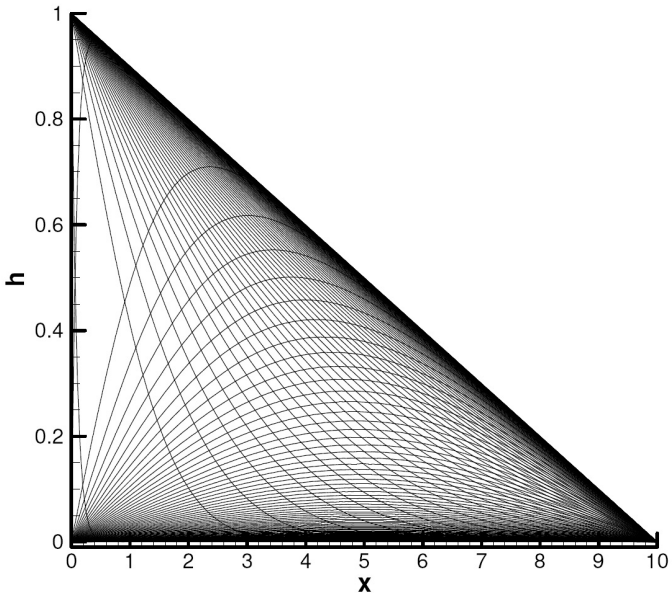

Figure 3.5: Envelope of the rising and falling profiles for the propagating front in test case 1 evaluated with the flux equation (no inertial effects taken into account).

Figure (3.5) shows the rising and falling profiles of the propagating front after the boundary condition changes from zero to 1m and from 1m to zero, evaluated with the flux equation in (1.11).

The solution obtained by considering the influence of the inertial terms is reported in figure (3.6) for both rising and falling profile cases. The spatial influence of the inertial terms is not easy to establish, the inertial effects on the profile shape seem to vanish before reaching the right end of the domain. In the other hand, figure (3.7a) reports the evolution in time of the difference between inertial and non-inertial solutions for both rising and falling limbs. It clearly shows that the difference tend to vanish as time advances, yet seems to proceed beyond the domain length. In fact it is forced to zero at the right end of the domain where the envelope seems to be convex and this implies that the asymptotic convergence of the two solutions is influenced by the domain boundary rather than the vanishing of inertial effects.

From the dimensional analysis of the previous section, if we enter figures (3.1a) and (3.1b) with the values of S_s and K_s used for this experiment, we see that the temporal inertial term exerts an influence of the same order of magnitude of the Darcy's terms within distances that range between $L1 \cong 0.3$m and $L2 \cong 10$m. Here the domain length is exactly 10m and therefore it is of the same magnitude of $L2$. In order to see if the inertial influence proceeds beyond this distance the domain length has been increased to 20m, figure (3.7b) shows the profiles difference in space and time. Here the influence of the domain boundary seems to be negligible, in fact the profile of the envelope is concave and reaches zero before the right end of the domain. Furthermore the envelope width seems to be negligible for distances in the range 10-15m.

However, this distance is clearly difficult to be evaluated exactly, yet it seems to agree very well with the dimensional analysis which states also that the advection term is some order of magnitude lower than the other terms for the lengths of interest in this case. To verify that, we may enter figure (3.2) with $H_r = 1.0$m (which log = 0) to discover that the advection term is to be taken into account in case of local gradients greater than 100, which might occur for very short timings and very close to the left boundary. As a demonstration we performed the same simulation by neglecting the advection term in equation (3.8) and the results were exactly the same.

Moreover, to demonstrate the influence of the right boundary in forcing the profiles difference due to the inertial effects to vanish, we performed an experiment in which the domain length was set to 5m. Figure (3.8) shows the envelope of the propagating profiles for both rising and falling limbs. From the graph it is evincible how the propagating profile rises a little bit above the equilibrium profile, and therefore exerting an inertial effect on the boundary. The result of that is the occurrence of a greater head gradient than that exhibited by the solution of the flux equation at L=5m. The difference is very small indeed in this case, yet it emphasizes the domain boundary influence in the problem solution.

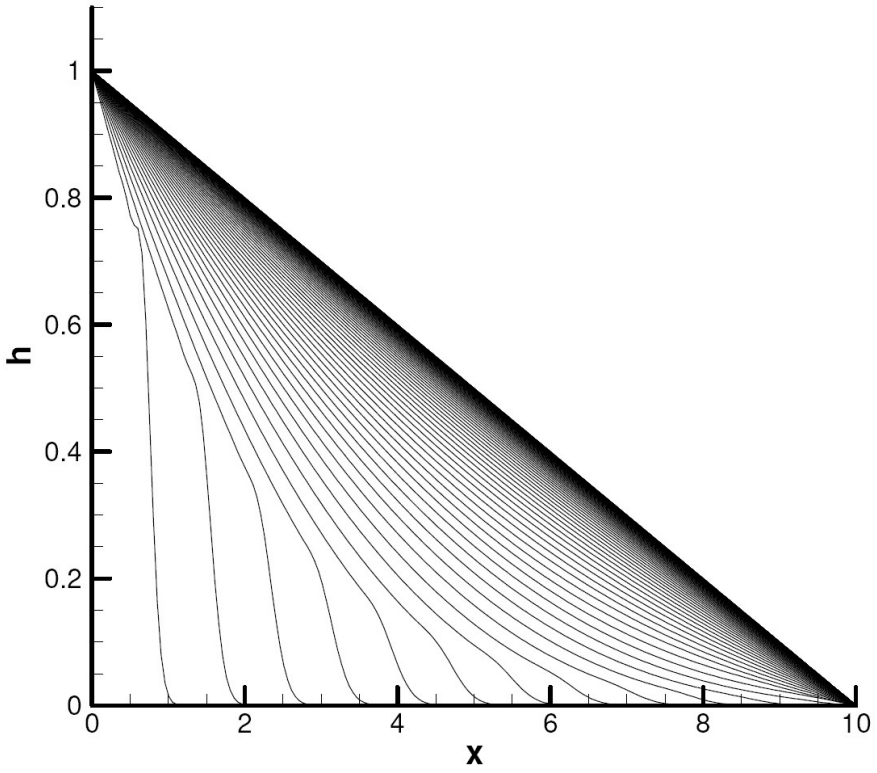

(a)

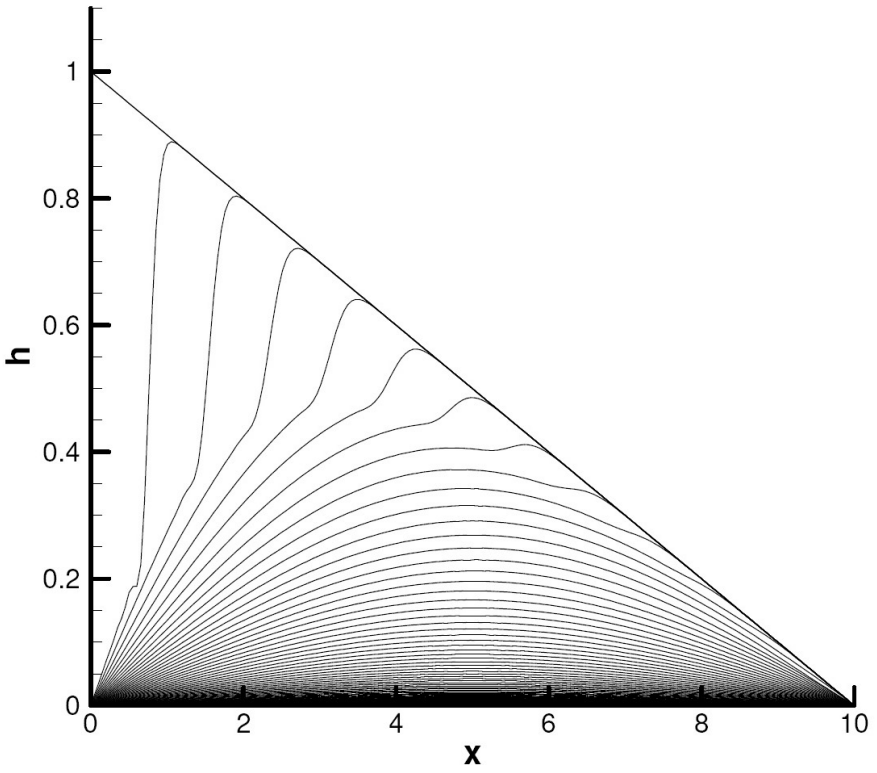

(b)

Figure 3.6: Propagating fronts for test case 1 evaluated with the inertial system: a)rising profiles envelope and b)falling profiles envelope.

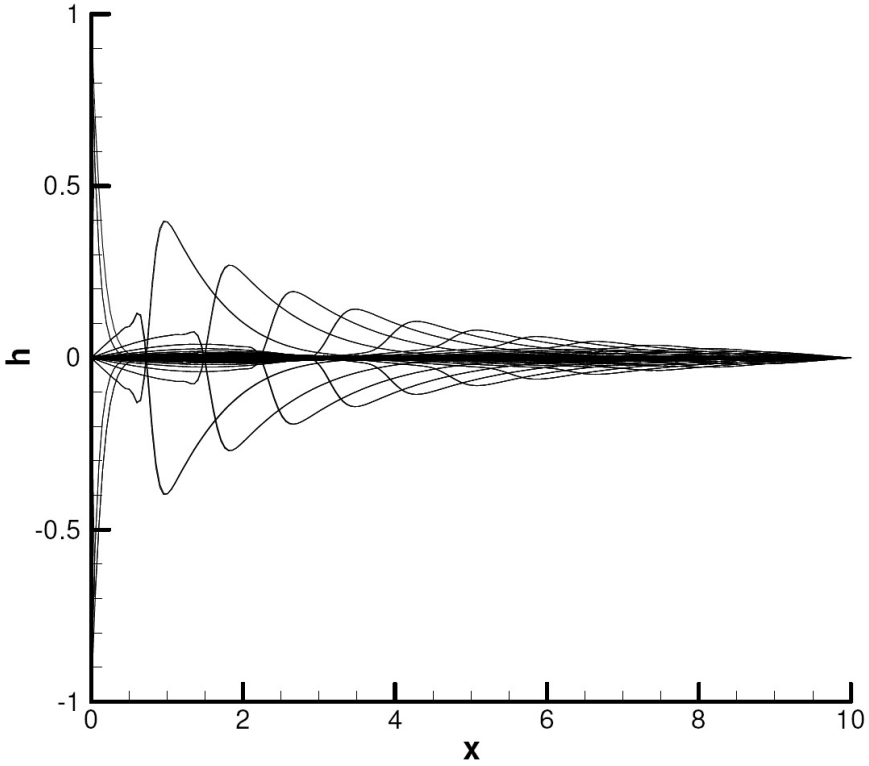

(a)

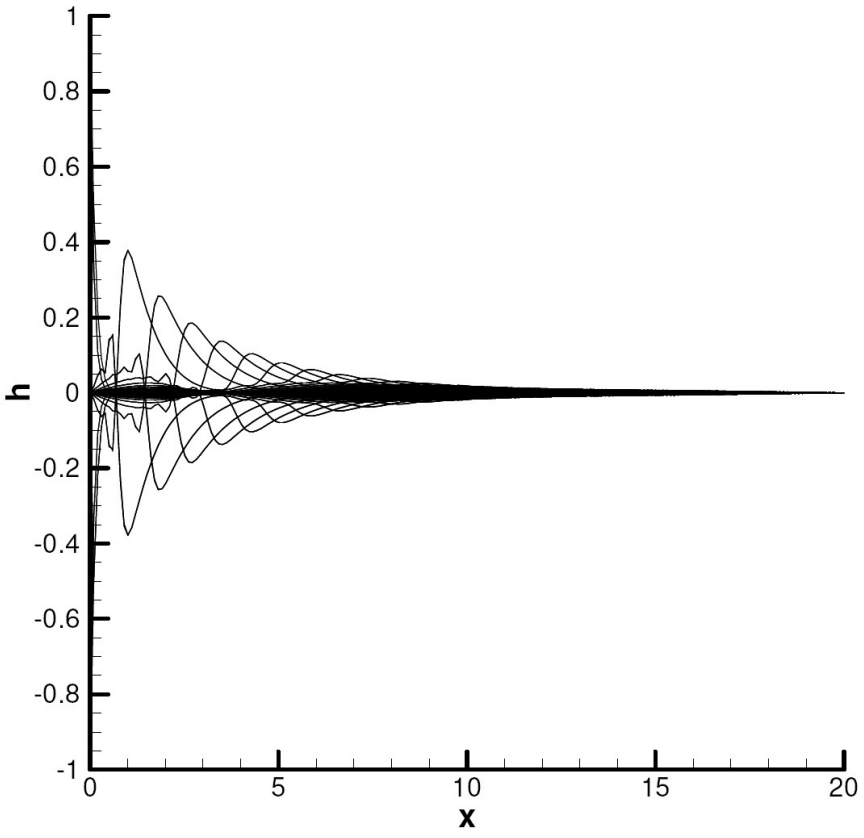

(b)

Figure 3.7: Profiles difference envelope in time between inertial and non-inertial solution for domain length of a)10m and b)20m.

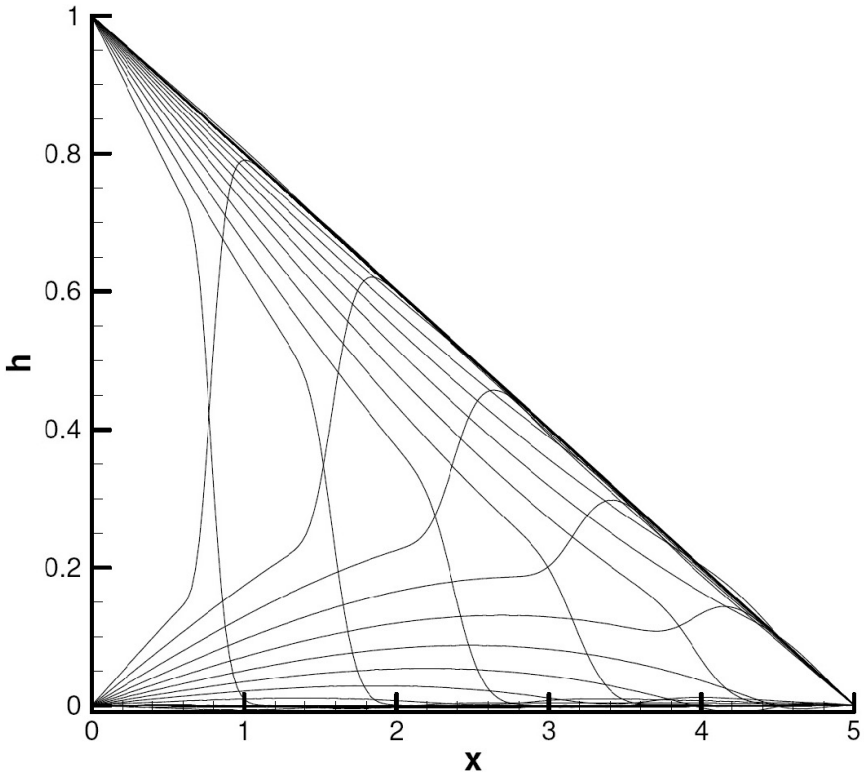

Figure 3.8: Propagating fronts envelope for test case 1 evaluated with the inertial system for a domain length of 5m.

Test Case 2

The second test case reported concerns a high frequency pulsating boundary condition. This test case has been reported because it shows clearly the extent of the inertial effects on the problem solution. A sinusoidal upstream Dirichlet boundary condition is imposed. The wave amplitude is very low and its frequency very high, its form is as follows:

$$\Delta h(t) = \frac{\pi}{2} \cdot 10^{-4} \sin\left[\frac{\pi}{2}\left(\frac{t}{3.2 \cdot 10^{-3}}\right)\right] \tag{3.29}$$

where t is time expressed in seconds and Δh is in meters. The domain properties are the same as those of the previous test case. As shown in figure (3.9) the influence length of the solution of the inertial system extends farther (figure (3.9a)) than that of the flux equation (figure (3.9b)). Figure (3.10) shows the envelope of the profiles difference in time and more important the extension of such differences. From this figure it is clear how the inertial solution extends the non-inertial one. In fact the wave propagates for almost double distances in the solution that takes into account of the inertial effects.

The dimensional analysis applied to this exercise leads to the same results as for the previous test case, reference lengths in the range $[0.3 - 15m]$, and no influence of the advection term for such lengths magnitude.

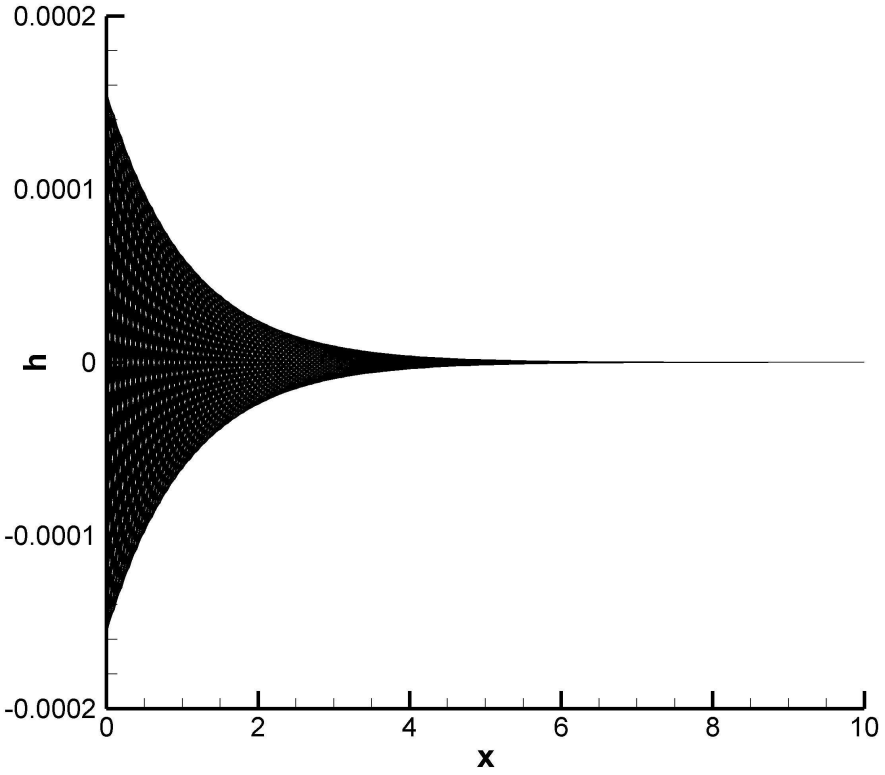

(a)

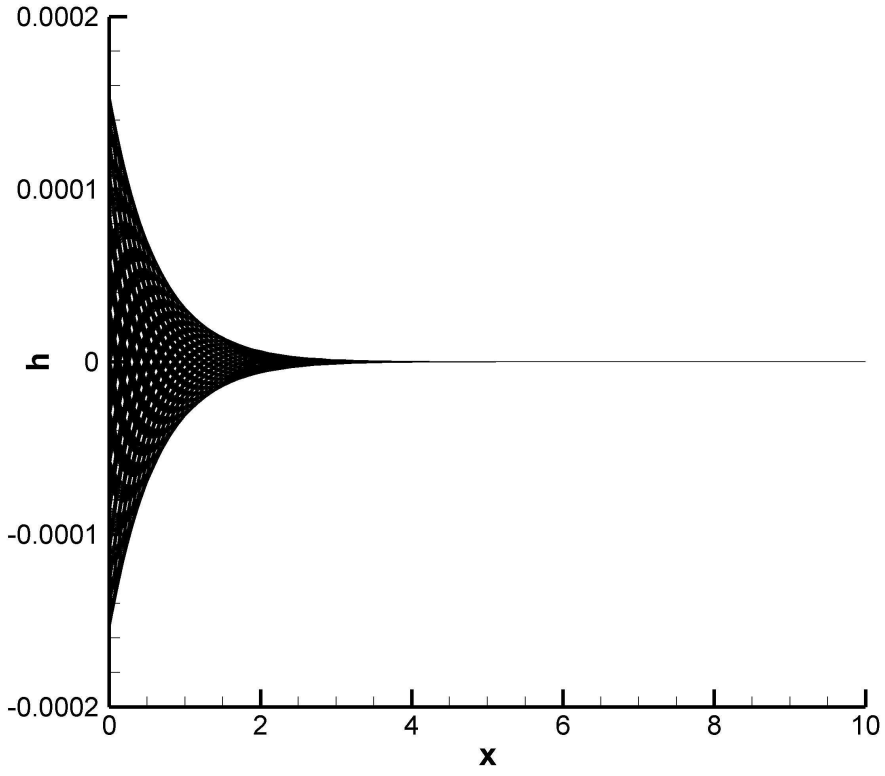

(b)

Figure 3.9: Profiles envelopes for test case 2 in which a high frequency wave is imposed as upstream boundary condition. Solution of a)the inertial system and b)the flux equation.

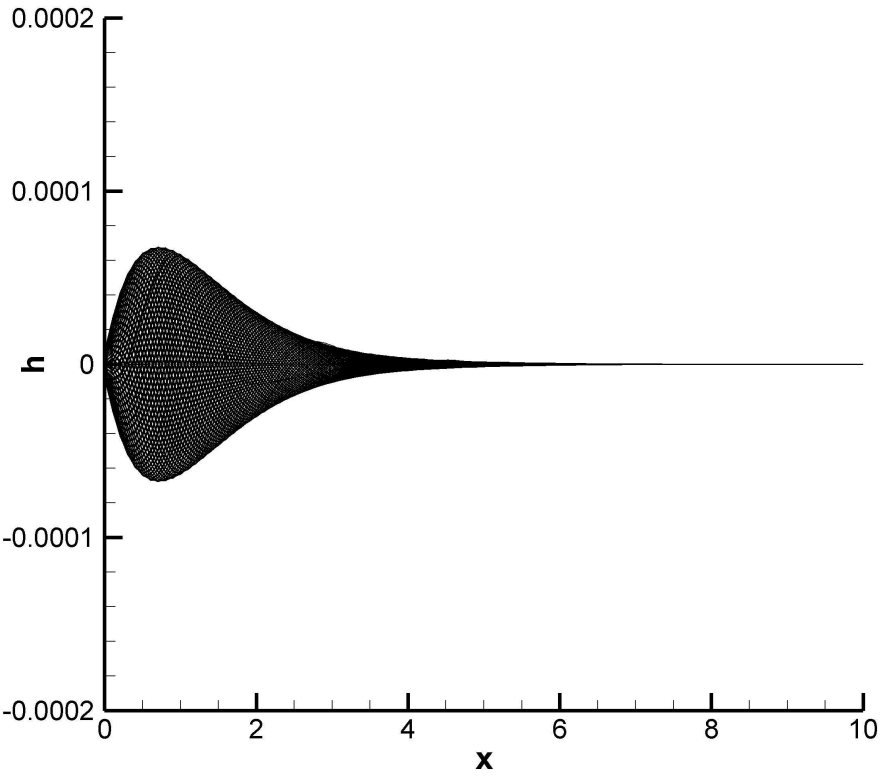

Figure 3.10: Profiles difference envelope for test case 2.

3.4 Summary

This chapter evidenced many aspects concerning inertial flow in saturated porous media. The equations that govern such phenomena are reported together with a dimensional and a numerical analysis. The dimensional analysis proposes the guidelines that allow to understand the situations in which we may have to consider the effects of inertia in practical applications. The comparison between the numerical simulations results and the dimensional analysis seems to agree fairly well in the reported test cases. Several further applications have been performed, yet the two reported are deemed to be representative of them all. However, none of them highlighted situations in which the advection term exerts appreciable influence to the flow dynamics. Such situations might arise when the Reynolds regime is high enough to imply turbulence occurrence, and this calls for the introduction of further terms in the momentum equation, but this is of no interests for the present study. However, objections may be done against the dimensional analysis validity in such cases, since for the definition of the scaling velocity the use the simple Darcy's law to find a representative value for such scaling parameter may not be valid.

In any case, our interests concern flows at low Reynolds number, and we deem that the reported analysis is fairly satisfactorily for such cases, although the numerical analysis

considers only the one dimensional case. Furthermore, these studies have been done as a former step for a problem that is going to be treated in the next chapter where unsaturated flow is analyzed.

4 Unsaturated Flow Modeling

4.1 Introduction

The most challenging aspects concerning subsurface flow are indeed the unsaturated porous media processes. A hundred years of studies could not fulfill all the lacunas related to this topic. All the improvements in our modeling capabilities to correctly describe the variably saturated porous media dynamics, are still not always satisfactory. The equation widely used for modeling such phenomena is the so called $Richards's$ equation which describes the water content evolution by means of the continuity equation and assuming the validity of mainly two closure relationships. In order to describe moisture fluxes within a porous matrix, the use of the $Darcy - Buckingham's$ law is necessary. Such law depends on the local suction gradients, while the variable that is conserved within the mass balance equation is the moisture content. This gap, one equation with two unknowns, call for the first closure model which aim is to link together these two unknowns. The second closure model is required for the description of the dependence between the moisture content and the actual hydraulic conductivity value. Furthermore, as for the saturated case, the equation describing the fluxes is a simplification of the momentum balance equation which though is now defined within a multi-phase framework (Bear and Bachmat, 1990). In the commonly adopted schemes for modeling flow in unsaturated soils only the dynamics of the wetting phase, water, are considered, while the dynamics of the second phase, air, are neglected. However the influence of air is taken into account by employing the first closure model, namely the water retention curve.

This physically based model is widely employed to simulate the variably saturated processes in hydrological applications, by using a distribute modeling framework. Unfortunately the performances of such model depends on our capability of characterizing the spatial variability of hydraulic properties, which is typically very limited, particularly in applications. Such parameters are highly variable in space and their poor characterization reflects negatively on the modeling accuracy. The output is that such distributed models often fail to predict the response timing and magnitude of natural systems such as hillslopes (Romanelli et al. (2006) and Rigon et al. (2006)). Furthermore there seem to be a lack between the theoretical basis on which the model relies and the real dynamics of unsaturated soil, which often reveal unexpected behaviors. First of all, objections on the validity of the water retention function have arisen after several experimental evidences

in which this function seems to depend on the rate of change of water content (see e.g. Hassanizadeh et al. (2002) and Shultze et al. (1999)). Moreover , in order to capture the fast response observed during intense storms, and the occurrence of preferential flow paths dual porosity or dual permeability models have been proposed (see e.g. Simunek et al. (2003) for an accurate review of these models).

In addition to these issues, some authors observed in field and laboratory experiments the occurrence of pressure waves that travel significantly faster than moisture propagation in soils subjected to infiltration. Montgomery et al. (2002) and Torres et al. (1998) monitored rainfall infiltration within the CB1 catchment, and observed a very fast response of the tensiometers placed deeply into the soil. Torres and Alexander (2002) and Rasmussen et al. (2000) noticed the same phenomena in soil column infiltration tests conducted in laboratory. They observed that the travel time of the pressure information related to the infiltration process was one to two order of magnitude faster than revealed by the moisture propagation process. Moreover Torres and Alexander (2002) and Germann and Di Pietro (1999) hypothesized the occurrence of inertial unsaturated flow as a consequence of a fast increase of the irrigation rate. They monitored a column subjected to variable rainfall, and surveyed an enhanced release of soil water due to the change of the rainfall intensity, and imputed such behavior to inertia occurrence in pore water flow.

This chapter analyzes the impact of the inertia terms of the momentum equation on flow in unsaturated soils subjected to a rapidly varying rainfall. The reason for this choice is that in the alps hillslopes are characterized by a shallow soil mantle of the order of one meter depth overlying bedrocks that may be either compact, and thus impermeable, or fractured. The runoff production will then involve a vertical infiltration process through this shallow soil mantle. This part of the process is an important part of the processes controlling runoff production at the hillslope scale. Therefore the water percolation mechanisms occurring in this unsaturated system are crucial for the correct modeling of the rainfall-runoff processes.

We decided to perform an extensive theoretical and numerical analysis of the experimental results reported by Torres and Alexander (2002) about the occurrence of non-darcian flow in column experiments subjected to highly variable irrigation rate. Unfortunately the authors did not report all the information required in order to perform accurate numerical simulations, therefore we performed a rather qualitative comparison between data and simulations.

4.2 Problem Statement

Here we report in detail the experimental setup and results obtained by Torres and Alexander (2002) about the occurrence of inertial type flow during drainage experiments in a laboratory soil column.

The experimental apparatus is composed of a cylindrical column of 80cm height and 14.6cm width. The column is filled with commercial standardized sand, with a narrow granulometric curve which mean grain size is 0.42mm and $10 - 90\%$ quantile range of $0.3 - 0.6$mm, packed 5cm increments to a height of 75cm. The sand bulk density was 1.54g/cm^3, mean porosity was $0.39\text{m}^3/\text{m}^3$, residual water content was $0.02\text{m}^3/\text{m}^3$ and saturated hydraulic conductivity $K_s = 3.7 \cdot 10^{-3}$m/s. The water retention curve exhibited hysteresis and was confined between zero suction and $-20, -40$cm (which means negative pressures between 0 and $-2, -4$KPa). Unfortunately they did not report the unsaturated hydraulic conductivity curve, so we can only hypothesize a standard trend for sandy soils. The bottom of the column was immersed in water till a depth of 2cm. The whole apparatus was positioned upon a high precision balance to measure weight changes from which to infer the column storage variations during the experiments. The column was instrumented with TDR probes and Tensiometers installed at 10cm intervals starting respectively from -15cm and -10cm from the top. Irrigation was provided by means of a 10 tubes peristaltic pump, with the aid of a mechanic shaker for allowing uniform rain distribution on top of the soil. Twelve irrigation experiments have been performed in which a low rainfall intensity is provided for 7-10 hours, then a spike increase of variable magnitude and duration is applied, and then back again to the pre-spike intensity for one hour. The instruments readings were monitored during the whole rainfall duration and for the time necessary for allowing the column to freely empty.

Figure (4.1) shows some of the results presented by Torres. In particular figure (4.1a) reports the inflow-outflow rate in time of the column monitored in one of the twelve experiments, while figure (4.1b) reports the evolution of the column storage in time. What is somewhat surprising in these figures is that after the column has been subjected to the spike rainfall rate, it reveals an enhanced drainage capacity. In fact the column storage in the pre-spike period is much greater than the column storage in the post-spike when pre-spike rainfall rate is set again on top of the column. It seems that the rain spike caused the column to release more water than expected according to the water retention curve and the common understanding of infiltration processes.

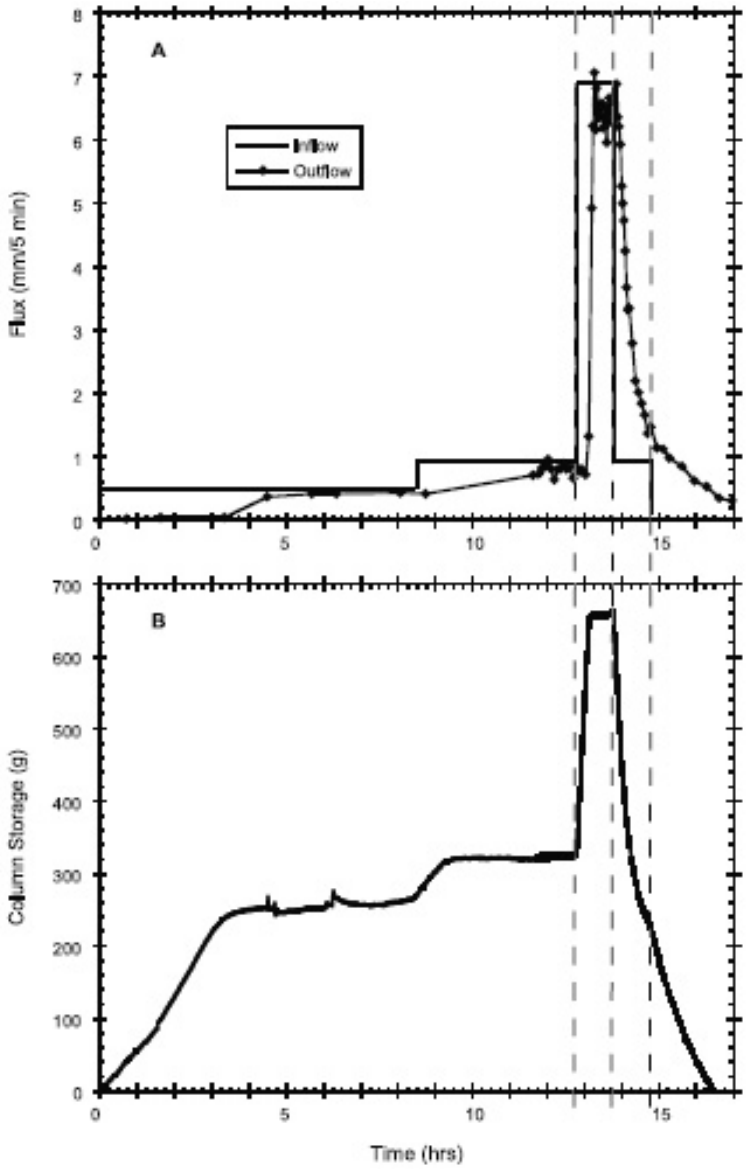

Figure 4.1: (a) Time series of column inflow and outflow. Flux is presented as mm per 5 min interval. The first vertical dashed line corresponds to the onset of a spike increase in irrigation rate. The second dashed line corresponds to the end of the spike and return to the background irrigation rate. The third dashed vertical line marks the end of irrigation. (b) Total column storage for the duration of the experiment. The increase at 8.5 hours corresponds to a time when water delivery tubes were unblocked and normal flow resumed (source Torres and Alexander (2002)).

Torres and Alexander (2002) argued that this effect is probably due to the occurrence of inertial type flow, which is to develop in the proximity of zero pressure heads, that is for this type of soil in the region of the water retention curve where a small change in suction relates to a large variation in water content. In our opinion these evidences are truthful, and not due to measurement errors since they are confirmed by all the instrument used within the experiments, i.e. by the TDR probes, tensiometers, precision balance and inflow-outflow readings.

In next paragraphs we report our studies where we tried to model such phenomena by employing the inertial terms within the governing equations for flow in variably saturated porous media. The governing equations written for a 1-D flow are the following:

$$C(\psi)\frac{\partial \psi}{\partial t} = -\frac{\partial(\theta(\psi)v_z)}{\partial z} \tag{4.1}$$

where $C(\psi)$ is defined in (1.28). And:

$$\frac{\partial v_z}{\partial t} + \frac{\partial(v_z^2/2)}{\partial z} = -gT(\theta(\psi))\frac{\partial \psi}{\partial z} - gT(\theta(\psi)) - \frac{gT(\theta(\psi))}{k(\theta(\psi))}\theta(\psi)v_z \tag{4.2}$$

First of all a dimensional analysis of equations (4.1) and (4.2) has been performed in order to understand the terms magnitude for the specific case of Torres's experiment. Numerical modeling is also presented and applied to this test case. Comparison with the Richards's equation is also provided. A discussion on the physical mechanism that governs the inertial-type flow highlighted by Torres is then presented.

4.3 Dimensional Analysis of The Governing Equations

In order to accomplish the dimensional analysis of equations (4.1) and (4.2), we need to repeat the steps performed during the same analysis we applied to the saturated case. The main difference is that we have now a non linear system of equations, and hence more variables should be considered. Consequently, the dimensional analysis for the variably saturated equations is more complicated and for this reason it is not possible to get general conditions for the occurrence of inertial effects in unsaturated flow. However, it is possible to apply such analysis to specific situations, such as the laboratory experiment of Torres and Alexander (2002) that is analyzed subsequently.

The first step is indeed the definition of scaling variables to be applied in the normalization process of the governing equations. All of them are of a similar form of those defined for the saturated case, yet the non-linear character of the unsaturated problem introduces additional difficulties. In fact, the non-dimensional form of the equation, and therefore the dimensional weights of the terms of the equation, depend on the system state.

4.3.1 The Scaling Variables For The Unsaturated Flow Case

The Reference Suction

As for the saturated case this reference value of the suction cannot be defined as function of domain properties. It depends on the changes induced by the boundary conditions, and more specifically on the variations of suction during the experiment. Since the boundary condition has different effects depending on the original state of the system, we may define the actual state and the solicited state. Therefore a quantity called ψ_r will refer to the actual state of the system, while the quantity called ψ_b will refer to the new system state which depends to the boundary condition. In this sense, the two reference suctions will be used for the non-dimensional form of the suction differentials:

$$\partial\psi^* = \frac{\partial\psi}{|\psi_b - \psi_r|} \tag{4.3}$$

There will be several non dimensional coefficients which depend to the system state, for convenience they will be evaluated with respect to the actual system state. This will lead to a safer analysis, which means that we are not going to overestimate the effects due to each single term.

The Variably Saturated Reference Time

Also in this case the most important scaling quantity is certainly the reference time, which refers to the temporal window that we want to analyze. Similarly to the saturated case, we defined the reference time as:

$$t_r = C(\psi_r)\frac{T(\psi_r)^2 L_r^2}{K(\psi_r)} \tag{4.4}$$

The non-linearity of the problem influences the reference time through the non-linear parameters $C(\psi)$, $K(\psi)$ and $T(\psi)$ which state respectively the slope of the retention curve, the unsaturated conductivity and the unsaturated tortuosity for a defined value of ψ. L_r is the reference length as defined for the saturated case. Using the reference time defined in (4.4) we can define the non dimensional time t^* as:

$$t^* = \frac{t}{t_r} \tag{4.5}$$

The Reference Unsaturated Velocity

As for the suction scaling variable the reference unsaturated velocity should be related to the real field dynamics that are to occur along the period of time in which the system will be simulated. Similarly to the saturated case the scaling velocity may be expressed as follows:

$$V_r = -\frac{K(\psi_r)}{\theta(\psi_r)}\left(1 + \frac{|\psi_b - \psi_r|}{L_r}\right) \tag{4.6}$$

The flow non-linearity is taken into account through the relative conductivity function, which depends to the state of the system. The non-dimensional velocity may then be defined as follows:

$$\partial v^* = \frac{\partial v}{V_r} \tag{4.7}$$

which may be employed for both velocity and differential velocity terms.

4.3.2 Non-Dimensional Form of The Variably Saturated Equations

We may now substitute into equations (4.1) and (4.2) the dimensional variables with the non dimensional coefficients multiplied by the scaling factors. This process will result, after some arrangements, in the following form of the continuity equation in (4.1):

$$\frac{\partial \psi^*}{\partial t^*} - \left(\frac{T(\psi_r)^2 [L_r + |\psi_b - \psi_r|]}{|\psi_b - \psi_r|} \right) \frac{\partial \theta^* v^*}{\partial z^*} = 0 \tag{4.8}$$

and the momentum equation in (4.2) becomes:

$$\frac{\partial v^*}{\partial t^*} + \left(\frac{V_r L_r C(\psi_r) T(\psi_r)^2}{K(\psi_r)} \right) v^* \frac{\partial v^*}{\partial z^*} + \left(\frac{g T(\psi_r)^3 C(\psi_r) L_r (|\psi_b - \psi_r|)}{V_r K(\psi_r)} \right) \frac{T^* \partial \psi^*}{\partial z^*} =$$

$$- \left(\frac{g T(\psi_r)^3 C(\psi_r) L_r^2}{V_r K(\psi_r)} \right) T^* - \left(\frac{g T(\psi_r)^3 C(\psi_r) L_r^2 \theta(\psi_r)}{K(\psi_r)^2} \right) \frac{T^* \theta^* v^*}{K^*} \tag{4.9}$$

For readability reasons, the reference velocity V_r has not been substituted into equation (4.9). Equations (4.8) and (4.9) represent the non-dimensional form of the 1-Dimensional vertical variably saturated flow model.

4.3.3 Analysis of The Non-Dimensional Coefficients

General Considerations

The non-dimensional coefficients in equations (4.8) and (4.9) depends on the field properties, boundary conditions and actual state of the system. Moreover, the field properties depend on the unsaturated coefficients used for the definition of the water retention curve and the relative conductivity functions. Therefore, the quantities that may be varied within the coefficients are several, if we employ a simple model such as the Brooks and Corey model for both the water retention curve and the relative conductivity function, we obtain eight reference quantities (K_s, γ, ψ_{cr}, θ_s, θ_r, ψ_r, ψ_b and L_r). In such circumstances it is prohibitive to perform a complete analysis which output should be the general conditions for the dimensional equivalence of the terms of the equations. However our objective is to study the occurrence of inertial effects in a specific soil type and for specific boundary conditions, therefore we may use the characteristics of the soil used within the laboratory experiments previously illustrated. The analysis will then focus on the specific conditions under which the experiments exhibited non-darcian flow. Unfortunately we cannot define accurately all the scaling factors, yet we may guess a representative value or a set of possible ones. However, as a next step in the analysis one may perform dimensional analysis by means of numerical simulations.

Dimensional Comparison of The Coefficients

Applying the dimensional analysis to our specific case, calls for the definition of the scaling variables previously defined. The first step is to approximate the water retention curve, from which we can evaluate a guess for $C(\psi)$. We employed the simple Brooks and Corey model in (1.22), for which we found approximate fitting parameters of $\gamma = 2.0$ and $\psi_{cr} = -0.06$m (The same model and parameters have been used for the relative conductivity function, for which unfortunately we do not have the real trend and hence we might have only a guess.

From the paper of Torres and Alexander (2002) we obtained the remaining scaling quantities but the reference length L_r. For this scaling variable we guessed three possible values, that is $L_r = 0.001$m which should be a representative value for a very sharp infiltrating front, $L_r = 0.01$m for an average yet still sharp front and $L_r = 0.1$m for a smoother front. From the TDR measurements we estimated a value for $\theta_r = 0.21\text{m}^3/\text{m}^3$ in the pre-spike region, while from the tensiometers readings we estimated $\psi_r = -0.09$m and $\psi_b = -0.06$m, respectively for the pre-spike and spike regions. These are all approximations since the instruments readings were affected by measurement errors. From these values, we could infer the approximate values for $C(\psi_r) = 3.65\text{m}^{-1}$ and $K(\psi_r) = 1.44 \cdot 10^{-4}$m/s. For simplicity the tortuosity factor has been set equal to unity in the calculations.

The analysis is focussed on studying the structure of the momentum equation (4.9), for which we already have the order of magnitude of the first term, in fact its coefficient is unity and hence of order zero. For convenience we may refer to the coefficients as Ci with $i = 1, 5$, where for instance $C1$ represents the first and $C5$ represents the last coefficients.

Table (4.1) reports the magnitude of each of the terms as a function of the reference length.

$L_r[m]$	$C1$	$C2$	$C3$	$C4$	$C5$
0.001	$1 \cdot 10^0$	$5.38 \cdot 10^{-1}$	$3.50 \cdot 10^2$	$1.16 \cdot 10^0$	$3.62 \cdot 10^2$
0.01	$1 \cdot 10^0$	$6.95 \cdot 10^{-1}$	$2.71 \cdot 10^4$	$9.04 \cdot 10^2$	$3.62 \cdot 10^4$
0.1	$1 \cdot 10^0$	$2.25 \cdot 10^0$	$8.35 \cdot 10^5$	$2.78 \cdot 10^6$	$3.62 \cdot 10^6$

Table 4.1: Momentum equation coefficients magnitude for different reference length values in the specific case of Torres experiments (Torres and Alexander, 2002).

It is evident that for all the reference lengths, quantifying how sharp is the front, the inertial terms are at least two to three orders of magnitude smaller than the other terms. Smaller differences arise when considering very sharp fronts (Lr=0.001), but also in this case the inertial terms can be neglected in comparison to the other terms. Furthermore the very conductive character of the analyzed soil together with the very sharp behavior of the water retention curve are extreme features for a soil, so that for moderate cases, such as a real sandy soil, one should expect larger differences. Nonetheless, boundary conditions exert a minor role on the relative importance of the terms Ci.

Indeed the above analysis is only qualitative since there is a lot of uncertainty in the definition of the scaling variables, therefore a numerical investigation may help in shedding new light in the dynamics controlling this problem.

4.4 Numerical Solution

4.4.1 Overview

In this section we report the numerical solution of equations (4.1) and (4.2) applied to the column test case exposed in the previous paragraphs. The numerical technique is the same used for the saturated case, therefore a staggered grid approach has been employed for this numerical problem where the two unknowns are respectively the water content θ and the fluid velocity in the vertical direction v_z. The aim is to verify the results of the non-dimensional analysis performed previously.

The staggered grid discretization to be used for the problem solution is depicted in figure (4.2), which is very similar to the one used in the saturated case, the only difference is that the conserved variable for the continuity equation is the water content.

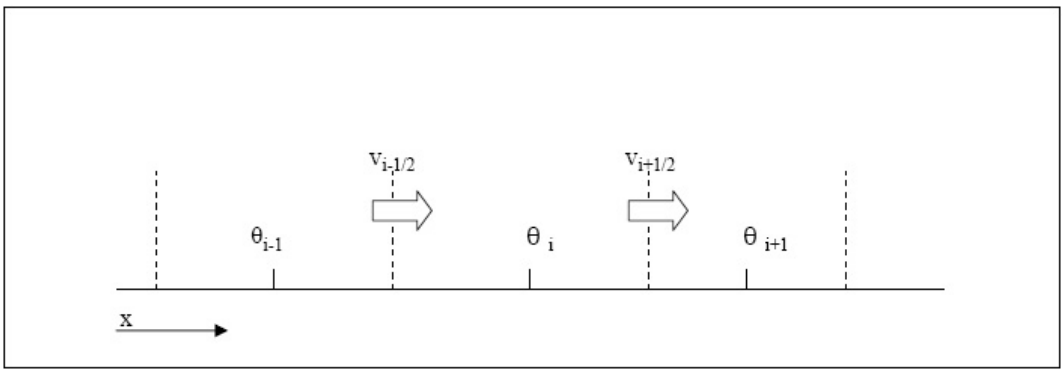

Figure 4.2: Staggered grid layout used for the solution of the inertial system of equations.

In order to obtain accurate mass balance we want to keep equation (4.1) in conservative form. For the particular discretization employed, this aspect involves a problem in the approximation of the numerical fluxes, because they depend to both unknown which unfortunately are not defined in the same point. In other words the numerical form of $\partial(\theta v_z)/\partial z$ has been implemented as:

$$\left.\frac{\partial \theta v}{\partial z}\right|_i^{n+1} = \frac{\overline{\theta_{i+1/2}^{n+1}} v_{i+1/2}^{n+1} - \overline{\theta_{i-1/2}^{n+1}} v_{i-1/2}^{n+1}}{\Delta z} \tag{4.10}$$

where for instance:

$$\overline{\theta_{i+1/2}^{n+1}} = \frac{\theta_i^{n+1} + \theta_{i+1}^{n+1}}{2} \tag{4.11}$$

which is implicit and therefore approximated within the Picard iterations.

The application of the boundary conditions is the same as for the saturated case.

4.4.2 Simulations Setup

The water retention function has been modeled with the model of van Genuchten (1980) in (1.24), which parameters has been set equal to $\alpha = 12.$ and $n = 3$ (see figure (4.4)). Initially, we did not take into account the hysteresis of the water retention function, subsequently we included it unfortunately without obtaining significant improvements. We will see later that such hysteretic trend has nothing to do with the non-darcian flow evidenced by the laboratory experiments.

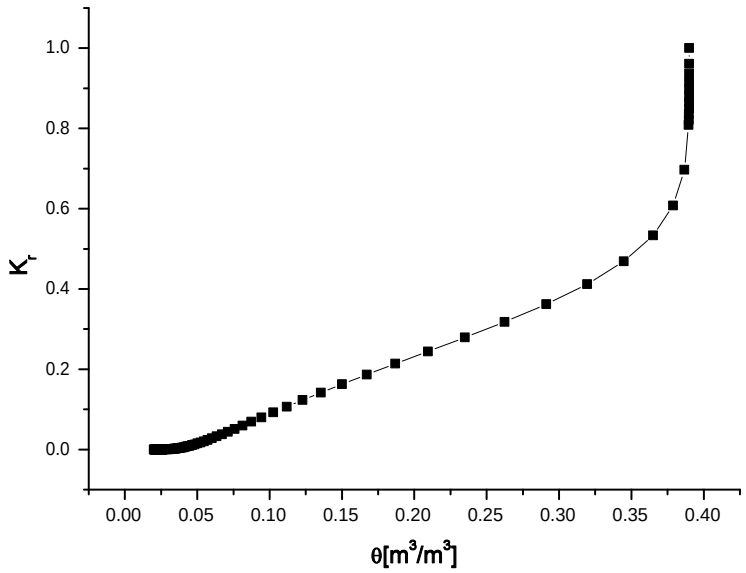

Figure 4.3: Calibrated relative conductivity function (Van Genuchten model with $\alpha = 12$ and $n = 1.55$)

The other parameters required for the simulations setup, and that we could infer from the published paper of Torres and Alexander (2002), are the column length, the rainfall rates and the saturated hydraulic conductivity. The main problem is that no relative conductivity trend has been reported by Torres and Alexander (2002), therefore we utilized a reasonable water retention curve. From the irrigation experiments of Torres and Alexander (2002) we could infer that in the pre-spike region, which is considered to be an equilibrium state, the inflow rate applied on top of the column gave rise to an average water content of approximately $0.21\text{m}^3/\text{m}^3$, while at the peak the water content increases to approximately $0.235\text{m}^3/\text{m}^3$.

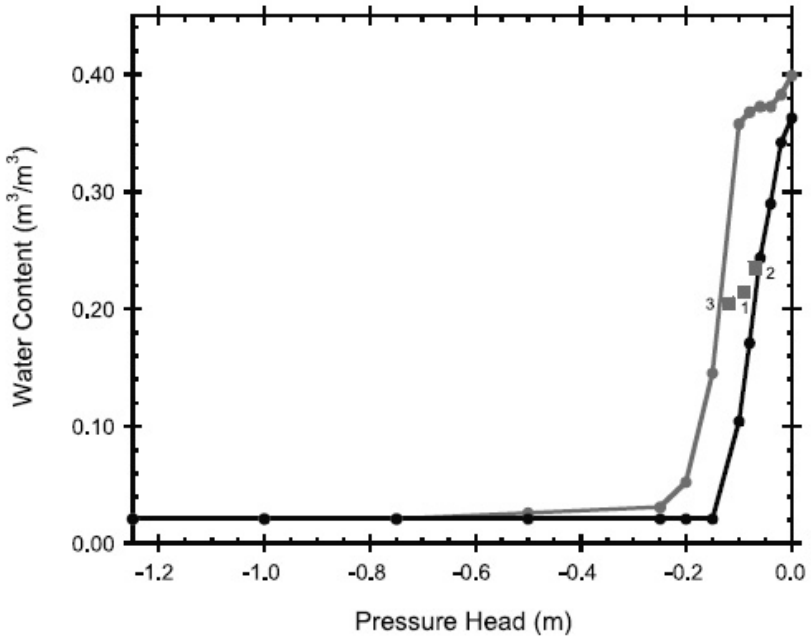

(a)

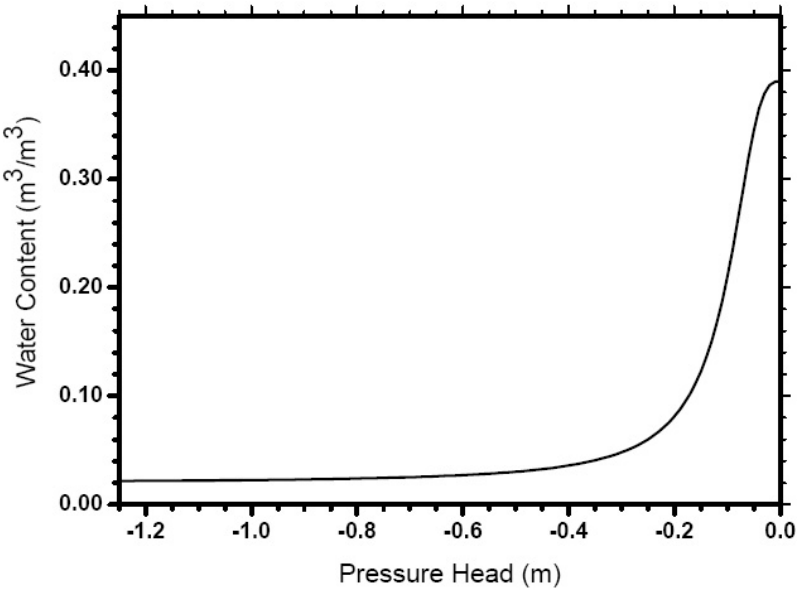

(b)

Figure 4.4: Water retention curve of a) Torres experiment (Torres and Alexander, 2002) and b) fitted for the numerical applications.

By employing the unsaturated conductivity model of van Genuchten (1980) with the same parameters used for the WRC, we were not able to obtain accurately the water content levels reported by Torres and Alexander (2002). Therefore we tried to calibrate the relative conductivity curve in order to obtain a reasonable agreement with experimental observations. The value of the parameters for the calibrated relative conductivity reported in figure (4.3) were $\alpha = 12$ and $n = 1.55$.

4.4.3 Results and Discussion

We simulated the experiment of Torres and Alexander (2002) by solving numerically equations (4.1) and (4.2), and compared the results in figure (4.5) with the solution of the Richards equation. As anticipated by the dimensional analysis no differences are observed between the two models. Additional simulations with different parameters of the van Genuchten's model and boundary conditions confirmed what suggested by the simulations of the above experiment.

Therefore the dimensional analysis is hereby confirmed by the numerical simulations, and hence we conclude that the non-darcian flow observed in the experiments cannot be explained as the effect of the inertia terms in the momentum equation as claimed by Torres and Alexander (2002) who referred to an early study of Germann and Di Pietro (1999).

However we noticed that, if we extrapolate the suction and water content profiles from the data reported by Torres and Alexander (2002), we see that their trend is very irregular as if no theoretical hydrostatic conditions are reached. Furthermore, if we employ the relative conductivity function evaluated with the same parameters as for the WRC ($\alpha = 12$ and $n = 3$), the water content profiles along the column would be less than those observed during the experiment. Therefore, it seems that the column is over-storing water. From these considerations one can envision the formation of a capillary barrier which shields subsurface percolation. A capillary barrier may form where a unit with relatively small pores or fractures overlies a unit with relatively large pores or fractures (Wu et al. (2002) and Montazer and Wilson (1984)).

This conceptual model is typically utilized in order to model flow in variably saturated porous formations composed by units with different textural and hydraulic properties. Common applications ranges from agriculture, where the objective is to contrast moisture reduction due to gravity in the root zone (Sinaj et al., 2002), or the hydraulic isolation of contaminated zones in order to prevent them from delivering pollutants to the surroundings (Rooney et al., 1998). A similar phenomenon may develop in soil because of local variability on formation's porosity.

In order to explain how this shielding mechanism acts let us consider a porous media with a known average water content. In such a situation water is held at the contact with the grains by the meniscuses that form because of capillarity effects. These meniscuses can sustain a certain amount of water before breaking and letting water to outflow the

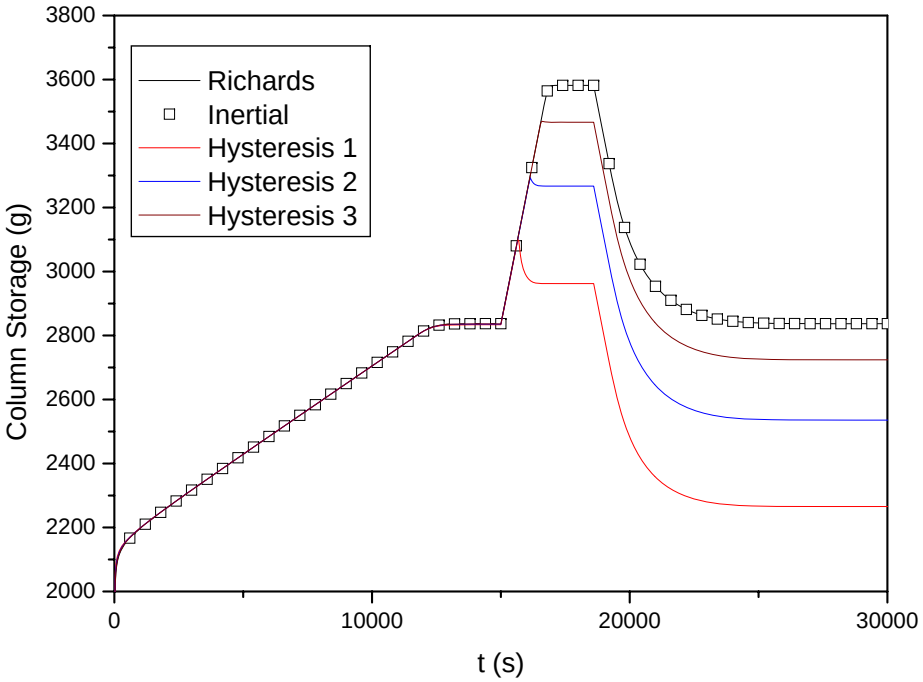

Figure 4.5: Comparison of the numerical evolution of the column storage simulated with all the considered models.

pores. Figure (4.6) shows a water drop on a flat surface having equilibrium contact angle equal to θ. If we give an inclination to the supporting surface, we see that the drop exhibit a different contact angle in its head and tail, called respectively advancing and receding angles, and the drop will not move until these angles reach their maximum value. See for instance the capillary tubes on the right of the figure, their aim is to explain the behavior of a moving meniscus. When the water level increases in the tube, the meniscus is allowed to move when its contact angle reaches a maximum advancing value θ_{max}. In the opposite, when the water level is decreased, the meniscus starts to recede after its contact angle reaches the minimum receding value θ_{min}. In any case the movement will occur after the driving forces (capillarity or gravity) overcome the friction between the wetting liquid and the tube material.

If we employ these two concepts to unsaturated porous media flow, we can assume that each pore behaves like a capillary tube with an irregular shape. Therefore a fine pore my either be connected with a smaller or a larger pore. In this scenario, a moving meniscus must first win the friction with the grain material and second it must deal with the capillary barrier effect at every change in the pore size.

If the pore structure of a soil is very regular, i.e. in every point the pore structure is

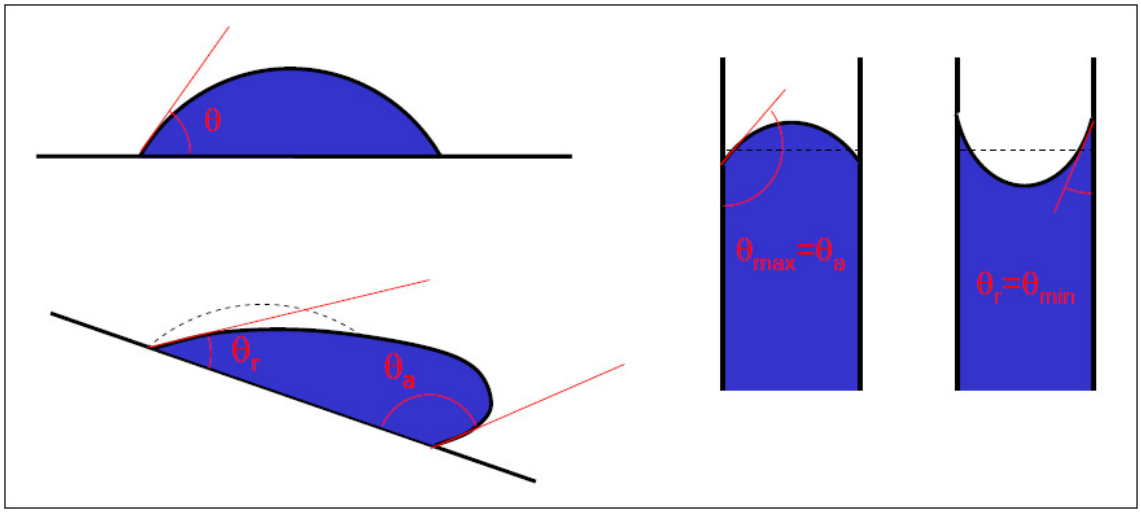

Figure 4.6: Hysteresis of the contact angle, where θ_a is the advancing angle and θ_r the receding angle.

the same, the capillary barrier does not develop. However the pore structure of a real soil is heterogeneous, and as such the pore distribution might reveal significant changes from point to point. Therefore the grains are not distributed regularly, but we might find zones of smaller and zones of larger grain sizes at a small scale. Therefore, stagnation zones originate requiring larger energy to be mobilized. This energy may be provided by increasing rainfall intensity which through the upper boundary condition transmit energy to the system. This mechanism creates stagnant zones where part of the infiltrating water is immobile and sustained by the meniscuses, while water flowing into larger pores bypass this less porous part of the porous formation because it requires less energy to drain.

The sustaining capability of the so formed capillary barriers will be effective until some threshold water content is reached. At such occurrence several mechanisms may exert a role in breaking the meniscuses. The overpressure above such zones or the lateral spreading of water right below the barriers might weaken the sustaining capillaries enough to allow the water outflow. From a conceptual point of view, the threshold water content above which the stagnant zones start to take part in the runoff process, might be identified with the moisture level at which the water within the soil is considered to be theoretically fully interconnected. This point is usually identified with the water content level at which the concavity of the WRC changes its sign. Figure (4.7) shows schematically the behavior of the conceptual model explained above. In the pre-spike, at low irrigation rate, stagnant zones forms above locally formed capillary barriers (figure (4.7a), the circle indicates the capillary barrier zone).

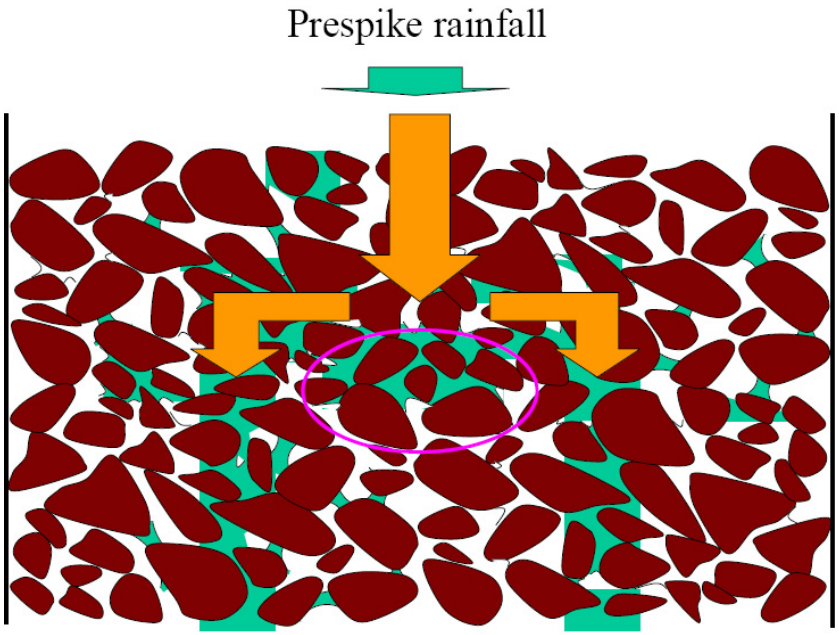

(a)

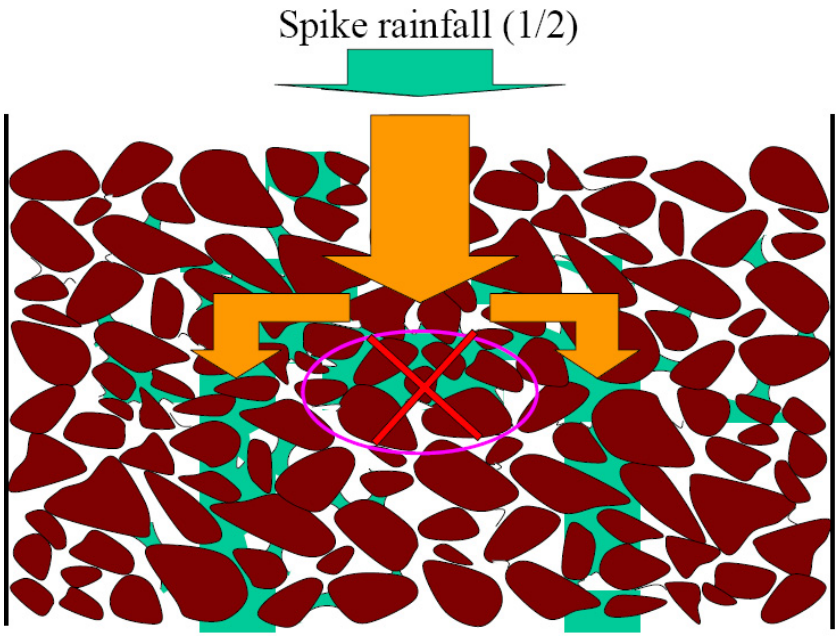

(b)

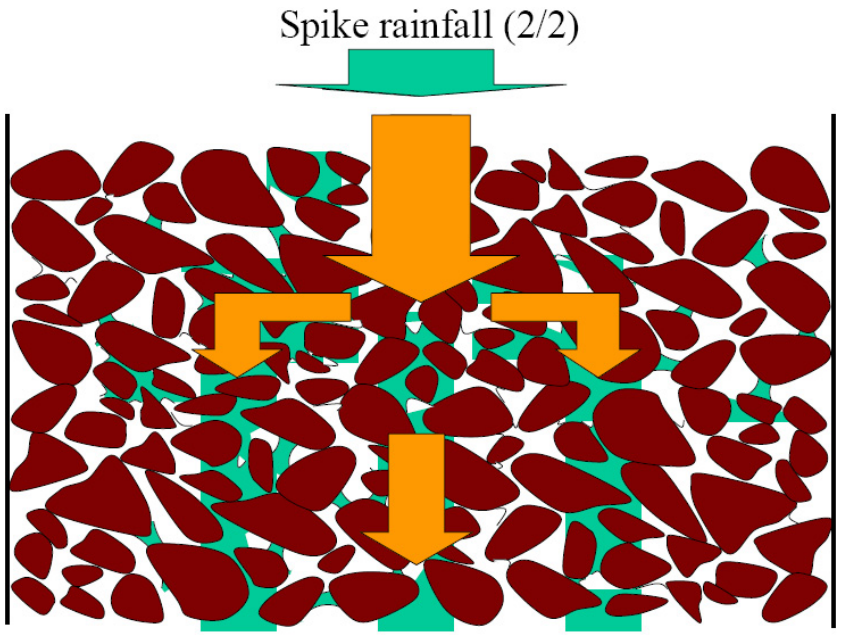

(c)

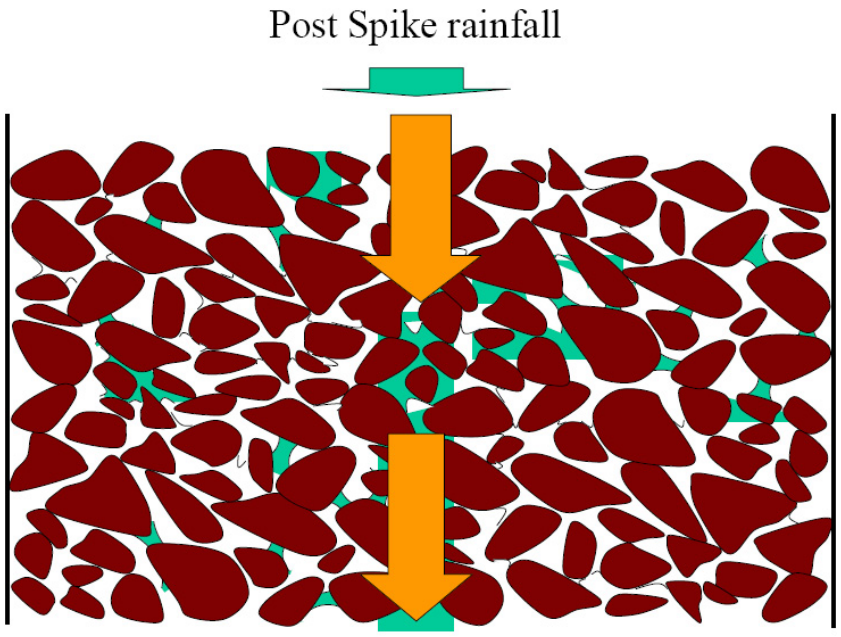

(d)

Figure 4.7: Conceptual application of the capillary barrier concept to the experimental evidences exposed by Torres and Alexander (2002).

In such situation the excess rainfall will bypass laterally the stagnant zone. When the irrigation rate increases significantly during the spike, the capillary barrier is weaken until rupture, and the stored water is released by the stagnant reservoirs (see figures (4.7b) and (4.7c)).

In the post-spike (figure (4.7d)), when irrigation rate is set again to a low intensity, since the capillary water is now fully interconnected throughout the soil, the stagnant zones are not allowed to reform. Therefore the soil exhibits a lower water content than in the pre-spike period. In this situation the moisture interconnection is ensured unless very dry conditions are reached again. In such conditions the capillary barriers are allowed to form again.

4.4.4 Numerical Application of The Capillary Barrier Concept

The problem now is how to find a mathematical model capable of describing the threshold mechanism at the base of the conceptual model exposed in the previous paragraph.

A way to proceed is to assume that the unsaturated conductivity function exhibits a sort of hysteretic behavior, with the only difference that its functioning is not the classical one, the only common aspect is that it is still based to the existence of two curves. In our scenario there are two threshold values of the water content to be defined. When the moisture level rises above the first one, there will be the establishment of full interconnected flow, while when it falls below the second threshold this will create again non-interconnected flow conditions.

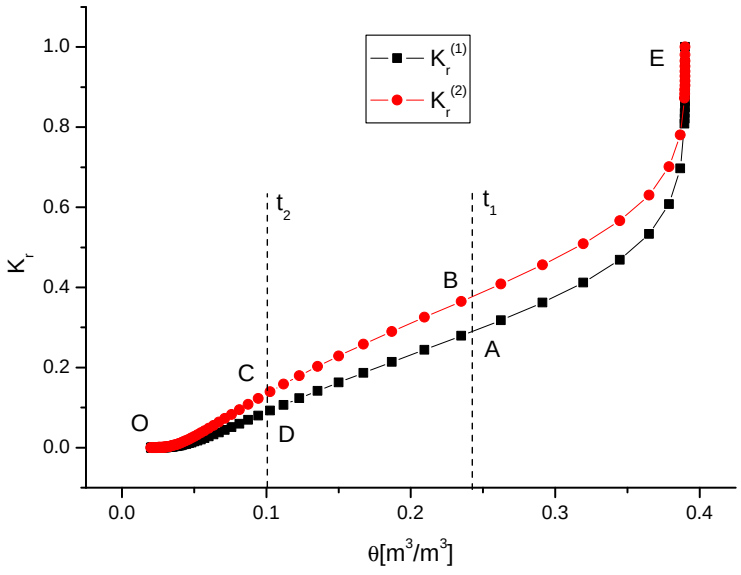

Figure 4.8: Hysteretic unsaturated conductivity function employed for the numerical simulations of the capillary barrier effect.

Let us analyze this model on the base of figure (4.8). Starting from a dry soil $\theta < t_2$, all the wetting and drying cycles are described along the $K_r^{(1)}$ curve in the segment (ODA) until the threshold moisture t_1 is reached. After this value has been exceeded, the moisture interconnection along the soil has been achieved, and hereafter the conductivity curve that is to be used for describing both wetting and drying cycles switches to $K_r^{(2)}$. The wetting and drying cycles will move along the segment (CBE). If the soil dries below the t_2 threshold, the soil moisture interconnection goes lost and the fluid motion switches again to curve $K_r^{(1)}$. Such type of threshold behavior is fairly observable in the experimental data reported by Wildenschild et al. (2001). The authors performed several laboratory experiments in order to measure the water retention and the relative conductivity of two different sandy soils. Starting from fully saturated conditions they measured the main drying curves of both water retention and conductivity functions. Especially for the well graded soil, the data reveal a trend similar to that of the $(EBCDO)$ curve in figure (4.8). These evidences perfectly agree with the threshold conceptual model explained above.

The simulations used with this type of conductivity model produced very good results. Figure (4.5) shows the evolution of the column storage evaluated numerically with the three different models, i.e. the Richards, the inertial and the conductivity hysteretic models.

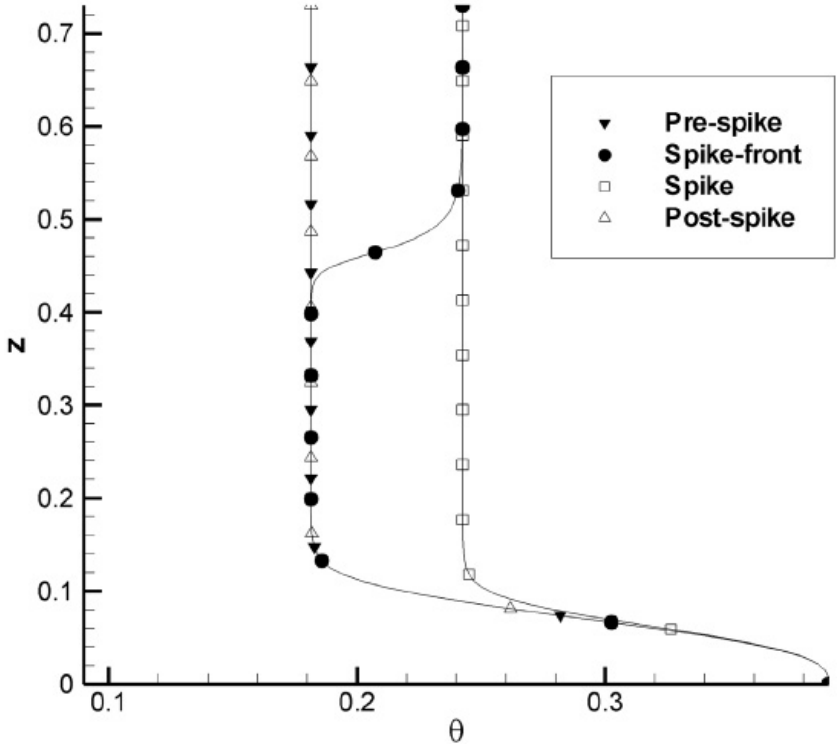

(a)

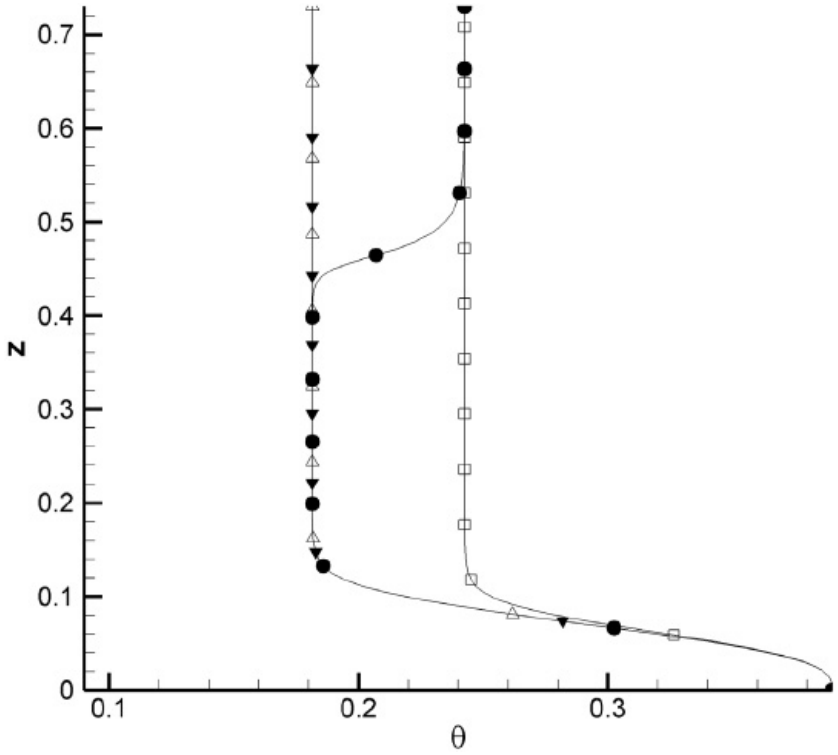

(b)

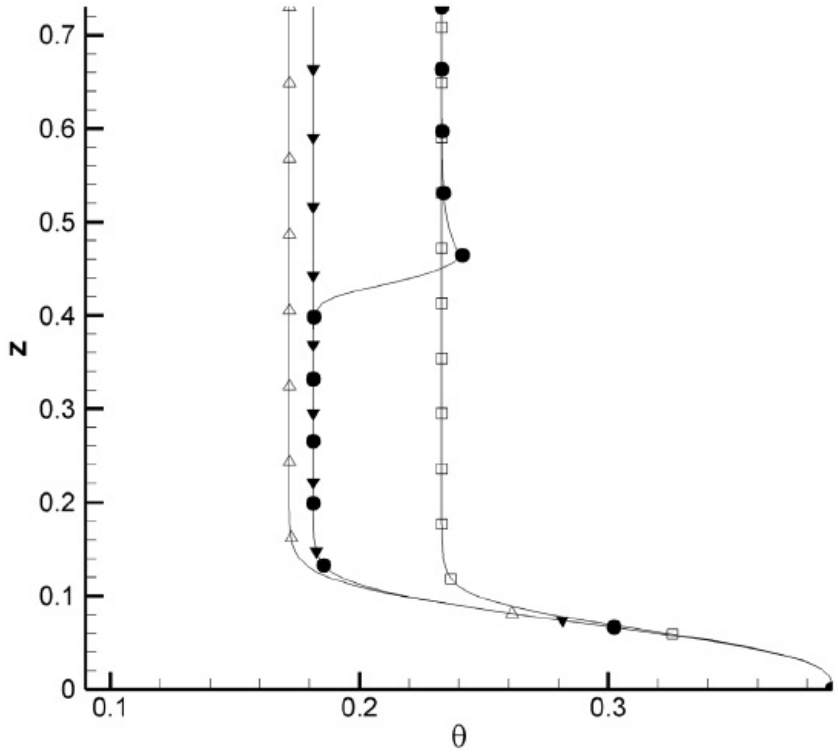

(c)

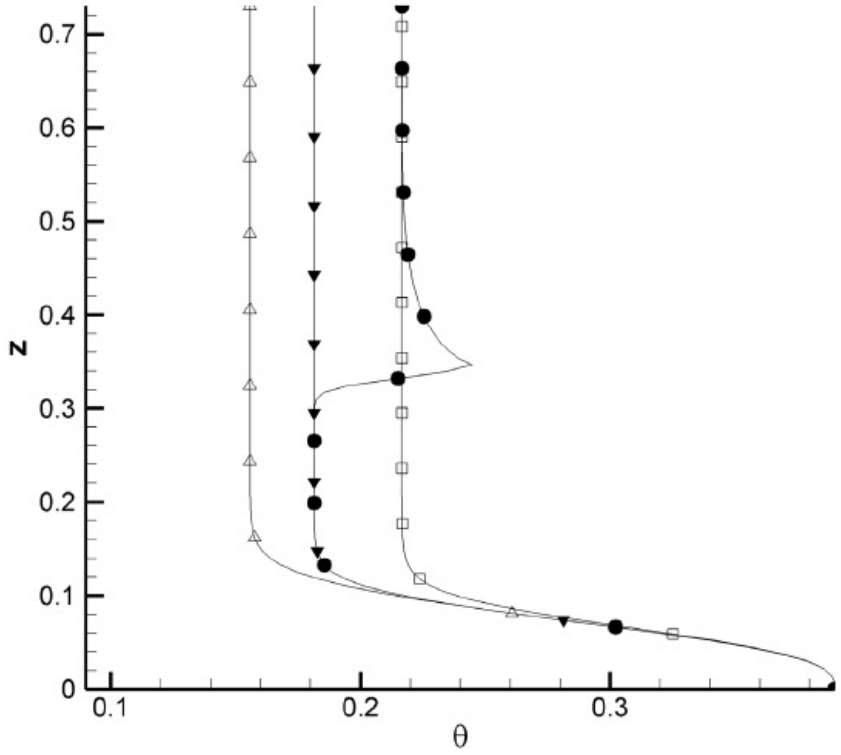

(d)

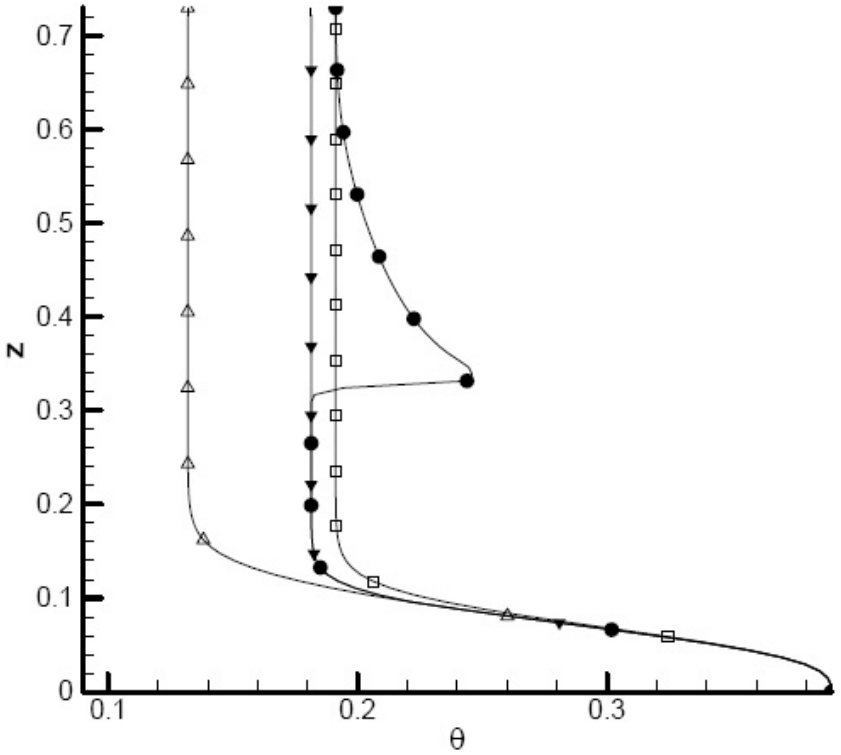

(e)

Figure 4.9: Pre-spike, spike and post-spike stationary profiles and spike advancing front profile evaluated numerically with a)Richards model, b)Inertial model and c),d) and e) with the threshold hysteretic conductivity model with the value for the n parameter of $K_r^{(2)}$ equal respectively to 1.6, 1.7 and 1.9.

As reported in the plot, the column storage simulated with the threshold hysteretic conductivity model is the only one that exhibit a qualitative agreement with the observed experimental results of Torres and Alexander (2002). Therefore the proposed conceptual schematization is capable of simulating correctly the phenomena highlighted in such experiments.

Figure (4.9) shows the numerical water content profiles evaluated with all the three models. The profiles are representative of the pre-spike, spike and post-spike regions and a spot of the propagation of the spike infiltrating front is reported too. Figures (4.9a) and (4.9b) represent the solution achieved with the Richards and the inertial models. They are exactly the same, no differences between these two models have been observed since the magnitude of the inertial terms have been found to be much lower than the Darcy-Buckingham's terms. Furthermore the pre- and post-spike profiles are equal, and this means that the column storage is conserved.

Figures (4.9c), (4.9d) (4.9e) show the moisture profiles evolution evaluated with the threshold hysteretic conductivity model for three different parameterization of the $K_r^{(2)}$ curve. The choice of the parameters has been done arbitrarily. Given the parameters for $K_r^{(1)}$ which are $\alpha = 12$ and $n = 1.55$, we modeled the three $K_r^{(2)}$ curves by setting the n parameter value to respectively 1.6, 1.7 and 1.9. The advancing spike front initially exceeds the upper threshold value which has been set to be equal to $t_1 = 0.24\text{m}^3/\text{m}^3$, that is approximately the water content at which the WRC concavity changes. As the front advances, it modifies the type of flow within the soil it went through from non-interconnected to interconnected, allowing the stagnant zones to release the previously stored water. This effect results in lower values of water content behind the advancing front peak and therefore revealing a decrease in the column storage.

Unfortunately the above simulations are not perfectly fitted to the experimental data because we did not have the real relative conductivity function, yet the results are rather satisfactory. However, in order to verify our speculations about the physical principle underlying the phenomena observed by Torres and Alexander (2002), we decided to design our own column experiments. The work is in progress, but in the next section a brief introduction to the design of the laboratory apparatus is reported and discussed.

4.5 Laboratory Experiment Design and Setup

After the theoretical and numerical considerations discussed in the previous section, we designed a laboratory column for infiltration experiments. The objectives are to further investigate the several experimental evidences encountered in literature and briefly mentioned in the introduction of the present chapter. However the first task is certainly to examine our theoretical speculations about the occurrence of threshold hysteretic-like

behavior of soils.

4.5.1 Column Design

The column body is composed of a series of independent 20cm long and 20cm internal diameter modules (see figure (4.10)). This feature allows us to choose the total height of the experimental apparatus. It has been designed in a modular way in order to allow the maximum experimental flexibility. Every module is linked with the neighboring ones by means of 8 screws, an o-ring ensures the stagnancy at each junction between two modules. The modules are laterally perforated in order to allow the column to be instrumented. The column is set over a filtrating base (figure (4.11)), where a perforated disk allows water to outflow while the porous material is avoided from passing through the filter by a geo-synthetic fabric membrane. The base outflow is routed through a tube which can be used for both the outflow in case of top infiltration experiments, and the inflow in case of bottom infiltration experiments.

Irrigation is provided by means of a rainfall head designed appositely for our experiments. This head is composed of a stagnant chamber where a peristaltic pump ensures inflow from a tap placed on top (figure (4.12a)), while water is delivered from the bottom through 300 needles which perfectly simulate rainfall drops (figure (4.12b)). Each needle acts like a capillary tube, therefore if we set a homogeneous pressure head on top of them, the outflow will be the same for all of them, since they obey to the Poiseuille's law. In order to ensure homogeneous pressure distribution over all the needles it is necessary to place the head perfectly horizontal. We tested the effective accuracy of the water distribution over the irrigation area with various head inflow rates and found satisfying results, the error is in the order of a few percentage (<5%). In order to fill the head chamber, a Venturi tube is applied on top and water is allowed to be sucked through the needles which draw water from a bottom placed reservoir. However some of the needles may be obstructed by air bubbles. In any case we observed that a very low number of needles do not take part in the irrigation process at a time, and they are homogeneously distributed over the irrigation area. Sometimes, simply hitting them a couple of time with some iron tool, i.e. a screw driver, triggers conduction since the air bubble is lead to flush away by the caused vibrations.

We performed also experimental tests in order to make sure that the geo-synthetic membrane do not modify the hydraulic behavior of the column, i.e. by acting like a low conducting layer. We tested it against simple infiltration experiments, where a homogeneous standardized sand of grain size between 0.8mm and 1.2mm has been used in 10cm increments, packed all in the same way, and at each of which the saturated hydraulic conductivity of the actual soil column has been experimentally measured.

Figure 4.10: Column module in PVC, 20cm high and 20 cm long.

Figure 4.11: Base of the column with perforated filter.

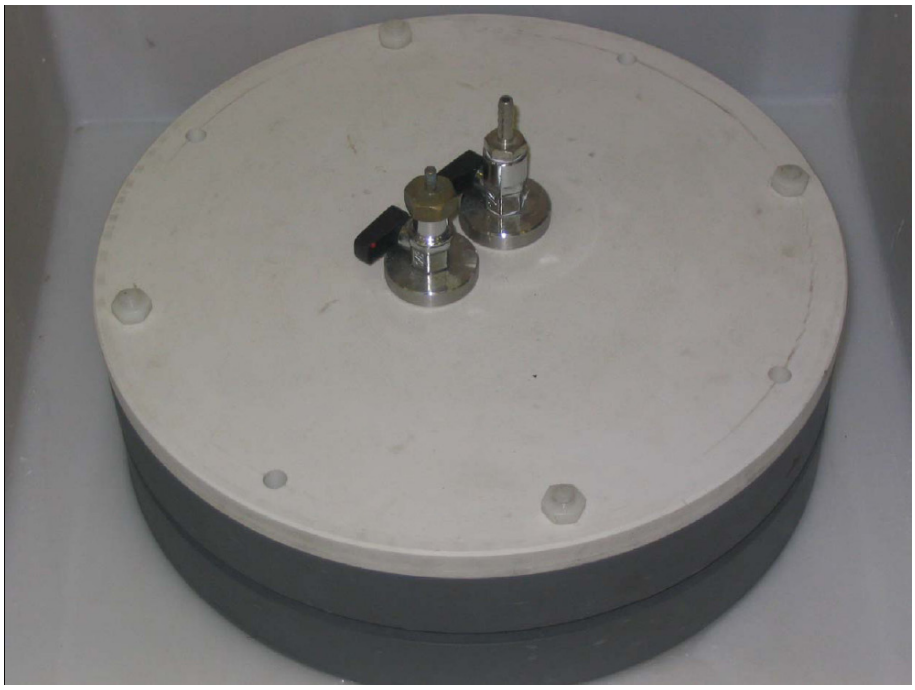

(a)

(b)

Figure 4.12: Column head, a) top view and b) bottom view.

Starting with 10cm soil column and ending with 80cm soil column a constant water level was applied on top of them. At stationarity, the outflow was collected in a pluviometer cup while the input was monitored by a precision balance. The saturated hydraulic conductivity was then measured on the basis of 10min constant flow rate experiments. For all the soil increments we measured approximately the same hydraulic conductivity, in the order of 10^{-4}m/s.

All these tests, performed in order to assess the correct behavior of the column parts, have produced satisfactory results. The next step is to test and calibrate all the instruments to be employed in the experiments.

4.5.2 Instrumentation Overview

In order to monitor unsaturated flow, suction and water content need to be accurately measured. We acquired so far 3 SWT5 minitensiometers provided by Delta-T engineering (UK) for accurate suction measurements in the range +100KPa to -85KPa, with accuracy of +/- 0.2KPa. We are aware that the minitensiometer's readings are very punctual and might be poorly representative of the real suction scenario, yet we chose them for their very low flux disturbance. Anyway, if they reveal to be unsuitable for our objectives we will switch to tensiometers with a bigger ceramic cup. For the moment we do not know their effective capability to capture representative values of the real suction distribution in soil, and this is why we decided to get only 3 of them.

In order to monitor water content, we acquired the Champbell Sci. TDR100 system with a SDMX50 multiplexer and 8 TDR probes 7.5cm long.

The column outflow is going to be monitored with a 0.2mm tip pluviometer, with declared accuracy of 1-2% of the total rainfall and which we tested with several rainfall rates.

A National Instruments DAQ card is to be used to acquire all the instruments readings by means of a Labview code which is actually under construction.

The last instrument we acquired is the peristaltic pump to be used for supplying water to the rainfall head, a Watson-Marlow 323D model has been selected together with 1.6mm and 3.2mm marprene tubes. We tested its pumping rate reliability, and the results are that it performs very well for RPMs in the range 2-200, for which the water discharge through the 1.6mm and 3.2mm tubes varies respectively between 0.75-50ml/min and 2.6-170ml/min. After the 200RPM the pump looses outflow steadiness. In our experiments we will need discharges in the range 10 to 100ml/min, therefore we may employ the 3.2mm marprene tube to maintain a reliably constant irrigation rate.

4.5.3 Ongoing Work

For the former column infiltration tests we decided to use an ideal sand with a uniform grain size distribution in the range between 0.075mm and 2mm. After we constructed the sand, we started the characterization of its hydraulic properties. The evaluation of the water retention curve is actually ongoing following the work of Tarantino and Tombolato (2005), the former surveyed points reveal that it will be contained between 0 and -5KPa suction (the sand used by Torres and Alexander (2002) was in the range 0,-2KPa). The apparatus used for the determination of the WRC is the load cell reported in figure (4.13) where suction measurements are collected by means of TN tensiometers (Tarantino, 2004) at various loads. The aim is to find a set of WRCs which depend to the soil compaction level. This is done in order to select an appropriate compaction level for which the WRC shape is not too narrow. In fact, a high compaction of the sandy soil lead to WRCs in the range 0,-1KPa, which would be too narrow for accurate readings made with our instrumentation.

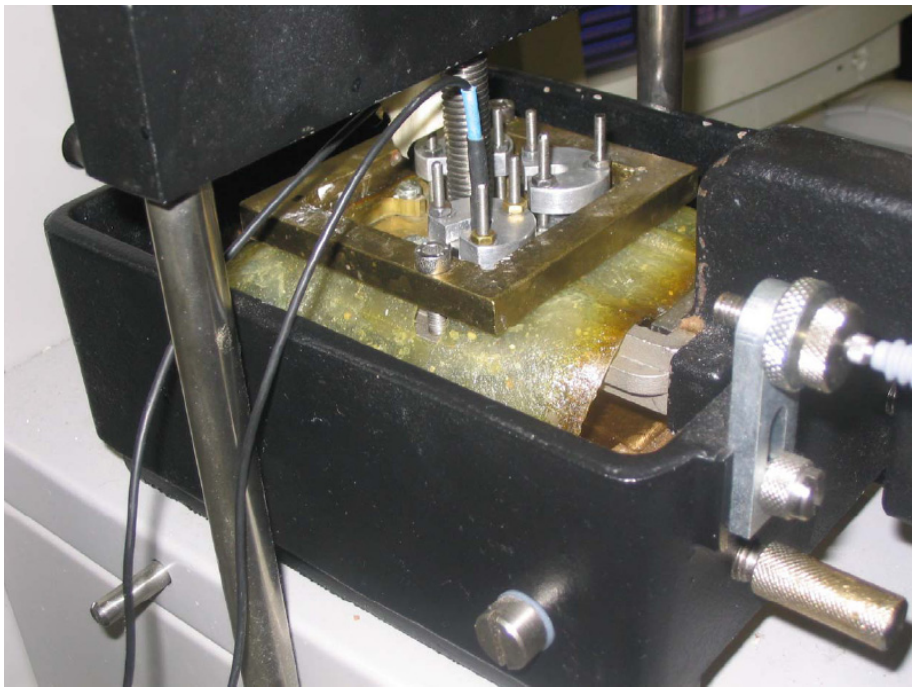

Figure 4.13: Load cell used for the measurement of the WRC related to the selected sandy soil.

The actual ongoing work is focussed onto many aspects such as the WRC measurement, the calibration of the measurement instruments and the continuation of the column modules construction. We deem that in two months time the whole apparatus will be ready for the former tests.

4.6 Summary

In this chapter we analyzed the inertial-type flow observed in laboratory tests by Torres and Alexander (2002) and formerly discussed by Germann and Di Pietro (1999). We performed numerical and theoretical analysis of the problem and hypothesized a conceptual model for its physical explanation. The occurrence of a threshold hysteretic type behavior of the unsaturated conductivity function has been hypothesized and numerical simulations have been performed to demonstrate the effectiveness of our speculations. However, since Torres and Alexander (2002) did not report all the required data, we could not perform accurate comparison between simulations and data. Therefore we designed our own experiments to further investigate the analyzed phenomena and to confirm our conjectures.

5 Conclusions

The work done in this thesis evidenced many aspects related to the actual way of modeling the subsurface flow processes. The importance to correctly modeling the porous media flow dynamics is crucial in many hydrological fields, such as aquifer restoration, risk assessment and runoff generation. Therefore the objectives of this work were to further investigate several issues concerning the uncertainty lying beneath our modeling capabilities of the real fields dynamics. In particular we studied two main aspects related to this problem.

The first one concerned an investigation on the reliability of numerical models for the solution of the flow equations in non-homogeneous cases (Chapter 2), with particular interests on the numerical models structure and their interaction with the variability of the hydraulic parameters field. For this problem we focussed the attention to the saturated stationary case, and with particular attention to the stochastic modeling of flow and transport phenomena. The results indicate that in presence of strong variability in the conductivity field, the numerical model we are to employ for the flow field solution may exert several type of drawbacks in the reliability of the approximate solution. The most important aspect arisen from this study concerns the way a scheme evaluate approximate inter-cell fluxes. This issue might have significant influence on the stochastic representativeness of the numerical solution with respect to the hydraulic conductivity field structure. In particular we found that the classical schemes, CG and MH, reveal a more robust behavior than newly proposed post-processing schemes in case of heterogeneous domain. Furthermore, since CG approximate the inter-cell fluxes by means of the arithmetic mean of the hydraulic properties, it leads to solutions that are more in line with second order stochastic solutions. In the other hand the MH employs the harmonic mean of hydraulic properties, and this lead to a smoother velocity flow field. It seems that this latter method solves the problem over a smoother hydraulic conductivity field than the original one.

The second main aspect studied concerns the investigation on the validity of the assumptions under which the momentum equation might be reduced to the Darcy's law in the saturated case (Chapter 3), and to the Darcy-Buckingham's law in the unsaturated case (Chapter 4). For the first case we compared the order of magnitude of the different terms within the momentum equation, and found some general guidelines that can help to understand in which cases the inertial terms in saturated flow can be neglected respect to the Darcy's terms. Furthermore we investigated numerically the reliability of

our dimensional analysis and found good agreement between them.

The second case concerned the occurrence of inertial-type flow in unsaturated soil. This work was based on some experimental evidences published recently by Torres and Alexander (2002) and formerly by Germann and Di Pietro (1999). We conducted a dimensional analysis of the governing equations in order to see whether the inertial terms in the momentum equation might have some effect in unsaturated flow, and found that the magnitude of such terms is far lower than those representative of the Darcy-Buckingham's law. We also confirmed numerically the dimensional considerations, where we found that considering or not the inertial terms lead to the same solution. After this finding, we further investigated the experimental problem from a theoretical point of view. Upon a conceptual explanation, we concluded that the observed effects are probably due to the occurrence of a threshold hysteretic-type behavior of the unsaturated conductivity function. We then modeled numerically our hypothesis and found that they might explain very well such false inertial effects. Unfortunately we could not perform an accurate comparison between the numerical results and the experimental data, because the authors did not report all the required information. However, we started to design our own experiments and hopefully we will confirm our speculations in next few months.

This unsaturated flow phenomena, if experimentally confirmed, might exert a relevant role in hillslope hydrology, shedding light to some unexpected behavior of the vadose zone dynamics.

List of Figures

1.1 Schematization of Darcy's law experiment. 8
1.2 Limits of the validity of Darcy's law related to Reynolds number values. . . 10
1.3 General shape of the unsaturated hydraulic conductivity: a) K(θ) ; b) K(h) ($h = z + \psi$) (Musy and Soutter, 1991). 12
1.4 General shape of the water retention curves for some types of soil. Taken from http://research.umbc.edu/ jgwo/Courses/CompSubHydrol-I /Homework01.html. 15

2.1 Mass balance control volume for CG scheme also referred to as Voronoi cell 25
2.2 Homogeneous domain for test case 1 with unitary hydraulic conductivity. . 28
2.3 Heterogeneous domain for test case 2, all the blocks report a conductivity value which is proportional to the unitary one (**I**). 30
2.4 Heterogeneous domain for test case 3, all the blocks report a conductivity value which is proportional to the unitary one (**I**). 32
2.5 Comparison between first order analytical solution according to Rubin (1990) and numerical longitudinal (a)u_{11}) and transversal (b)u_{22}) velocity covariance functions for $\sigma_Y^2 = 0.2$. 38
2.6 Comparison between first order analytical solution according to Rubin (1990) and numerical longitudinal (a)u_{11}) and transversal (b)u_{22}) velocity covariance functions for $\sigma_Y^2 = 1$. 39
2.7 Comparison between first order analytical solution according to Rubin (1990) and numerical longitudinal (a)u_{11}) and transversal (b)u_{22}) velocity covariance functions for $\sigma_Y^2 = 2$. 40
2.8 Comparison between first order analytical solution according to Rubin (1990) and numerical longitudinal (a)u_{11}) and transversal (b)u_{22}) velocity covariance functions for $\sigma_Y^2 = 4$. 41
2.9 Flux balance for (a) MH over a squared control volume coincident with two triangular elements (Cordes and Kizelbach, 1996) and (b) CG over the extended Voronoi cell. 43
2.10 Hydraulic conductivity values CDFs of the real (RE), modified CG and MH fields for RE variances of a) 0.2, b)1, c)2 and d)4. 46

2.11 First effective moment comparison between the first order solution (σ_Y^2) and the transport solutions based on CG and MH flow fields for conductivity field variances of a) 0.2, b)1, c)2 and d)4. 51
2.12 Evolution of the plume barycenter velocity for the two numerical schemes for conductivity field variances of a) 0.2, b)1, c)2 and d)4. 53
2.13 Trends of the second effective moments Vs the first effective moment for conductivity field variances of a) 0.2, b)1, c)2 and d)4. 55

3.1 Upper (a) and lower (b) values for the reference distance L_r for which the temporal inertial term is of the same order of magnitude as the Darcy's terms. 66
3.2 Upper (a) and lower (b) values for the reference distance L_r for which the advection inertial term is of the same order of magnitude as the Darcy's terms. 68
3.3 Staggered grid layout used for the solution of the inertial system of equations. 70
3.4 Convergence trend at each second of the solution of the saturated inertial system obtained for the test case in which the upstream boundary condition is a square wave. 74
3.5 Envelope of the rising and falling profiles for the propagating front in test case 1 evaluated with the flux equation (no inertial effects taken into account). 75
3.6 Propagating fronts for test case 1 evaluated with the inertial system: a)rising profiles envelope and b)falling profiles envelope. 77
3.7 Profiles difference envelope in time between inertial and non-inertial solution for domain length of a)10m and b)20m. 78
3.8 Propagating fronts envelope for test case 1 evaluated with the inertial system for a domain length of 5m. 79
3.9 Profiles envelopes for test case 2 in which a high frequency wave is imposed as upstream boundary condition. Solution of a)the inertial system and b)the flux equation. 80
3.10 Profiles difference envelope for test case 2. 81

4.1 (a) Time series of column inflow and outflow. Flux is presented as mm per 5 min interval. The first vertical dashed line corresponds to the onset of a spike increase in irrigation rate. The second dashed line corresponds to the end of the spike and return to the background irrigation rate. The third dashed vertical line marks the end of irrigation. (b) Total column storage for the duration of the experiment. The increase at 8.5 hours corresponds to a time when water delivery tubes were unblocked and normal flow resumed (source Torres and Alexander (2002)). 86
4.2 Staggered grid layout used for the solution of the inertial system of equations. 93

4.3 Calibrated relative conductivity function (Van Genuchten model with $\alpha =$ 12 and $n = 1.55$) . . . 94
4.4 Water retention curve of a) Torres experiment (Torres and Alexander, 2002) and b) fitted for the numerical applications. . . . 95
4.5 Comparison of the numerical evolution of the column storage simulated with all the considered models. . . . 97
4.6 Hysteresis of the contact angle, where θ_a is the advancing angle and θ_r the receding angle. . . . 98
4.7 Conceptual application of the capillary barrier concept to the experimental evidences exposed by Torres and Alexander (2002). . . . 100
4.8 Hysteretic unsaturated conductivity function employed for the numerical simulations of the capillary barrier effect. . . . 101
4.9 Pre-spike, spike and post-spike stationary profiles and spike advancing front profile evaluated numerically with a)Richards model, b)Inertial model and c),d) and e) with the threshold hysteretic conductivity model with the value for the n parameter of $K_r^{(2)}$ equal respectively to 1.6, 1.7 and 1.9. . . . 104
4.10 Column module in PVC, 20cm high and 20 cm long. . . . 107
4.11 Base of the column with perforated filter. . . . 107
4.12 Column head, a) top view and b) bottom view. . . . 108
4.13 Load cell used for the measurement of the WRC related to the selected sandy soil. . . . 110

List of Tables

1.1 Saturated hydraulic conductivity and capillary rise for some soil types (Freeze and Cherry, 1979). 9
1.2 Soil hydraulic parameters for van Genuchten and Brooks and Corey models for eleven soil classes (Shao and Irannejad, 1999). 14
1.3 Grain size ranges for typical soil classes (Zaradny, 1993) 14

2.1 Euclidean norm for 6 refinement levels and convergence rate for piezometric heads evaluated with the standard Galerkin SG and the mixed hybrid MH schemes in test case 1. 29
2.2 Euclidean norm for 6 refinement levels and convergence rate for the module of velocity evaluated with the classical Galerkin CG, Yeh and the mixed hybrid MH schemes for test case 1. 29
2.3 Euclidean norm for the 4 higher refinement levels and convergence rate for piezometric heads evaluated with the standard Galerkin SG and the mixed hybrid MH schemes in test case 2. 31
2.4 Euclidean norm for the 4 higher refinement levels and convergence rate for the module of velocity evaluated with the classical Galerkin CG, Yeh, Zhou ZB and the mixed hybrid MH schemes for test case 2. 31
2.5 Euclidean norm for 6 refinement levels and convergence rate for piezometric heads evaluated with the standard Galerkin SG and the mixed hybrid MH schemes in test case 3. 33
2.6 Euclidean norm for 6 refinement levels and convergence rate for the module of velocity evaluated with the classical Galerkin CG, Yeh, Zhou ZB and the mixed hybrid MH schemes for test case 3. 33
2.7 Non-dimensional velocity field variances for longitudinal ($u'_{11}(0,0)$) and transversal ($u'_{22}(0,0)$) components. Second-order analytical values reported in Hsu et al. (1996) 37
2.8 Mean and variance of the real and modified conductivity fields for the four heterogeneity levels considered. 47

3.1 Resulting rates for the convergence test of the inertial system. The convergence rates attest around order 2. 73

4.1 Momentum equation coefficients magnitude for different reference length values in the specific case of Torres experiments (Torres and Alexander, 2002). 91

References

Ackerer, P., R. Mosé, P. Siegel, and G. Chavent, 1996: Reply to cordes and kinzelbach (1996). *Water Resour. Res.*, **32**, 1911–1913.

Andrade, J. S., U. M. S. Costa, M. P. Almeida, H. A. Makse, and H. E. Stanley, 1999: Inertial effects on fluid flow through disordered porous media. *Physical Review Letters*, **82**, 5249–5252.

Arbogast, T., L. C. Cowsar, M. F. Wheeler, and I. Yotov, 2000: Mixed finite element methods on non-matching multiblock grids. *SIAM J. Num. Anal.*, **37**, 1295–1315.

Bear, J., 1972: *Dynamics of Fluids in Porous Media*. Elsevier, New York.

Bear, J. and Y. Bachmat, 1990: *Introduction to Modeling of Transport Phenomena in Porous Media*. Kluwer Academic Publishers, London.

Bellin, A., 2000: Sulle problematiche connesse con la modellazione tridimensionale del flusso e del trasporto nelle formazioni marcatamente eterogenee. *In: XXVII Convegno di Idraulica e Costruzioni Idrauliche*.

Bellin, A. and Y. Rubin, 1996: Hydrogen: a new random field generator for correlated properties. *Stoch. Hydrol.*, **10**.

Bellin, A., P. Salandin, and A. Rinaldo, 1992: Simulation of dispersion in heterogeneous porous formations: statistics, first-order theories, convergence of computations. *Water Resour. Res.*, **28**, 2211–2227.

Bergamaschi, L. and M. Putti, 1999: Mixed finite elements and newton-like linearization for the soltion of richards equation. *Int. J. Numer. Methods Eng.*, **45**, 1025–1046.

Brezzi, F. and M. Fortin, 1991: *Mixed and Hybrid Finite Element Methods*. Springer-Verlag, Berlin.

Brooks, R. H. and A. T. Corey, 1964: *Hydraulic properties of porous media*. Colorado state university, Fort Collins.

Brutsaert, W., 1966: Probability laws for pore-size distribution. *Soil Sci.*, **101**, 85–92.

— 2005: *Hydrology, An Introduction*. Cambridge University press, New York.

Chin, D. A. and T. Wang, 1992: An investigation of the validity of first-order stochastic dispersion theories in isotropic porous media. *Water Resour. Res.*, **28**, 1531–1542.

Cordes, C. and W. Kizelbach, 1992: Continuity velocity fields and path lines in linear, bilinear, and trilinear finite elements. *Water Resour. Res.*, **28**, 2903–2911.

— 1996: Comment on 'application of the mixed hybrid finite element approximation in a groundwater flow model: Luxury or necessity?' by mosé et al. (1994). *Water Resour. Res.*, **32**, 1905–1909.

Dagan, G., 1989: *Flow and Transport in Porous Formations*. Springer-Verlag, New York.

Darcy, H. P. G., 1856: *Les Fountaines Publiques de la Ville de Dijon*. Paris, France: Victon Dalmont.

Englert, A., J. Vanderborght, and H. Vereecken, 2006: Prediction of velocity statistics in three-dimensional multi-gaussian hydraulic conductivity fields. *Water Resour. Res.*, **42**, doi:10.1029/2005WR004014.

Firdaouss, M., J. L. Guermond, and P. L. Quéré, 1997: Nonlinear corrections to darcy's law at low reynolds numbers. *j. Fluid Mech.*, **343**, 331–350.

Forchheimer, P., 1901a: Wasserbewegung durch boden. *Z. Vereines deutscher Ingnieure*, **49**, 1736–1741.

— 1901b: Wasserbewegung durch boden. *Z. Vereines deutscher Ingnieure*, **50**, 1781–1788.

Forsyth, P. A., 1991: A control volume ginite element approach to napl groundwater contamination. *SIAM J. Sci. Stat. Comput.*, **12**, 1029–1057.

Fourar, M., G. Radilla, R. Lenormand, and C. Moyne, 2004: On the non-linear behavior of a laminar single-phase flow through two and three-dimensional porous media. *Adv. in Water Res.*, **27**, 669–677.

Freeze, R. A. and J. A. Cherry, 1979: *Groundwater*. Prentice Hall, Englewood Cliffs, N.J.

Gardner, W. R., 1958: Some steady-state solutions of the unsaturated moisture flow equation with application to evaporation from a water table. *Soil Sci.*, **85**, 228–232.

Germann, P. F. and L. Di Pietro, 1999: Scales and dimensions of momentum dissipation during preferential flow in soils. *Water Resour. Res.*, **35**, 1443–1454.

Hassan, A., J. H. Cushman, and J. W. Delleur, 1998: A monte carlo assessment of eulerian flow and transport perturbation models. *Water Resour. Res.*, **34**, 1143–1163.

Hassanizadeh, S. M., M. A. Celia, and H. K. Dahle, 2002: Dynamic effect in the capillary pressure-saturation relationship and its impacts on unsaturated flow. *Vadose Zone Journal*, **1**, 38–57.

Hassanizadeh, S. M. and W. G. Gray, 1993: Thermodynamic basis of capillary pressure in porous media. *Water Resour. Res.*, **29**, 3389–3405.

Hsu, K. C. and S. P. Neuman, 1997: Second-order expressions for velocity moments in two- and three- dimensional statistically anisotropic media. *Water Resour. Res.*, **33**, 625–637.

Hsu, K. C., D. Zhang, and S. P. Neuman, 1996: Higher-order effects on flow and transport in randomly heterogeneous porous media. *Water Resour. Res.*, **32**, 571–582.

Jakeman, A. J. and G. M. Hornberger, 1993: How much complexity is warranted in a rainfall-runoff model? *Water Resour. Res.*, **29**, 2637–2649.

Kirchner, J. W., 2003: A double paradox in catchment hydrology and geochemistry. *Hydrological processes*, **17**, 871–874.

Kumar, P., 2004: Layer averaged richards equation with lateral flow. *Adv. Water Resour.*, **27**, 521–531.

Levy, A., S. Sorek, G. Ben-Dor, and B. Skews, 1996: Wave propagation in saturated rigid porous media: analytical model and comparison with experimental results. *Fluid Dynamics Research*, **17**, 49–65.

McDonnell, J. J., 1990: A rationale for old water discharge through macropores in a steep, humid catchment. *Water Resour. Res.*, **26**, 2821–2832.

— 2003: Where does water go when it rains? moving beyond the variable source area concept of rainfall-runoff response. *Hydrological processes*, **17**, 1869–1875.

McGlynn, B. L. and J. J. McDonnell, 2003: Quantifying the relative contributions of riparian and hillslope zones to catchment runoff. *Water Resour. Res.*, **39**, 1310–1330.

McGlynn, B. L., J. J. McDonnell, J. Seibert, and C. Kendall, 2004: Scale effects on headwater catchment runoff timing, flow sources, and groundwater-streamflow relations. *Water Resour. Res.*, **40**, doi:10.1029/2003WR002494.

Meissner, U., 1972: A mixed finite element model for use in potential flow problems. *Int. J. Numer. Methods Eng.*, **6**, 467–473.

Montanari, A. and S. Uhlenbrook, 2004: Catchment modelling: towards an improved representation of the hydrological processes in real-world model applications. *Journal of Hydrology*, **291**, 159.

Montazer, P. and W. E. Wilson, 1984: Conceptual hydrologic model of flow in the unsaturated zone, yucca mountain, nevada. *U.S. Geol. Surv. Water Resour. Invest. Rep.*, **84**, 4345.

Montgomery, D. R. and W. E. Dietrich, 2002: Runoff generation in a steep, soil-mantled landscape. *Water Resour. Res.*, **38**, doi: 10.1029/2001WR000822.

Montgomery, D. R., W. E. Dietrich, and J. T. Heffner, 2002: Piezometric response in shallow bedrock at cb1: Implications for runoff generation and landsliding. *Water Resour. Res.*, **38**, 1274–1292.

Mosé, R., P. Siegel, P. Ackerer, and G. Chavent, 1994: Application of the mixed hybrid finite element approximation in groundwater flow model: Luxury or necessity? *Water Resour. Res.*, **30**, 3001–3012.

Mualem, Y., 1976: A new model for predicting the hydraulic conductivity of unsaturated porous media. *Water Resour. Res.*, **12**, 513–522.

Musy, A. and M. Soutter, 1991: *Physique du sol*. Presses Polytechniques et Universitaires Romandes, Lausanne.

Neal, C. and P. T. W. Rosier, 1990: Chemical studies of chloride and stable oxygen isotopes in 2 conifer afforested and moorland sites in british uplands. *Journal of Hydrology*, **115**, 269–283.

Neuman, S. P. and V. Di Federico, 2003: Multifaced nature of hydrogeologic scaling and its interpretation. *Review of Geophysics*, **41**, 1014, doi:10.1029/2003RG000130.

Putti, M. and C. Cordes, 1996: Triangular mixed finite elements vs finite differences and finite volumes in groundwater flow modelling. *International conference on computing methods and water resources XII, Aldana AA et al. (eds) Computational Mechanics and Applied Sciences: Elsevier Southampton, London*, 61–68.

— 1998: Finite element approximation of the diffusion operator on tetrahedra. *SIAM J. Sci. Comput.*, **19**, 1154–1168.

Rasmussen, T. C., R. H. B. Jr., J. F. Dowd, and A. G. Williams, 2000: Tracer vs. pressure wave velocities through unsaturated saprolite. *SSSAJ*, **64**, 75–85.

Raviart, P. A. and J. M. Thomas, 1977: A mixed finite element method for second order elliptic problems. in i. galliani and e. magenes, editors. *Mathematical Aspects of the Finite Elements Method*, **606 in Lecture Notes in Mathematics, New York**.

Reddy, J. N., 1993: *An introduction to the Finite Element Method*. McGraw-Hill, New York.

Richards, L. A., 1931: Capillary conductio of liquids through porous mediums. *Physics*, **1**, 318–333.

Rigon, R., G. Bertoldi, and T. M. Over, 2006: Geotop: A distributed hydrological model with coupled water and energy budgets. *Journal of Hydrometeorology*, **7**, 371–388.

Romanelli, M., D. J. Cavalli, and A. Fiori, 2006: Sulla generazione del deflusso nei versanti a forte pendenza. *Atti del XXX Convegno di Idraulica e Costruzioni Idrauliche*.

Rooney, D. J., K. W. Brown, and J. C. Thomas, 1998: The effectiveness of capillary barriers to hydraulically isolate salt contaminated soils. *Water, Air, and Soil Pollution*, **104**, 403–411.

Rubin, Y., 1990: Stochastic modeling of macrodispersion in heterogeneous porous media. *Water Resour. Res.*, **26**, 133–141 (Correction, Water Resour. Res., 26(10),2631,1990).

— 2003: *Applied Stochastic Hydrogeology*. Oxford University Press.

Russo, D., I. Russo, and A. Laufer, 1997: On the spatial variability of parameters of the unsaturated hydraulic conductivity. *Water Resour. Res.*, **33**, 947–956.

Salandin, P. and V. Fiorotto, 1998: Solute transport in highly heterogeneous aquifers. *Water Resour. Res.*, **34**, 949–961.

Segerlind, L. J., 1987: *Applied finite element analysis*. J. Wiley and Sons, New York.

Shao, Y. and P. Irannejad, 1999: On the choice of soil hydraulic models in land-surface schemes. *Boundary-Layer Meteorology*, **90**, 83–115.

Shultze, B., O. Ippisch, B. Huwe, and W. Durner, 1999: Dynamic nonequilibrium during unsaturated water flow. *Reprint from: M. Th. van Genchten, F. J. Leij and L. Wu(ed.) Proc. Int. Workshop on Characterization and Measurement of the Hydraulic Properties of Unsaturated Porous Media*, 22–24.

Simunek, J., N. J. Jarvis, M. T. van Genuchten, and A. Gardenas, 2003: Review and comparison of models for describing non-equilibrium and preferential flow and transport in the vadose zone. *Journal of Hydrology*, **272**, 14–35.

Sinaj, S., C. Stamm, G. S. Toor, L. M. C. T. Hendry, H. J. Di, K. C. Cameron, and E. Fossard, 2002: Phosphorous exchangeability and leaching losses from two grassland soils. *J. Environ. Qual.*, **31**, 319–330.

Skjetne, E. and J. L. Auriault, 1999: New insights on steady, non-linear flow in porous media. *Eur. J. Mech. B/Fluids*, **18**, 131–145.

Sklash, M. G., 1990: Environmental isotope studies of storm and snowmelt runoff generation. *In: Anderson, M. G., Burt, T. P.(Eds.), Process Studies in Hillslope Hydrology*, 401–435.

Sorek, S., D. Levi-Hevroni, A. Levy, and G. Ben-Dor, 2005: Extensions to the macroscopic navier-stokes equation. *Transport in Porous Media*, **61**, 215–233.

Srivastava, R. and M. L. Brusseau, 1995: Darcy velocity computations in the finite element method for multidimensional randomly heterogeneous porous media. *Adv. in Water Resources*, **18**, 191–201.

Tarantino, A., 2004: Panel report: Direct measurement of soil water tension. *In Proc. Third Int. Conference on Unsaturated Soils, Recife*, **3**, 1005–1017.

Tarantino, A. and S. Tombolato, 2005: Coupling of hydraulic and mechanical behaviour in unsaturated compacted clay. *Géotechnique*, **55**, 307–317.

Torbjörn, L. and G. Rehbinder, 1993: Transient flow towards a well in an aquifer including the effect of fluid inertia. *Applied Sci. Res.*, **51**, 611–623.

Torres, R., 2002: A threshold condition for soil-water transport. *Hydrol. Process.*, **16**, 2703–2706.

Torres, R. and L. J. Alexander, 2002: Intensity-duration effects on drainage: Column experiments at near-zero pressure head. *Water Resour. Res.*, **38**, 1240–1251.

Torres, R., W. E. Dietrich, D. R. Montgomery, S. P. Anderson, and L. loague, 1998: Unsaturated zone processes and the hydrologic response of a steep, unchanneled catchment. *Water Resour. Res.*, **34**, 1865–1879.

Uchida, T., Y. Asano, T. Mizuyama, and J. McDonnell, 2004: Role of upslope soil pore pressure on lateral subsurface storm flow dynamics. *Water Resour. Res.*, **40**, doi: 10.1029/2003WR002139.

van Genuchten, M. T., 1980: A closed-form equation for predicting the hydraulic conductivity of unsaturated soils. *Soil Sci. Soc. J.*, **44**, 892–898.

Wenniger, J., S. Uhlenbrook, N. Tilch, and C. Leibundgut, 2004: Experimental evidence of fast groundwater responses in hillslope/floodplain area in the black forest mountains, germany. *Hydrological Processes*, **12**, 3305–3322.

Wheeler, J. A., M. F. Wheeler, and I. Yotov, 2002: Enhanced velocity mixed finite element methods for flow in multiblock domains. *Comput. Geosci.*, **6**, 315–332.

Wildenschild, D., J. W. Hopmans, and J. Simunek, 2001: Flow rate dependence of soil hydraulic characteristic. *SSSAJ*, **65**, 35–48.

Wu, Y. S., W. Zhang, L. Pan, J. Hinds, and G. S. Bodvarsson, 2002: Modeling capillary barriers in unsaturated fractured rock. *Water Resour. Res.*, **38**, 1253, doi:10.1029/2001WR000852.

Yeh, G. T., 1981: On the computation of darcian velocity and mass balance in the finite element modeling of groundwater flow. *Water Resour. Res.*, **17**, 1529–1534.

Zaradny, H., 1993: *Groundwater Flow In Saturated And Unsaturated Soil*. A.A. Balkema Publishers, Brookfield.

Zehe, E. and G. Bloeshl, 2004: Predictability of hydrologic response at the plot and cachment scales: Role of initial conditions. *Water Resour. Res.*, **40**, doi: 10.1029/2003WR002869.

Zhou, Q., J. Bensabat, and J. Bear, 2001: Accurate calculation of specific discharge in heterogeneous porous media. *Water Resour. Res.*, **37**, 3057–3069.

Acknowledgements

For my research, thank you:

To professor Alberto Bellin, for theoretical and financial supports, but especially for being a very good soul.

To professor Mario Putti, for the same reasons cited above... a part from the financial one.

To professor Riccardo Rigon, for being always available for explanations.

To professor Alessandro Tarantino and to Sara Tombolato, for laboratory support.

To Lorenzo Forti, for his highly technical laboratory work.

To Laura Martuscielli and Elena Uber, for all the bureaucratic part and for being very patient.

To Cristobal Castro and Martin Kaeser, for some numerical help... and fun.

For many reasons, thank you:

To Marta Castagna, Andrea Bertagnoli, Bruno Majone and Maddalena Stanchina, for being my very patient room mates.

To Stefano Serafin, Stefano De Toni and Elena Berté for being very nice lunch-mates... and friends.

To Marco Baratieri, for "geo-statistical" reasons.

To Roberto Tonezzer and Federica Castaman, for laboratory help and for funny moments.

To Dorje Dawa, Stefano Endrizzi and Silvia Simoni, for sharing with me these three years.

To Luciano Giovannini, for being very patient in administrative matters.

To Patrizia Pederzolli, Lorenzo Perghem and Giulia Fiorini, for being my very best friends.

And to anyone else, ...for everything else.

§

And very special thanks to my family: mom, dad, Renzo and Serena (The list of reasons is too long).

And to my girlfriend Elisa.

§